FINITE ELEMENT ANALYSIS OF LABORATORY MODEL EXPERIMENTS ON BEHAVIOR OF SHALLOW FOUNDATIONS UNDER GENERAL LOADING

A THESIS SUBMITTED TO
THE GRADUATE SCHOOL OF NATURAL AND APPLIED SCIENCES
OF
MIDDLE EAST TECHNICAL UNIVERSITY

BY

HASAN EMRE OKTAY

IN PARTIAL FULFILLMENT OF THE REQUIREMENTS
FOR
THE DEGREE OF MASTER OF SCIENCE
IN
CIVIL ENGINEERING

FEBRUARY 2012

Approval of the thesis:

FINITE ELEMENT ANALYSIS OF LABORATORY MODEL EXPERIMENTS ON BEHAVIOR OF SHALLOW FOUNDATIONS UNDER GENERAL LOADING

submitted by **HASAN EMRE OKTAY** in partial fulfillment of the requirements for the degree of **Master of Science in Civil Engineering Department, Middle East Technical University** by,

Prof. Dr. Canan Özgen
Dean, Graduate School of **Natural and Applied Sciences** _____

Prof. Dr. Güney Özcebe
Head of Department, **Civil Engineering** _____

Prof. Dr. B. Sadık Bakır
Supervisor, **Civil Engineering Department, METU** _____

Examining Committee Members:

Prof. Dr. M. Yener Özkan
Civil Engineering Dept., METU _____

Prof. Dr. B. Sadık Bakır
Civil Engineering Dept., METU _____

Assist. Prof. Dr. Nejan Huvaj Sarıhan
Civil Engineering Dept., METU _____

Assist. Prof. Dr. M. Tolga Yılmaz
Engineering Sciences Dept., METU _____

Dr. Onur Pekcan
Civil Engineering Dept., METU _____

Date: _____

I hereby declare that all information in this document has been obtained and presented in accordance with academic rules and ethical conduct. I also declare that, as required by these rules and conduct, I have fully cited and referenced all material and results that are not original to this work.

Name, Last Name: HASAN EMRE OKTAY

Signature :

ABSTRACT

FINITE ELEMENT ANALYSIS OF LABORATORY MODEL EXPERIMENTS ON BEHAVIOR OF SHALLOW FOUNDATIONS UNDER GENERAL LOADING

Oktay, Hasan Emre
M.S., Department of Civil Engineering
Supervisor : Prof. Dr. B. Sadık Bakır

February 2012, 161 pages

In this study, a series of laboratory model experiments carried on shallow foundations is intended to be simulated through numerical modeling. The laboratory model tests were conducted by Fukui et al. (2005), over square shaped, shallow surfacial foundations located over air-dried Toyoura sand. Tests included centered vertical and combined loading cases on sand with 60% and 80% relative densities. Plastic limit loads obtained from numerical analyses and available analytical solutions in literature are compared to the laboratory test results and the differences are discussed.

Employment of Mohr - Coulomb yield criterion and linear elasticity, resulting in linear elastic perfectly plastic constitutive law, is one of the most common practices in modeling geotechnical problems. Accuracy of this approach for the modeled experiments is judged by comparison of analyses results with experimental findings and solutions in literature. Finite element method is utilized for modeling purposes, with Mohr-Coulomb yield criterion and linear elastic behavior. Abaqus 6-10.2 is selected as the analysis software, and two and three dimensional models are used in the analyses. Analyses, the results of which are compared with experimental findings, aim employment of associated flow rule. Additional analyses are con-

ducted with varying dilation angles in order to examine the influence of unassociated flow rule on eccentric and concentric loading results.

Differences between the results of numerical analyses and experimental observations varied between 2% and 34%. Main reason of the difference is attributed to employed soil behavior modeling approach in analyses and the eccentric placement of model weight in monotonic horizontal loading experiments. In the case when this eccentric placement is accounted for in numerical models, it is seen that the difference diminished to vary between 8% and 18%, and order of the difference was similar for similar experiment cases. Therefore, based on this condition, it is seen that results of the modeled experiments are consistent, while in general they are somewhat higher than the results obtained from analyses and solutions in literature. Difference between the results of analyses and average of selected solutions in literature in both cases is at most 9%.

Finite element method employing Mohr-Coulomb failure criterion could provide results in close agreement with solutions in literature that inherently assume Mohr-Coulomb failure criterion as well. However, the same accuracy could not be obtained for experiments due to uncertainties involved in the material properties as well as the insufficiencies of the model to represent the behavior precisely. Finite element method has the potential to consider more advanced material models. Nonetheless, employment of Mohr-Coulomb failure criterion provides results with sufficient accuracy for most cases.

Keywords: finite element method, Abaqus, general loading conditions, shallow foundations, bearing capacity

ÖZ

YÜZEYSEL TEMELLERİN GENEL YÜKLEME KOŞULLARI ALTINDAKİ DAVRANIŞINI İNCELEYEN LABORATUVAR MODEL DENEYLERİNİN SONLU ELEMANLAR YÖNTEMİ İLE ANALİZİ

Oktay, Hasan Emre
Yüksek Lisans, İnşaat Mühendisliği Bölümü
Tez Yöneticisi : Prof. Dr. B. Sadık Bakır

Şubat 2012, 161 sayfa

Bu çalışmada yüzeysel temeller üzerinde yapılan bir seri laboratuvar model deneyinin sayısal yöntemler ile modellenmesine çalışılmıştır. Laboratuvar model deneyleri havada kurutulmuş Toyoura kumu üzerine yerleştirilen kare biçimli sığ temeller üzerinde Fukui et al. (2005) tarafından yapılmıştır. Deneyler dikey ve genel yükleme koşulları altındaki temellerin %60 ve %80 rölatif yoğunluktaki kum üzerinde yer alan testlerini içermektedir. Sayısal analizlerden ve literatürdeki mevcut çözümlerden elde edilen limit plastik yükler, laboratuvar deney sonuçları ile karşılaştırılmış ve farklar irdelenmiştir.

Zemin mekaniği problemlerini modellemede en yoğun olarak kullanılan uygulamalardan biri Mohr-Coulomb akma kriteri ve doğrusal elastikiyetin kullanılması ve neticede doğrusal elastik mükemmel plastik davranış elde edilmesidir. Bu yaklaşımın modellenen deneyler için hassasiyeti analiz sonuçlarının deneysel bulgular ve literatürdeki mevcut çözümlerin sonuçları ile karşılaştırılması ile değerlendirilmiştir. Sayısal modelleme yöntemi olarak, sonlu elemanlar yöntemi Mohr-Coulomb akma kriteri ve doğrusal elastik davranış ile birlikte kullanılmıştır. Abaqus 6-10-2, analiz yazılımı olarak seçilmiş ve analizlerde iki ve üç boyutlu modeller kullanılmıştır. Sonuçları deneysel bulgular ile karşılaştırılan analizler ilişkili akma koşulunu

kullanmayı hedeflemiştir. İlişkisiz akma koşulunun analiz sonuçları üzerindeki etkisini irdelemek amacıyla farklı dilatasyon açıları ile dikey ve genel yükleme koşullarını modelleyen ek analizler yapılmıştır.

Sayısal modeller ile deneysel gözlemler arasındaki fark %2 ila %34 arasında değişmiştir. Farkın ana sebebi, analizlerde kullanılan zemin davranışı modelleme yaklaşımına ve monotonik yatay yükleme deneylerinde model ağırlığının merkezde olmayacak şekilde konumlandırılmasına bağlanmıştır. Dengelenmemiş model ağırlığının kurulan sayısal modellerde göz önüne alınması durumunda ise bu farkın kapanarak %8 ila %18 arasında değiştiği ve benzer deneyler arasında benzer mertebelerde kaldığı görülmüştür. Buna gözlemden ötürü, laboratuvar deney bulgularının analiz sonuçları ve literatürdeki çözümlerden genel olarak bir miktar yüksek olmakla birlikte, tutarlı olduğu görülmektedir. Analiz sonuçları ile literatürden seçilen sonuçların ortalaması arasındaki fark ise her halükarda en fazla %9 olarak bulunmuştur.

Mohr-Coulomb akma kriterini kullanan sonlu elemanlar yöntemi, literatürde yine Mohr-Coulomb akma kriterini kabul eden çözümlere çok yakın sonuçlar sağlayabilmektedir. Ancak, aynı hassasiyet malzeme parametrelerindeki belirsizliklerden, ve modelin gerçek davranışı tamamen yansıtamadığından ötürü deneyler için elde edilememiştir. Sonlu elemanlar yönteminin daha gelişmiş malzeme modellerini kullanabilme potansiyeli bulunmaktadır. Bununla beraber, bu analiz yöntemi pek çok amaç için yeterli hassasiyette sonuçlar vermektedir.

Anahtar Kelimeler: sonlu elemanlar yöntemi, Abaqus, genel yükleme koşulları, yüzeysel temeller, taşıma kapasitesi

To My Family

ACKNOWLEDGEMENTS

First, I would like express my thanks to my supervisor Prof. Dr. Bahadır Sadık Bakır for his guidance, recommendations, motivation and hours he spent throughout my thesis study.

I am grateful to Ahmet Kuşyılmaz and Serhat Melik for their friendship, kindness, support and suggestions.

I wish also like to express my appreciation to Sevinç Ünsal Oral and Volkan Kaltakçı for their kindness.

The numerical calculations reported in this study were performed at TUBITAK ULAKBIM, High Performance and Grid Computing Center (TRUBA Resources). I would like to thank to Murat Ulubay from METU Computer Center, Sefa Arslan and Emrah Akkoyun from TRUBA Resources for their excellent technical support and encouragement.

Finally, and most importantly, I would like to thank to my dear family for their continuous support and encouragement throughout the study.

TABLE OF CONTENTS

LIST OF TABLES

TABLES

LIST OF FIGURES

FIGURES

LIST OF ABBREVIATIONS AND SYMBOLS

B	Width of the shallow foundation
B'	Effective width of foundation due to eccentric loading
c	Cohesion of soil
CPUS	Number of central processing unit cores utilized in calculations
D_r, D_R	Relative density of soil
E	Modulus of elasticity
e	Load eccentricity
$f_{cd}, f_{qd}, f_{\gamma d}$	Embedment depth factors for bearing capacity, considering cohesion, surcharge at foundation level, and unit weight of soil
$f_{ci}, f_{qi}, f_{\gamma i}$	Load inclination factors for bearing capacity, considering cohesion, surcharge at foundation level, and unit weight of soil
$f_{cs}, f_{qs}, f_{\gamma s}$	Shape factors for bearing capacity, considering cohesion, surcharge at foundation level, and unit weight of soil
F_f	Maximum shear resistance of soil - foundation interface
F_n	Normal force acting on soil - foundation interface
FEM	Finite Element Method
G	Shear Modulus
$G_\circ$	Small strain shear modulus
H_{CoG}	Height of center of gravity of the foundation model from base of foundation
H_{LP}	Height of experiment load application point on foundation model from base of foundation
i_c, i_q, i_γ	Load inclination factors for bearing capacity, considering cohesion, surcharge at foundation level, and unit weight of soil
I	Moment of inertia
k_h	Ratio of the horizontal to vertical components of the resultant force acting on foundation

$K_\circ$	Coefficient of at rest earth pressure
M_{arm}	Moment arm
M_y	Yield (ultimate) moment for foundation
N_c, N_q, N_γ	Bearing capacity factors for cohesion, surcharge at foundation level, and unit weight of soil
q_s	Surcharge pressure
RD	Relative density of soil
s_c, s_q, s_γ	Shape factors for bearing capacity, considering cohesion, surcharge at foundation level, and unit weight of soil
s_γ^{circ}	Shape factor for bearing capacity of circular foundations, considering unit weight of soil
$T.S.$	This study
V	Vertical component of the resultant force acting on the foundation
V_{max}, V_u	Ultimate vertical load the foudation could carry under centered vertical loading condition
W	Weight of foundation model
α	Angle of the resultant force acting on the foundation with respect to vertical
Δx_v	Horizontal displacement of vertical load application point
Δx_{CoG}	Component of horizontal displacement of center of gravity of foundation model due to tilt of the foundation
δ_{max}	Maximum dry density of soil
δ_{min}	Minimum dry density of soil
δ_o	Horizontal displacement of the load application point in monotonic horizontal loading experiments at maximum horizontal load
δ_{tip}	Displacement of the loading point of a cantilever supported beam at loading direction
ϕ	Angle of internal friction of soil
ψ	Dilatancy angle
γ	Unit weight of soil
μ	Friction coefficient for Coulomb friction rule
ν	Poisson's ratio of soil
Θ	Tilt angle of foundation

CHAPTER 1

INTRODUCTION

1.1 General

Finite element method is a valuable tool for geotechnical engineering considering its capability to enable solution of specific problems with complex geometries and demanding material models, for which analytical solutions may not exist. Mohr - Coulomb failure criterion is one of the most commonly used yield criterion to define plasticity of soils in finite element method. One of the difficulties with finite element method is the verification of the analysis results. Accuracy and reliability of finite element method analyses employing Mohr - Coulomb yield criterion for bearing capacity problems under general loading conditions is investigated by modeling laboratory model experiments and comparing results with solutions in literature.

1.2 Literature Review

Bearing capacity defines the load that a foundation can sustain at the state immediately before failure. In this section a review of studies in literature on ultimate bearing capacity of shallow foundations under centered vertical and combined loading is presented with emphasis on square shaped foundations resting on cohesionless soil without surcharge and for rough soil-foundation interface.

Traditional approach for bearing capacity calculation, which is suggested by Terzaghi (1943), involves the independent assessment of the influence of soil cohesion, overburden, and weight of the soil beneath the footing on bearing capacity. His expression in its most basic form is presented in Equation 1.1. The idea behind this equation is that there exist three main

contributions to the ultimate bearing pressure for a foundation. These contributions are due to the soil cohesion (c), the surcharge (q_s), and the soil self weight (γ).

Bearing capacity factors (N_c, N_q, N_γ) determine the extent of these contributions to the bearing capacity (q_u). Bearing capacity factors (N_c, N_q, N_γ) are defined to depend only on the internal friction angle of the soil. Among these, soil self weight contribution was the least agreed upon by the researchers as stated by Michalowski (1997). Later, Martin (2005) was able to obtain precise value for N_γ for rough or smooth footing assumptions, and associated flow rule condition by employing method of characteristics.

Bearing capacity equation when employed in its basic form as presented in Equation 1.1 is representative for the strip foundations (i.e., due to plane strain assumption) resting on soil surface and subjected to centered vertical loading. This equation is extended to be applicable to more general cases to account for the influence of foundation shape, depth of embedment and loading conditions involving inclined and eccentric loading by introduction of modification factors to the equation.

$$q_u = cN_c + q_sN_q + 0.5\gamma BN_\gamma \tag{1.1}$$

Bearing capacity equation is given in Equation 1.2 as presented by Das (1997) with the introduced factors to account for the shape, inclination, and embedment depth of foundations. For footings that are positioned below ground level, embedment depth factors (f_{cd}, f_{qd}, $f_{\gamma d}$), for loading conditions involving horizontal loading, load inclination factors(f_{ci}, f_{qi}, $f_{\gamma i}$), and to consider the foundation shape, shape factors (f_{cs}, f_{qs}, $f_{\gamma s}$) are utilized to modify the components in Equation 1.1 as presented in Equation 1.2.

$$q_u = cN_cf_{cs}f_{cd}f_{ci} + q_sN_qf_{qs}f_{qd}f_{qi} + 0.5\gamma BN_\gamma f_{\gamma s}f_{\gamma d}f_{\gamma i} \tag{1.2}$$

There are a number of numerical, analytical, and experimental studies in literature which aim to obtain the factors employed in Equation 1.2. Sieffert and Bay-Gress(2000) compared analytical formulations for the factors in Equation 1.2 as presented in Figure 1.1. These formulations are mainly based on the proposals of Terzaghi (1943), Meyerhof (1963), Hansen (1970) and Vesic (1973). It is observed that, the bearing capacity estimated by Equation 1.2 depends strongly on the selected formulation and among these Meyerhof's proposal yields

the highest results. Yilmaz (2004) stated that a unique methodology to estimate the bearing capacity does not exist for application, and further studies are required on this topic.

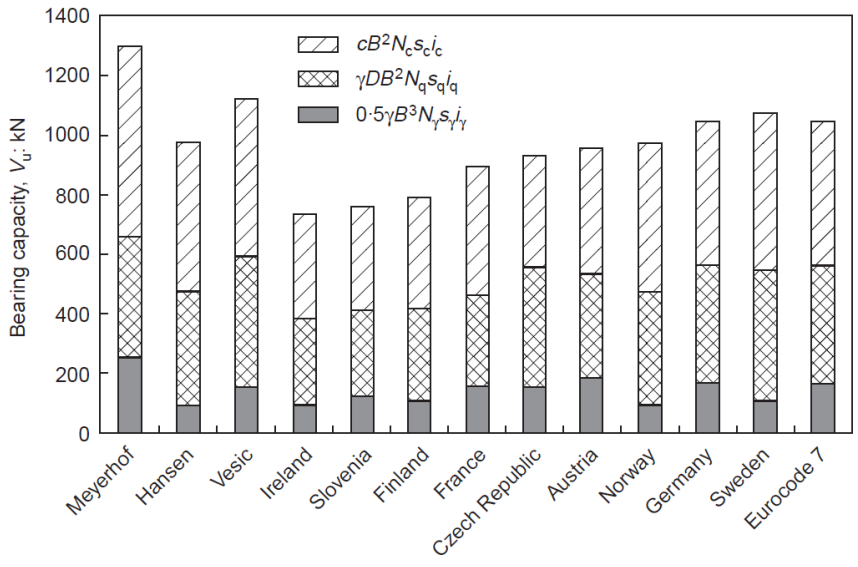

Figure 1.1: Comparison of analytical formulations and design codes of countries for an example problem by Sieffert and Bay-Gress(2000)

Bearing capacity factors are defined to depend only on the internal friction angle of the soil. Actually, these factors are shown to depend on cohesion, unit weight, foundation breadth and surcharge pressure (Michalowski, 1997). However, these dependencies are not considered in design for simplicity. In addition to the uncertainty of the magnitude of the factors employed in Equation 1.2, suitability of the equation itself is of question as well. Although the summation of the contributions of cohesion, surcharge and soil weight on ultimate bearing capacity is not strictly correct (Yilmaz, 2004, Zhu and Michalowski, 2005) this approach was adopted for application for its simplicity. Nonetheless it is shown by Bolton and Lau (1993) that the approximation due to this superposition is on the safe side.

Bolton and Lau(1993) investigated bearing capacity factors under vertical loading by using method of characteristics. This method avoids the assumption of arbitrary slip surfaces and produces zones within which equilibrium and plastic yield are simultaneously satisfied for given boundary stresses. They have considered strip and circular foundations resting on Mohr-Coulomb soil with rough or smooth soil - foundation interfaces. They have confirmed that the Terzaghi's approach of superposition of bearing capacity terms provides safe solutions. Additionally they have confirmed that Cox (1962) solution is mathematically acceptable. Moreover

bearing capcity factors N_q and N_γ are observed to be very sensitive to the value of ϕ. Interface condition between soil and foundation bottom is also found to have strong influence on the bearing capacity.

Michalowski (1997) investigated N_γ factor using upper bound limit analysis. The effect of non-associativity of the soil on this factor is investigated by employing the approach proposed by Drescher and Detournay (1993) in their study. It is observed that N_γ is sensitive to angle of dilation ψ and drops significantly with the decrease in ψ. Accordingly, they have concluded that the influence of non-asssociative flow rule should be considered in design.

Frydman and Burd (1997) investigated N_γ for strip foundation by finite difference method and finite element method analyses. It is found that for smooth footings with $\phi < 35°$, ψ has almost no effect on N_γ. For rough footings, however, very significant decrease in N_γ was found with decrease in ψ. For example, for rough soil - footing interface on soil with $\phi = 30°$ $N_\gamma = 21.7$ for $\psi = \phi$, and $N_\gamma = 16.7$ for $\psi = 0$. They have concluded that numerical techniques can be utilized for investigations of foundation load capacity.

Martin (2005) employed method of characteristics to obtain bearing capacity factors for strip and circular foundations with rough or smooth soil foundation interface conditions. He proved that for strip foundations results of the study were exact. On the other hand, for circular foundations results were not exact, as indicated by Loukidis and Salgado(2009), due to the assumption on the magnitude of intermediate principal effective stress at failure and its implication of occasional overlapping of the stress characteristic lines. In addition to publishing exact N_γ values, Martin (2005) commented that the method of characteristics is not a versatile method and has developed a software, that has casted away the error due to superposition of contributions of cohesion, surcharge and soil weight.

Loukidis and Salgado (2009) studied centered vertical bearing capacity of strip and circular foundations on sand with finite element method employing Mohr-Coulomb failure criterion. Focus of the study was on bearing capacity factors N_q and N_γ and corresponding shape factors for circular foundations. Influence of non-associativity of flow rule on bearing capacity factors was investigated with employment of realistic pairs of internal friction angle and dilation angle values as well. Influence of non-associativity of flow rule on ultimate bearing capacity was concluded as significant. Based on the analysis results, equation for N_γ and N_q presented in Equation 1.3 depending on dilation angle in addition to internal friction angle

was presented. For circular foundations, they have compared the finite element method analysis results with the results of Martin (2005), concluding that bearing capacity results obtained from finite element analyses can be in very close agreement with rigorous analytical methods. Shape factors, s_q and s_γ (Equation 1.4) were proposed for associated flow rule, which indicate higher bearing capacity of circular foundations compared to strip foundations, for high internal friction angles.

$$N_q = \frac{1 + \sin\phi}{1 - \sin\phi} e^{F(\phi,\psi)\pi \tan\phi} \tag{1.3a}$$

$$N_\gamma = (N_q - 1)\tan(1.34\phi) \tag{1.3b}$$

$$F(\phi,\psi) = 1 - \tan\phi(\tan(0.8(\phi - \psi)))^{2.5} \tag{1.3c}$$

$$s_\gamma^{circ} = 1 + \left(0.26\frac{1 + \sin\phi}{1 - \sin\phi} - 0.73\right) \tag{1.4}$$

Lyamin et al. (2007) studied the bearing capacity of strip, circular, square and rectangular foundations in sand, considering embedment depth, with finite-element limit analysis. In this technique, separate analyses are conducted to obtain rigorous upper and lower bounds of the desired result. Analyses for the upper and lower bounds are conducted with different finite element types and governing equations. Based on the average of results of upper and lower bound analyses, and their comparison with results of Martin (2005), equations for shape and depth factors for surcharge and soil weight contributions were suggested. It is commented that shape factor for soil weight contribution for circular foundations is slightly higher than that of square foundation. Additionally, a new ultimate bearing capacity equation was proposed which combine the influence of surcharge and soil weight in to a single quantity, in order to remove the error due to superposition discussed for Terzaghi (1943) bearing capacity equation.

Siddiquee et al. (1999) conducted finite element method simulations of the laboratory model experiments on strip foundation resting on Toyoura sand. They have conducted a parametric study to identify the significance of the factors influencing the bearing capacity, including confining pressure, anisotropy, non-linear strain hardening and softening, dilatancy and strain localization into shear bands. Their results present that as the number of influencing factors

accounted for in the analyses increases, ultimate bearing capacity obtained from the analyses decreases, resulting in better agreement with the laboratory model experiments. They have concluded that only when these influences are taken into account, results of physical model tests could be reasonably simulated by finite element method, and that the isotropic perfectly-plastic modeling of the deformation and strength property of sand are overly simplified approximations to be employed in finite element method analyses.

Approaches for obtaining the plastic limit loads for the bearing capacity of foundations subjected to eccentric and inclined loading could be grouped in two categories. The first group employs the traditional approach where Equation 1.2 is used by utilizing adjustment factors for eccentricity and inclination in the similar manner to the shape factors mentioned in Section 1.2. As discussed by Randolph et al. (2004), this approach is replaced by use of interaction envelopes defined in vertical, horizontal and moment spaces. This is the second group and an envelope proposed by Butterfield and Gottardi (1994) is shown in Figure 1.2.

Meyerhof bearing capacity equation together with Meyerhof's effective width rule is one of the most commonly used methods in estimation of the foundation load carrying capacity under eccentric and inclined loading. Note that for this equation shape factor utilization is not allowed by the formulation, since for loading with inclination Meyerhof has published the ultimate bearing capacity formula without shape factors. This is due to the fact that the plane strain assumption has significant effect on vertical bearing capacity, whereas it does not have such significance for inclined and eccentric loaded foundations. To take into account the eccentricity, effective width calculated according to Equation 1.5 of the foundation is used instead of full breadth of foundation. As for the inclination, inclination factors presented in Equation 1.6 are employed. In this equation α is the angle of inclination of the resultant force with respect to vertical.

$$B' = B - 2e \tag{1.5}$$

$$i_q = \left(1 - \frac{\alpha}{90^\circ}\right)^2 \tag{1.6a}$$

$$i_\gamma = \left(1 - \frac{\alpha}{\phi}\right)^2 \tag{1.6b}$$

The other method used in this study is that proposed by Paolucci and Pecker (1997). Paolucci and Pecker (1997) presents a method for the evaluation of seismic effects on the ultimate bearing capacity of shallow foundations on Mohr-Coulomb soils based on the kinematic approach of the yield design theory. This solution is an upper bound solution for the loading conditions involving inclination and eccentricity. Kinematic mechanism employed in their study allowed the uplift of the foundation under strong load eccentricities. Based on the obtained results they proposed an empirical formula presented in Equation 1.7, which defines an interaction envelope in vertical, moment and horizontal load space. This series of equation is organized in such a way that, for known breadth (B), ultimate bearing capacity under vertical loading (V_{max}), load eccentricity (e), magnitude of horizontal load acting on foundation (H); vertical load carrying capacity V of the foundation can be computed, by considering effect of inclination (first multiplier), inertial body forces (second multiplier) and eccentricity (third multiplier). In this study, test results and finite element analyses results for monotonic horizontal loading cases are compared with the proposal by Paolucci and Pecker (1997) by only considering the eccentricity and load inclination components of the equation.

$$V = \left(1 - \frac{k_h}{0.85}\right)^3 \cdot \left(1 - \frac{k_h}{\tan\phi}\right)^{0.35} \cdot \left(1 - \frac{2e}{B}\right)^{1.8} \cdot V_{max} \tag{1.7a}$$

$$k_h = H/V_{max} \tag{1.7b}$$

Butterfield and Gottardi (1994) utilized model test results on cohesionless soils from different authors. Relationship presented in Equation 1.8 is found between M, V, and H.

$$\left(\frac{V}{V_u}(V_u - V)\right)^2 = \left(\frac{H}{0.52}\right)^2 + \left(\frac{M_y}{0.35B}\right)^2 - \left(2.4\frac{M_y H}{B}\right) \tag{1.8}$$

One of the studies from which Equation 1.8 was derived is Georgiadis and Butterfield (1988). This study investigated the response of footings on sand, under eccentric and inclined loads. The experimental program included several tests on surface footings subjected to different eccentric and inclined load combinations. All of the experiments in the study were conducted on a foundation model that lies on the surface of a sand having peak internal friction angle of 46°. The footing model was made of steel and it was 50 mm wide and 400 mm long.

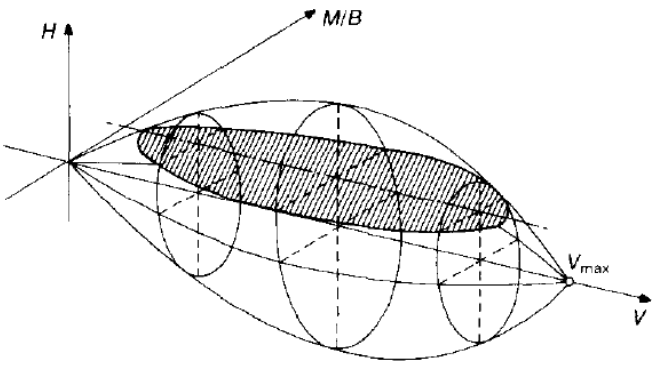

Figure 1.2: Failure envelope defined in vertical load, horizontal load and moment space defined by Butterfield and Gottardi (1994)

Loukidis et al. (2008) employed the finite element method in determination of collapse loads of strip footings subjected to combined loading resting on purely frictional soil following Mohr-Coulomb failure criterion. They considered effect of non-associativity as well. Based on the analyses results, they suggested a failure locus in vertical load, horizontal load and moment space, and described the failure surface by two different expressions. Equation 1.9 is the one which provides poorer fit to the analysis results but has a simpler form. In this equation V is the vertical load capacity under inclined and eccentric loading, e is the eccentricity, B is the breadth of the foundation, α is the angle of the loading with respect to vertical, V_{max} is the ultimate bearing capacity of foundation under vertical loading. The other form, which is stated to fit better with the analysis results, is employed in this study for the comparison in Chapter 4.

$$V = \left(1 - \sqrt{3.7\left(\frac{e}{B}\right)^2 + 2.1(\tan\alpha)^2 + 1.5\frac{e}{B}\tan\alpha}\right)^2 \cdot V_{max} \tag{1.9}$$

1.3 Objective and Scope

This study aims to make simulation of a set of laboratory model experiments using finite element method. Experiments include monotonic vertical and horizontal loading tests The tests were conducted on square shaped shallow foundation models, which are positioned on the surface of air-dried Toyoura Standard Sand (Fukui et al., 2005). Test cases involve Toyoura sand with 60% and 80% relative densities and loading conditions which yield different

moment to base-shear ratios.

Simulation method is chosen as implicit Finite Element Method (FEM) utilizing linear elastic perfectly plastic Mohr-Coulomb constitutive model. For all experiment cases both 2D plane strain and 3D FEM analyses are conducted. Abaqus 6-10.2 is utilized as the software for the FEM analyses. Calculated values of plastic limit loads of square shallow foundations on granular soils under general loading conditions through FEM analyses are compared with the Fukui et al. (2005) tests' results and with analytical solutions available in literature.

Other aims of this thesis include the discussions on the influence of unassociated flow rule, plane strain assumption, second order moments on conducted FEM analyses.

1.4 Outline

This study is composed of seven chapters and three appendices, which are organized as described below.

In Chapter 1, objective and scope of the study together with literature review for the modeled problem are presented.

In Chapter 2, the simulated laboratory model experiments are introduced.

In Chapter 3, details of the finite element analyses are presented. After a basic introduction of the finite element method, features of Abaqus software, which is employed in this study are presented. Following this background, layout of monotonic vertical loading and horizontal loading analyses are presented separately together with the employed modeling decisions. Afterwards, verification studies are presented. Then, consequences of the compromises made to increase computational efficiency of the analyses are evaluated. Finally, material properties employed in analyses are discussed.

In Chapter 4, results of experiments, analyses, and available solutions in literature are presented, compared and discussed. Details of the FEM modeling, such as the material parameters are presented.

In Chapter 5, differences observed between the results of experiments and analyses presented in Chapter 4 are further investigated and explanations are provided for.

In Chapter 6, influence of the unassociated flow rule, plane strain assumption and second order moments are discussed, based on analyses results.

In Chapter 7, conclusions are presented together with the recommendations for further studies.

In Appendix A, load versus sliding and foundation tilt angle curves obtained for monotonic horizontal loading analyses, the results of which were presented in Chapter 4, are provided together with experiment measurements.

In Appendix B, deformed meshes and distribution of vertical components of stresses and deformations of the finite element method analyses, the results of which were presented in Chapter 4, are given.

In Appendix C, computational costs of a number of the analyses, the results of which were presented in this study, are provided.

CHAPTER 2

DETAILS OF THE MODELED EXPERIMENTS

2.1 Overview of the Experiments

All experiment cases are conducted on 2 m thick layer of Toyoura Standard Sand having relative density of either 80% or 60%. Foundation models are placed at the center of the soil surface and have square shape with 0.5 m breadth. In order to ensure rough interface between foundation and soil, sandpaper is glued to the bottom face of the models. In cases conducted on sand with 80% relative density, 1 m thick layer of Kashima Sand with identical unit density was placed under the Toyoura Sand layer. Dimensions of the deep soil tank employed in experiments are given as 3 m wide, 4 m long and 11 m deep.

Experiments were conducted on a special basic research projects laboratory of the Public Works Research Institute (PWRI) (Fukui et al., 2005). General view of the soil tank with experiment models for centered vertical loading and horizontal loading tests are presented in Figure 2.1

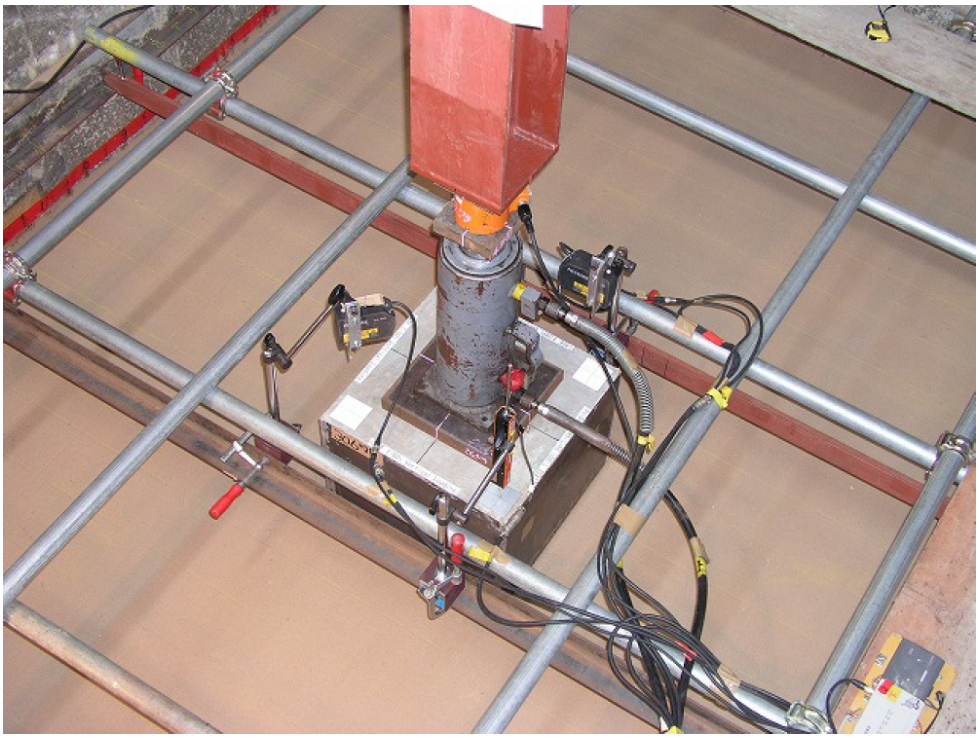

(a) Centered Vertical Loading Test

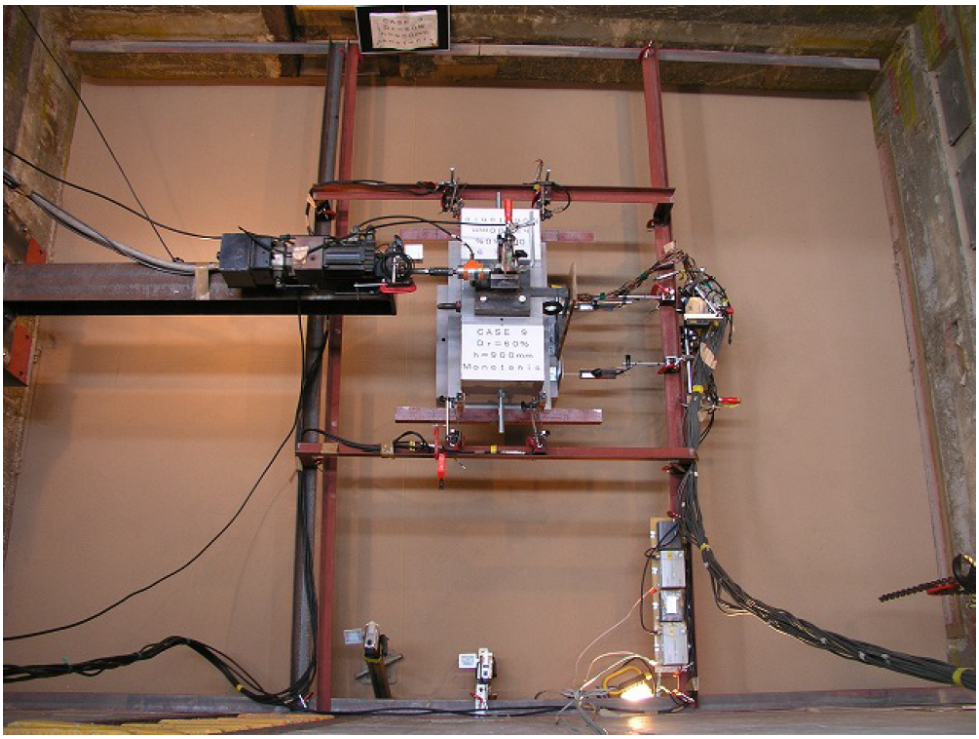

(b) Horizontal Loading Test

Figure 2.1: General view of the experiments (Fukui et al., 2005)

2.2 Experiment Cases and Purposes

Fukui et al. (2005) has conducted eleven experiment cases in the framework of their experimental work. Six of the cases were cyclic horizontal loading experiments, three of the cases were monotonical horizontal loading experiments, and two of the cases were monotonical centered vertical loading experiments. Cases can be grouped according to model used, and relative density of the employed Toyoura Sand as expressed in the following paragraphs. A summary of the tests is provided in Table 2.1. Employed foundation models are introduced in Section 2.3.

Two of the cases are monotonic vertical loading experiments conducted on Model V. Cases in this group are named as Case 1 and Case 2. Varying parameter in this group of tests is the relative density of the test medium. Case 1 is conducted on sand with 80% relative density, and Case 2 is conducted on sand with 60% relative density. Both of these experiment cases are simulated in this study.

Three of the cases are horizontal loading experiments run on Model H, underlain by sand with 80% relative density. Cases in this group are named as Case 3, Case 4 and Case 5. Varying parameter in this group is the horizontal load application method. In Case 3, horizontal load is applied monotonically; in Case 4, horizontal load is applied as one sided cyclic load; and finally in Case 5, horizontal load is applied as alternating cyclic load. For cyclic loading experiments of this group, Type II loading pattern is used. Only Case 3 is simulated in this group of tests.

Three of the cases are horizontal loading experiments run on Model L, underlain by sand with 80% relative density. Cases in this group are named as Case 6, Case 7 and Case 8. Varying parameter in this group is the horizontal load application method and employed load pattern. In Case 6, horizontal load is applied monotonically; in Case 7, horizontal load is applied as alternating cyclic load with Type I loading pattern; and finally in Case 8, horizontal load is applied as alternating cyclic load with Type II loading pattern. Only Case 6 is simulated in this group of tests.

Three of the cases are horizontal loading experiments run on Model L, underlain by sand with 60% relative density. Cases in this group are named as Case9, Case10 and Case11. Varying parameter in this group is the horizontal loading method and load pattern used. In Cases 9

horizontal load is applied monotonically; in Case 10 horizontal load is applied as alternating cyclic load with Type I loading pattern; and finally in Case 11 horizontal load is applied as alternating cyclic load with Type II loading pattern. Only Case 9 is simulated in this group of tests.

Table 2.1: Summary of the model tests, after Fukui et al. (2005)

Case	Model	Loading patterns		D_r (%)	Preparing the ground*
Case 1	Model V	Vertical loading		80	a
Case 2				60	a
Case 3	Model H	Monotonic horizontal loading		80	b
Case 4	(High pier)	Onesided-cyclic horizontal loading	Type II		b
Case 5		Alternating-cyclic horizontal loading			b
Case 6	Model L	Monotonic horizontal loading		80	a
Case 7	(Low pier)	Alternating-cyclic horizontal loading	Type I		b
Case 8			Type II		b
Case 9	Model L	Monotonic horizontal loading		60	a
Case 10	(Low pier)	Alternating-cyclic horizontal loading	Type I		b
Case 11			Type II		b

a, b: Method of sand replacement as discussed in Section 2.5
a: The entire (2m thick) sand layer was replaced.
b: Only 1m thick sand layer was replaced.

For monotonic centered vertical loading cases, load application is load controlled, with 0.2kN/s loading speed, until maximum force is reached. After reaching of the maximum force, load control was converted to displacement control with 0.5 mm/s loading speed. During horizontal loading tests, load application was either monotonic or cyclic, whereas the load was displacement controlled.

It is inferred that, monotonic vertical loading experiments provide guidance on the angle of dilation and Young's Modulus of the soil used in experiments. Moreover bearing capacity under general loading is often presented as a function of vertical bearing capacity in the literature. Monotonic horizontal loading experiments are conducted in order to determine the horizontal displacement to be employed in displacement controlled dynamic loading experiments.

2.3 Foundation Models Employed in Experiment Cases

Experiment cases employ three different foundation models. Two of these models are used in horizontal loading experiment cases in order to apply horizontal loading at different heights. The remaining one model is utilized in the vertical loading experiment. Models are named as ”vertical loading experiment model” (Model V), ”high pier model” (Model H) and ”low pier model” (Model L).

Model V consisted of a cube shaped steel shell filled with concrete. Horizontal face dimensions of the model were 0.5 x 0.5 m. Model H and Model L, shown in Figure 2.2, consisted of cap, pier and foundation parts and are employed in horizontal loading cases. Cap is composed of the weight placed on top of the pier and loading point apparatus which is attached on top of the weight. Pier is made of H Beams measuring 200 x 200 x 8 x 12 mm. Horizontal face dimension of the foundation was 500 x 500 mm. Load cells were attached to the bottom of the foundation. Weights of Model H and Model L were 8.924 kN and 8.728 kN respectively. Major difference between Model H and Model L is the height of the horizontal loading point from ground, which is 1300 mm for Model H and 900 mm for Model L. Due to weight placed on top of the pier, center of gravity of the models lie on the pier with 427 mm and 700 mm above from foundation base for Model L and Model H respectively.

2.4 Measuring Instruments Employed in Experiments

Figure 2.3 and Figure 2.4 presents the location of modeling instruments attached to foundation models employed in horizontal loading experiments. Table 2.2 presents the details of these instruments, including the quantity measured by each instrument and units of measurement.

Vertical displacements are measured at four corners of the square foundation and at top of the model corresponding to center. Horizontal displacements are measured at five locations. Horizontal force is measured at load application point. Eleven load cells are placed at footing base, each of which measures both horizontal and vertical forces.

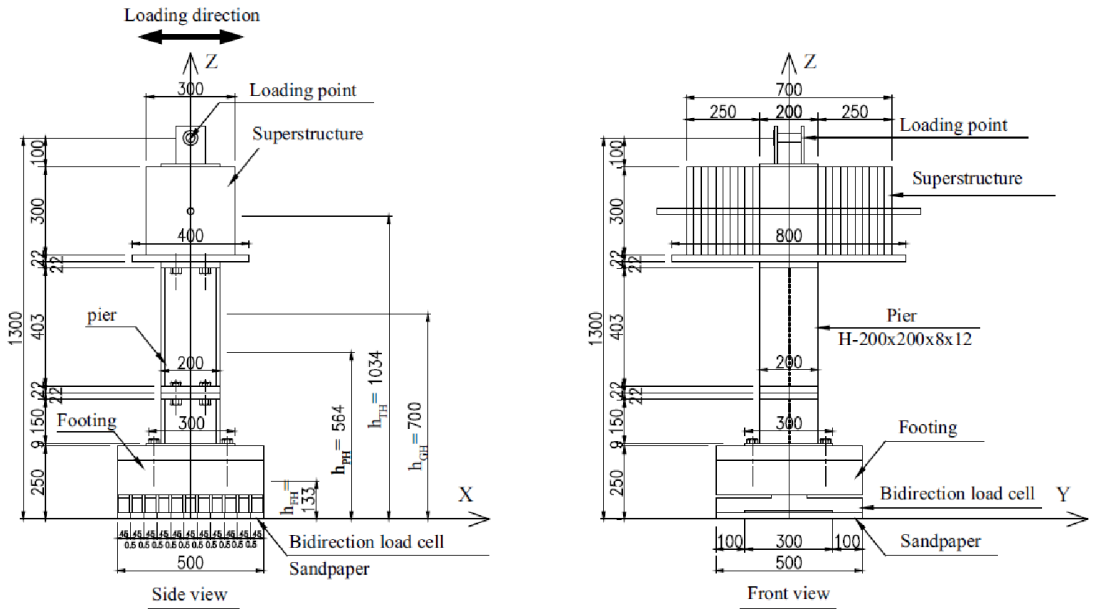

(a) High Pier Model (Model H)

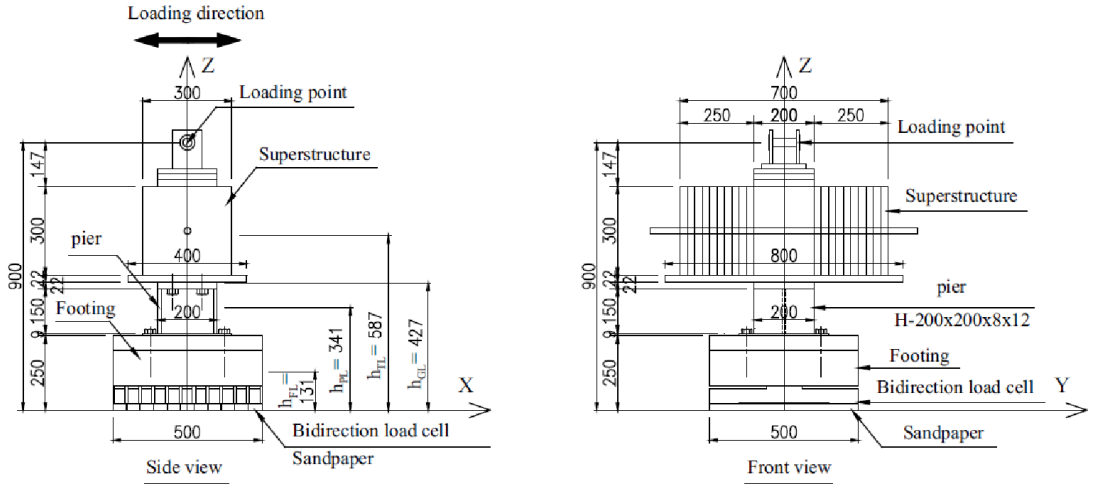

(b) Low Pier Model (Model L)

Figure 2.2: Models used in horizontal loading experiments, after Fukui et al. (2005)

Table 2.2: Measuring instruments attached to horizontal loading experiment models (Fukui et al., 2005)

Ch	Name	Measurement item	Measurement point	Unit	Positive sign
1	D-HT	Horizontal displacement	Loading point	mm	Southward
2	Load	Loading force	Loading point	kN	Push
3	D-HM	Horizontal displacement	Pier	mm	Southward
4	D-HL	Horizontal displacement	Footing	mm	Southward
5	D-VC	Vertical displacement	Model top	mm	Upward
6	D-VF1	Vertical displacement	Footing (SW)	mm	Upward
7	D-VF2	Vertical displacement	Footing (SE)	mm	Upward
8	D-VB1	Vertical displacement	Footing (NW)	mm	Upward
9	D-VB2	Vertical displacement	Footing (NE)	mm	Upward
10	P-H01	Reaction shear force	Footing bottom (S)	kN	Southward
11	P-H02	Reaction shear force	Footing bottom	kN	Southward
12	P-H03	Reaction shear force	Footing bottom	kN	Southward
13	P-H04	Reaction shear force	Footing bottom	kN	Southward
14	P-H05	Reaction shear force	Footing bottom	kN	Southward
15	P-H06	Reaction shear force	Footing bottom	kN	Southward
16	P-H07	Reaction shear force	Footing bottom	kN	Southward
17	P-H08	Reaction shear force	Footing bottom	kN	Southward
18	P-H09	Reaction shear force	Footing bottom	kN	Southward
19	P-H10	Reaction shear force	Footing bottom	kN	Southward
20	P-H11	Reaction shear force	Footing bottom (N)	kN	Southward
21	P-V01	Reaction vertical force	Footing bottom (S)	kN	Push
22	P-V02	Reaction vertical force	Footing bottom	kN	Push
23	P-V03	Reaction vertical force	Footing bottom	kN	Push
24	P-V04	Reaction vertical force	Footing bottom	kN	Push
25	P-V05	Reaction vertical force	Footing bottom	kN	Push
26	P-V06	Reaction vertical force	Footing bottom	kN	Push
27	P-V07	Reaction vertical force	Footing bottom	kN	Push
28	P-V08	Reaction vertical force	Footing bottom	kN	Push
29	P-V09	Reaction vertical force	Footing bottom	kN	Push
30	P-V10	Reaction vertical force	Footing bottom	kN	Push
31	P-V11	Reaction vertical force	Footing bottom (N)	kN	Push
32	D-HF1	Horizontal displacement	Footing (E)	mm	Southward
33	D-HF2	Horizontal displacement	Footing (W)	mm	Southward

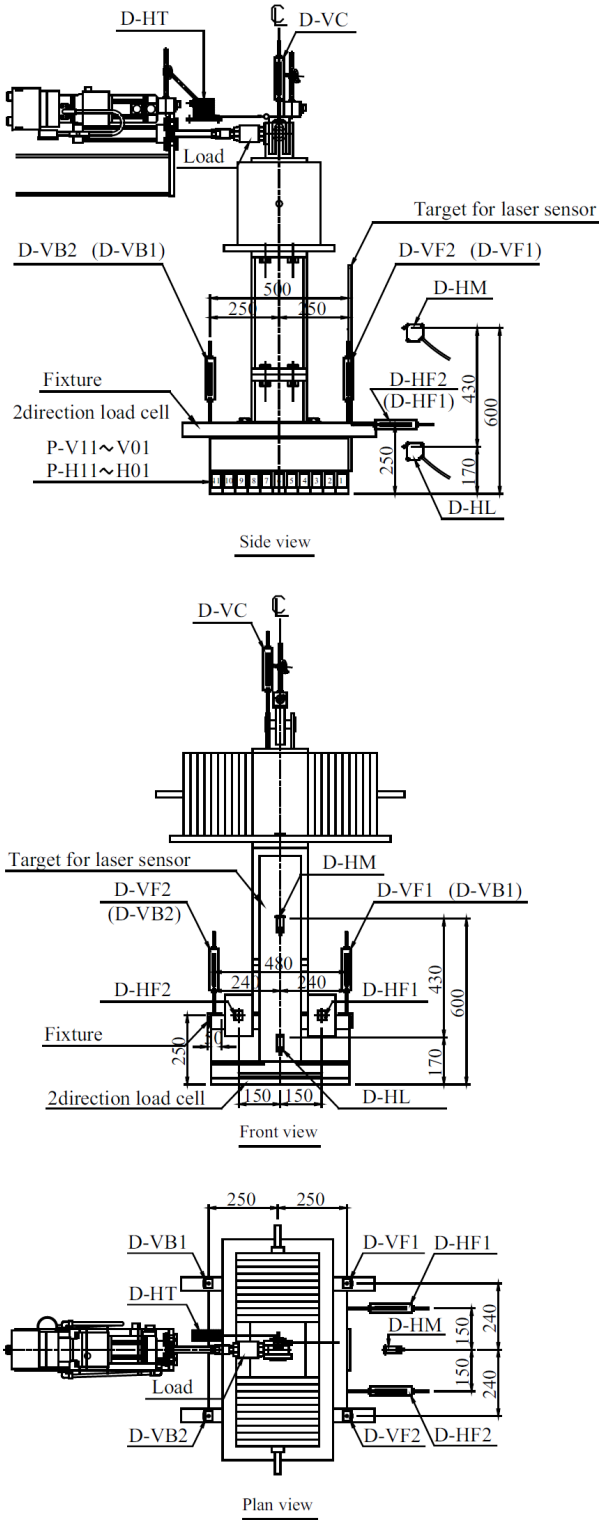

Figure 2.3: Measuring instruments attached to High Pier Model (Model H) (Fukui et al., 2005)

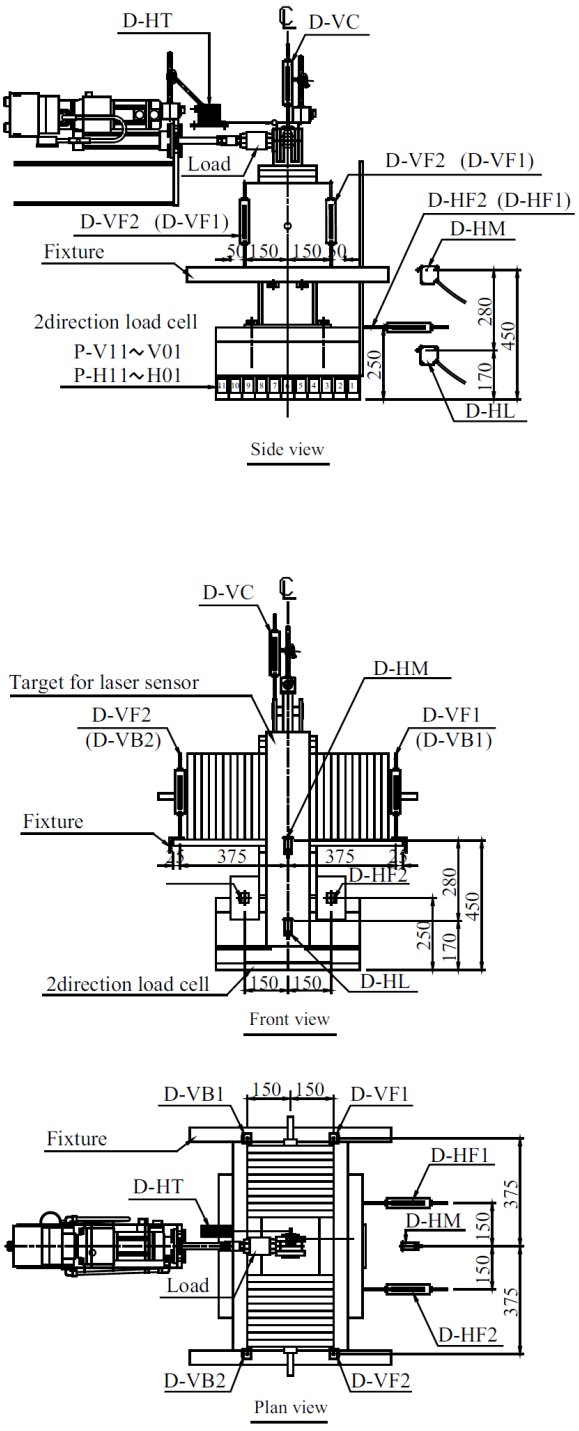

Figure 2.4: Measuring instruments attached to Low Pier Model (Model L) (Fukui et al., 2005)

2.4.1 Bidirectional Load Cells

In horizontal loading experiments eleven load cells were placed at footing base, each of which measures both horizontal and vertical forces. Each of these load cells was verified with a universal testing machine under vertical and shear loading conditions as shown in Figure 2.5. In verification of normal load sensors, load was applied with 1.961kN steps up to 19.613 kN, whereas in verification of shear load sensors load was increased with 0.196kN load steps up to 1.961 kN. Each test was conducted twice and calibration value was calculated by finding the mean slope of the tests in a primary regression analysis by Fukui et al. (2005). Results of two experiments on a single load cell for normal and shear load sensor verification are shown in Figure 2.6. Table 2.3 presents the results of the verification experiments for all load cells, conducted before the actual experiments.

It is inferred in this study that obtained magnitudes in the verification experiments were the strains recorded by load cells and the applied force in universal testing machine as shown in Figure 2.6. Then the relationship between these magnitudes were obtained by calculation of the slopes in these figures with primary regression analysis. Therefore in Figure 2.6 and Table 2.3, the ϵ_p and ϵ_s are the vertical and shear strains recorded by the load cells, respectively. Similarly, P and S are the vertical and shear forces, respectively, applied to the load cells by universal testing machine. In Table 2.3, P/ϵ_p, S/ϵ_s are presented indicating the linear relationship between strains measured by the load cells and applied loading. Taking note that these magnitudes are presented in Table 2.2, it is inferred that strains measured by load cells are converted to their respective forces with these magnitudes.

Under vertical loading verification tests the load cells were not expected to report shear forces, likewise under shear loading verification tests, the load cells were not expected to report vertical forces. These unexpected recordings are presented in Figure 2.6 and Table 2.3 as shear load and vertical load interference.

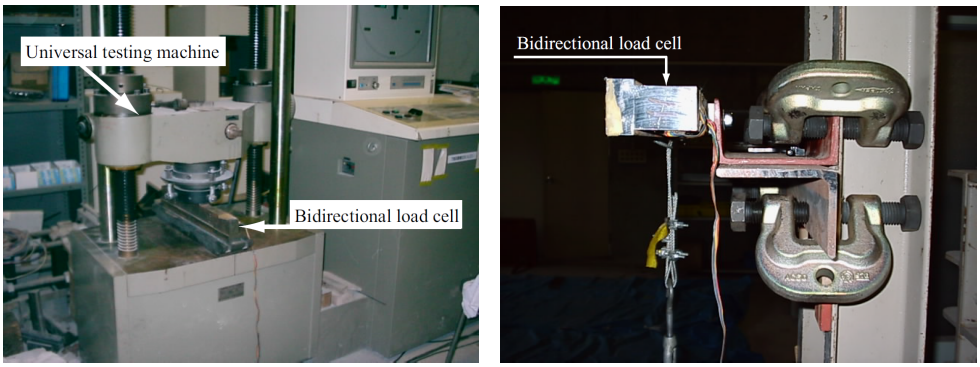

(a) Normal Loading (b) Shear Loading

Figure 2.5: Verification of vertical and shear sensors of load cells in universal testing machine (Fukui et al., 2005)

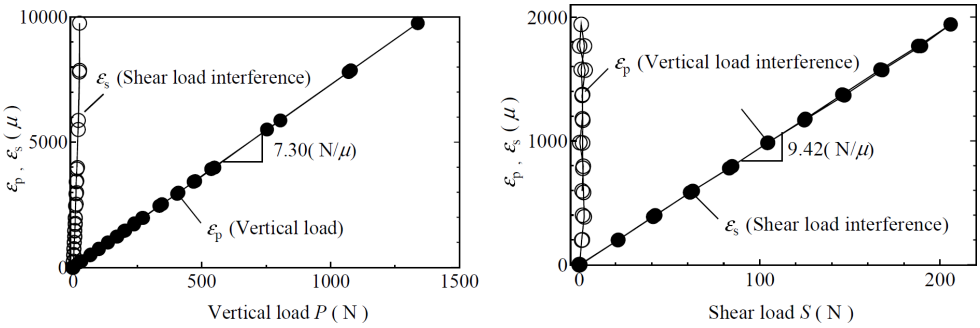

(a) Normal Loading (b) Shear Loading

Figure 2.6: Example of test results for vertical and shear loads verification (Fukui et al., 2005)

Table 2.3: Results of verification tests on load cells conducted before experiments (Fukui et al., 2005)

No	P/ε_p	P/ε_s	Interference (%)	S/ε_s	S/ε_p	Interference (%)
1	8.861	203.759	4.349	7.122	697.255	1.021
2	8.904	236.939	3.758	7.054	406.897	1.734
3	8.563	−337.195	−2.539	7.271	171.110	4.249
4	8.810	147.174	5.986	7.178	379.454	1.892
5	9.077	−271.008	−3.350	7.195	833.633	0.863
6	8.740	−451.799	−1.934	7.123	176.423	4.037
7	8.381	−340.151	−2.464	7.257	130.556	5.559
8	8.722	201.663	4.325	7.223	254.610	2.837
9	8.840	1001.108	0.883	7.086	306.000	2.316
10	8.673	−257.204	−3.372	7.192	299.490	2.401
11	8.930	1056.456	0.845	7.159	244.751	2.925

2.5 Method of Sand Placement

Figure 2.7 presents the procedure employed in preparation of the sand layers according to the desired relative density. When the relative density was changed among subsequent test runs the entire 2m thick layer was removed and new sand was placed, however when the same relative density is employed between subsequent experiments, only the 1 m of the layer was replaced. This was achieved thanks to the blue plastic and veneer (12 mm thick) were placed between the sand layers to simplify the replacement. Table 2.4 presents the densities for each experiment case modeled in this study. In this table, layer 1 is the deepest layer, whereas layer 8 is the closest layer to the soil surface.

Table 2.4: Density of each layer of sand for all experiment cases

Case	Overall density g (g/cm^3)									D_r
	layers 1	layers 2	layers 3	layers 4	layers 5	layers 6	layers 7	layers 8	layers all	(%)
Case 1	1.603	1.596	1.607	1.605	1.599	1.601	1.608	1.589	1.601	80
Case 2	1.540	1.537	1.533	1.544	1.540	1.539	1.542	1.532	1.538	60
Case 3	(1.602)	(1.606)	(1.600)	(1.604)	1.608	1.603	1.600	1.608	1.604	80
Case 6	1.602	1.606	1.600	1.604	1.599	1.595	1.604	1.597	1.601	80
Case 9	1.542	1.539	1.539	1.534	1.554	1.532	1.539	1.539	1.540	60

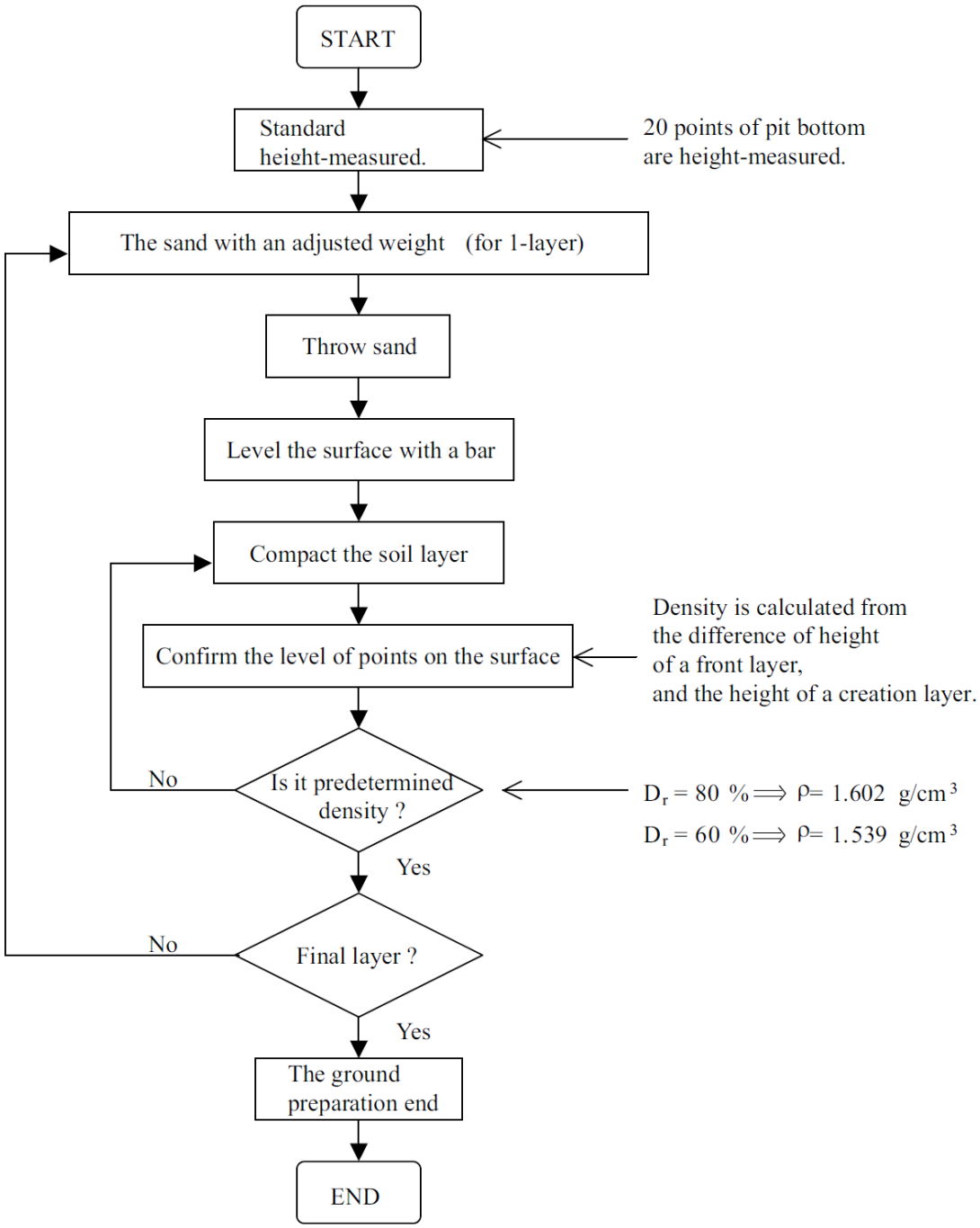

Figure 2.7: The procedure employed for preparation of the sand layers for the desired relative density

2.6 Geotechnical Properties of Toyoura Standard Sand in Experiments

Material properties given by Fukui et al. (2005) are presented in Table 2.5. Figure 2.8 presents shear modulus degradation and damping curves obtained from cyclic triaxial tests. In Section 3.7 material properties employed in finite element analyses are presented based on this information.

Table 2.5: Summary of physical properties of Toyura Sand used in experiments, after Fukui et al. (2005)

Item	Symbol	Unit	Value
Specific gravity	G_s	g/cm^3	2.655
Maximum diameter	-	mm	0.85
50 percent diameter	D_{50}	mm	0.170
30 percent diameter	D_{30}	mm	0.151
Coefficient of uniformity	U_c	-	1.4
Maximum dry density	ρ_{dmax}	g/cm^3	1.664
Minimum dry density	ρ_{dmin}	g/cm^3	1.364
Internal friction angle (for D_r = 60%)	ϕ	°	39.9
Internal friction angle (for D_r = 80%)	ϕ	°	42.1
Cohesion	c	kPa	0
Density (for D_r = 80%)	ρ	g/cm^3	1.602
Density (for D_r = 60%)	ρ	g/cm^3	1.539

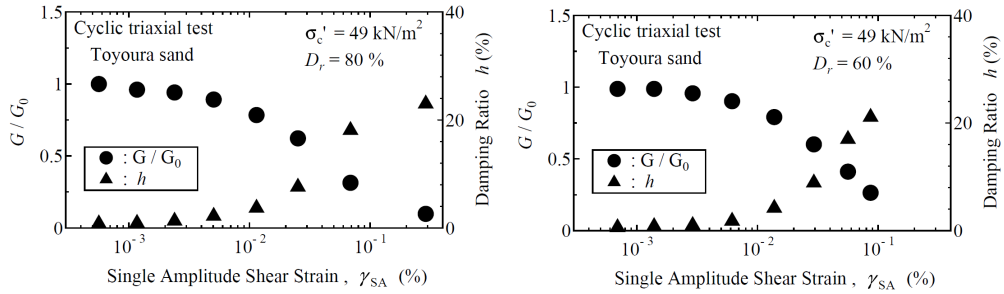

(a) For D_R = 80% (b) For D_R = 60%

Figure 2.8: Shear modulus degradation and damping, after Fukui et al. (2005)

CHAPTER 3

MATERIAL PARAMETERS AND METHOD USED IN THE FINITE ELEMENT ANALYSES

3.1 Field of Study

In this study, static, displacement based nonlinear finite element method analyses are conducted for plastic limit load calculations with granular material.

Soil is modeled as continuum with two dimensional quadrilateral or three dimensional hexahedral continuum elements that are utilizing quadratic shape functions and reduced integration scheme. Linear elastic perfectly plastic material model is selected for soil. Mohr-Coulomb yield surface is utilized as plasticity definition. Effect of unassociativity of the flow rule for plasticity is considered.

Foundation loads are either directly applied on soil continuum as prescribed displacements, or applied via discontinuous constraints with contact interactions. Interaction between soil continuum and foundation which is modeled as a discrete rigid body is enforced with penalty method. As contact interaction approach, contact pairs approach is utilized with surface to surface contact discretization together with finite sliding contact tracking. Frictional behavior of the contact is modeled to obey Coulomb friction rule with constant friction coefficient and pressure overclosure behavior of the contact is selected to enable separation after contact. The contact algorithm used in Abaqus is presented in Figure 3.1.

Newton's method is used as the solution strategy for nonlinear response. Line search algorithm is employed to ensure robustness of Newton's method. In order to deal with numerical instabilities adaptive automatic stabilization is utilized.

3.2 Finite Element Method Overview

This section reviews the basics of the finite element method. It includes a fast derivation of the method, compiled from books by Bathe (1996), Chandrupatla and Belegundu (1997), Potts and Zdravkovic (1999), Reddy (2004) and Abaqus Documentation (2010) as to provide a basis of reference for the explanations for the modeling choices presented in Section 3.4.

As stated in Abaqus Documentation (2010): "First step of any finite element simulation is to discretize the actual geometry of the structure using a collection of finite elements. Each finite element represents a discrete portion of the physical structure. The finite elements are joined by shared nodes. The collection of nodes and finite elements is called the mesh." Distribution of analysis variables are approximated within each element according to the magnitudes of that variables at that element's nodes.

Finite element method is used to solve a governing equation under given boundary conditions. For mechanical stress-strain analyses, which are conducted in this study, finite element method can make use of principle of virtual work as the governing equation. This principle is presented in Equation 3.1 and states that: "the equilibrium of a body requires that for any compatible small virtual displacements imposed on the body in its state of equilibrium, the total internal virtual work is equal to the total external work." (Bathe, 1996)

$$\int_V \epsilon^T \sigma \, dV = \int_V U^T F_B \, dV + \int_A U_A^T F_A \, dA + \sum_i U_i^T R_i \tag{3.1}$$

Left hand side of this equation represents internal work done due to deformation of the body, and right hand side of the equation considers external work done by the applied loads on the body. In this equation σ and ϵ are the virtual stresses and strains within the body, U terms are the virtual displacements, V is the volume of the body, F_B is the body force (such as gravitational force) acting on the body, U_A is the displacement of the nodes that makes up the surface with area A, F_A is the distributed force applied on that area and U_i is the displacement of a single node where reaction force R_i is applied on.

Considering employment of principle of virtual work in finite element method as the governing equation, terms in the equation could be reevaluated as follows. All terms at the right hand side of the equation except virtual displacements, namely F_A, A, R_i, F_B, V are part of

the problem definition. Hence values of these parameters are known. These variables are defining the boundary conditions for which the solution of the governing equation is sought. U terms are the unknown nodal displacements that would satisfy the governing equation for the boundary conditions. U, U_A, U_i could be considered as the same variable since they are represented with vector U. Considering virtual displacements do not depend on variables of integrations in Equation 3.1, they could readily be taken out of the integrals. By multiplying both sides of the Equation 3.1 with U (note that $U.U^T = 1$), and denoting $\int_V \epsilon^T \sigma \, dV$ term as stiffness matrix (K) this equation reduces to Equation 3.2b.

$$K = \int_V \epsilon^T \sigma \, dV \tag{3.2a}$$

$$KU = \int_V F_B \, dV + \int_A F_A \, dA + \sum_i R_i \tag{3.2b}$$

Remembering that except the nodal displacements, right hand side of the Equation 3.1 which concerns external forces is composed of known values, all of the terms at the right hand side of Equation Equation 3.2b can be evaluated numerically such that each body force, surface pressure and boundary condition is converted to representative forces or displacements acting at the finite element nodes. Sum of these forces for each node is held by the load vector (P) in Equation 3.3. Note that this evaluation might not strictly be considered as part of finite element method, since the results of the evaluation is an input for the finite element method. This input defines the boundary conditions for which the solution satisfying the governing equation (i.e., principle of virtual work) will be found by finite element method.

$$KU = P \tag{3.3}$$

It will be explained that once the nodal displacements (U) are known, the stresses (σ) and strains (ϵ) in each finite element can be determined. Hence the only remaining unknown term in Equation 3.1 is the nodal displacements. Therefore in a stress analysis displacements of the nodes (U) are the fundamental variables that are calculated.

In order for the stiffness matrix (K) presented in Equation 3.2a to be computed, relationships of nodal displacements with stresses and strains within the body is required.

Relationship between strains and nodal displacements is defined by the chosen element type. Such a relationship exists since displacement of any spatial location within a finite element is approximated according to the displacements of that element's nodes. Approximation is done by a polynomial function named as shape function which is defined within the finite element type utilized for discretization of the body. By differentiating this function according to requested strain direction, desired strains could be obtained. This relationship is shown in Equation 3.4. Note that approximation of strains according to nodal displacements is one of the main sources of errors in finite element method.

$$\epsilon = BU \tag{3.4}$$

Relationship between stresses and strains is defined by the chosen material model. This relationship is formulated in Equation 3.5, where C is the constitutive matrix.

$$\sigma = C\epsilon \tag{3.5}$$

An example constitutive matrix, for linear elastic material model with plane strain assumption is given in Equation 3.6. It is worth to note that terms in this matrix only depend on material constants namely elasticity modulus, and Poisson's ratio, which are part of the problem definition.

$$C = \frac{E}{(1+\nu)(1-2\nu)} \begin{bmatrix} 1-\nu & \nu & 0 \\ \nu & 1-\nu & 0 \\ 0 & 0 & \frac{1-\nu}{2} \end{bmatrix} \tag{3.6}$$

By substituting Equations 3.4 and 3.5 into Equation 3.2a for strains and stresses, right hand side of the equation is found as shown as stiffness matrix (K) in Equation 3.7.

$$K = \int_V B^T C B \, dV \tag{3.7}$$

It is important to note that obtaining the stiffness matrix (K) requires evaluation of an integral. Therefore a numerical integration method is essential for finite element method. For numer-

ical integration, Gauss Quadrature method, which requires the evaluation and summation of the term to be integrated for certain number of data points, can be utilized.

After computation of stiffness matrix, Equation Equation 3.2b becomes a system of linear equations which could be solved for U by solution techniques such as Gauss Elimination. After obtaining the displacements (U) from Equation 3.3, strains and stresses throughout the problem domain could be computed with Equations 3.4 and 3.5.

Boundary conditions are enforced by methods such as elimination approach or penalty approach. These methods are composed of modifying the terms of stiffness matrix (K) and load vector (P) or displacement vector (U) shown in Equation 3.3 once the system of equations is constructed in matrix form for the given boundary conditions. It is worth to note that the penalty method is an approximate approach, where a boundary condition is assigned by means analogous to placing a spring with high stiffness to the enforced degree of freedom, whereas elimination method is an exact method where the specific terms of the stiffness matrix is removed. Chandrupatla et al. (1997) has further details on formulation of stiffness matrix, and implementation details of finite element method.

At this point, introduction of finite element method in its basic form is completed. With features introduced up to this point, problems employing linear material model and for which small deformation assumption holds could be analyzed. Additionally, it is worth to note that, these type of analyses could complete in a single calculation step and do not require iterations. Additional features such as considerations of non-linear material behavior or discontinuous boundary conditions are implemented by introduction of iterations into the calculation. Calculation procedure utilized in Abaqus for analysis containing discontinuous constraints is shown in Figure 3.1 as an example for introduction of iterations in finite element method. Until this point non-linear behavior has not been considered. Although, ability to model non-linear load - displacement behavior is one of the essential features of finite element code for analyzing geotechnical problems in which material behavior is generally non-linear. In addition to the material, large deformations of the modeled bodies are another source of non-linearity. In this study, consideration of both material and geometric non-linearities have been appeared as a necessity in order to adequately model the experiments.

For linear elastic material definitions C matrix is composed of constant numbers whereas for non-linear material behavior C matrix depends on the strain magnitude. Material non-

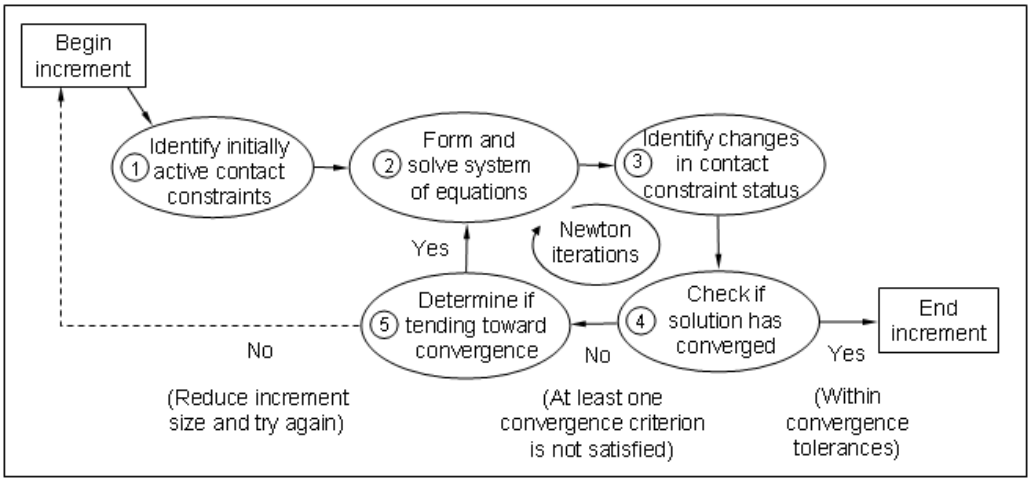

Figure 3.1: Contact algorithm used in Abaqus (Abaqus Documentation, 2010)

linearity is taken into account by recalculating the C matrix throughout the analysis, according to the strain magnitudes in the elements. Note that strains in elements depend on the nodal displacements.

There are a number of solution strategies for non linearity problems modeled with finite element method. Considering only material non-linearity, one of the differences of these methods is on how often, the changes in strains should be considered.

As an example, if tangent stiffness method is utilized (Figure 3.2(a)), C matrix is recomputed at the beginning of each load increment, according to the calculated stresses at the previous load increment. Therefore each load increment would conclude with a single iteration. On the other hand, if Modified Newton - Raphson method is utilized, a number of additional iterations are conducted within the load increment. In these iterations strains which were found previously according to the given load increment are utilized once more to update the C matrix and a new load increment is found with this matrix. Difference of these load magnitudes are checked for a given error tolerance and if the error magnitude is not found as acceptable, a new iteration is conducted, this time setting the load difference as the load increment. After an acceptable error is reached, nodal displacements corresponding to load increment is computed by summing all nodal displacements found in the iterations. Figure 3.2(b) illustrates one load increment, which completes in 5 iterations of this procedure.

For the sake of completeness, it is also worth to note that elastic strains and plastic strains

are evaluated separately by separate elastic and plastic constitutive matrices. Total strain is obtained by summation of elastic and plastic strains. This and similar implementation details are not mentioned in this section. Potts and Zdravkovic (1999) provide more detailed explanations and comparisons of different solution strategies for nonlinear problems.

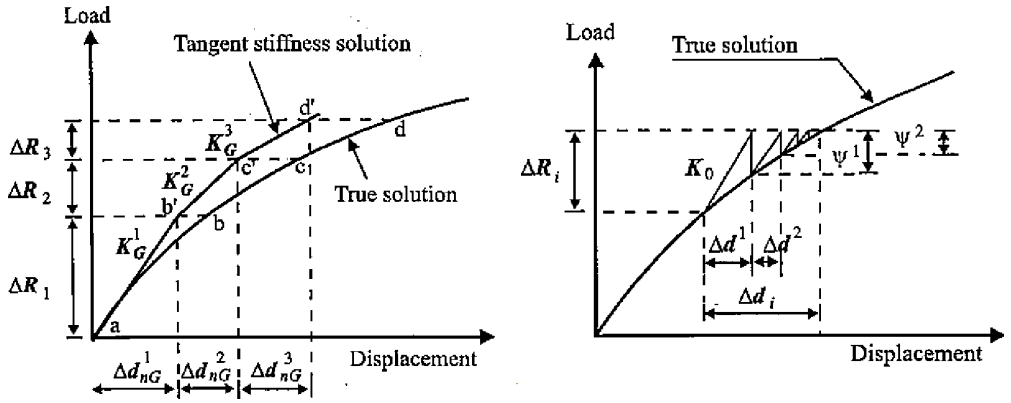

(a) Tangent Stiffness Method (b) Modified Newton Raphson Method

Figure 3.2: Illustrations of Solution Strategies for Non-Linear Problems After Potts and Zdravkovic(1999)

In order to take geometrical nonlinearity into account, B matrix is updated throughout the analysis similar to C matrix as described in above paragraphs. One other source of nonlinearity is the discontinuous constraints which are utilized for soil foundation contact interaction. If the soil and foundation are contacting these constraints are enforced, if they get separated these constraints are suppressed and not used. This prevents the artificial sticking of the soil to the foundation for cases showing uplift behavior. Figure 3.1 shows the algorithm used by Abaqus for the discontinuous constraint enforcement.

3.3 Abaqus Finite Element Code

3.3.1 General

Abaqus is a commercial, general purpose simulation tool which is used in different engineering fields. It is based on finite element method and has a large number of predefined element formulations and material models. It has means to solve contact interactions between bodies and has multiple methods for solving problems with non-linear behavior. Additionally it has

a graphical user interface for preprocessing of input files and post processing of the results.

Abaqus has been chosen as the finite element analysis software in this study for the following reasons: First, Mohr-coulomb yield criterion is readily available. Second, it has capability to conduct three dimensional analyses. Third, in literature studies on geotechnical engineering problems using this software are available. And the final reason is the availability of software license.

As a general purpose finite element software, Abaqus enables the use of a number of different technologies developed for finite element method. Generally, it has more than one means for modeling a physical phenomenon and multiple choices of algorithms to be used for finding the solution of the modeled problems. One of the valuable features of the software might be that, for any chosen method, it has predefined values of configuration parameters for that method, that would yield acceptable solutions in a general sense. Although modifications to the predefined parameters may be needed for the specific problem to be modeled, advices and guidelines for these modifications, with their possible consequences are documented.

Abaqus analysis product Abaqus/Standard requires an ASCII text file as input. This file contains all aspects of the model, from coordinates of the nodes, to the analysis steps, and requested output variables. Users can edit or create this file from scratch manually, or could use preprocessor software such as Abaqus CAE which has a graphical user interface for this purpose. In 6.10-2 version of Abaqus used in this study, not all, but most of the features of Abaqus analysis product could be utilized from within Abaqus CAE. For the not yet implemented features, input files could be modified by hand and Abaqus CAE could store these modifications. In this study Abaqus CAE is used for Abaqus input file generation.

As output, Abaqus can save the values of a certain variable at a selected entity throughout the analysis; or it can record the state of the whole model for a certain variable. The former is called a history output request, whereas the latter is called a field output request according to Abaqus Documentation (2010). These requests are written to an output database file, which is in a binary format that can be read by Abaqus CAE. Other forms of output format exists in which history output could be saved in binary or ASCII file formats and opened by third party software.

3.3.2 Element Types

There are a number of continuum element geometries and formulations available in Abaqus. With combination of these selections, over 20 element types are available in Abaqus software for 3 dimensional stress-displacement analyses. Main differences among element types are the element geometry, integration scheme, and order of shape function.

In Abaqus Documentation (2010), it is advised to use hexahedral (brick-shaped) elements wherever possible for 3D analyses, since they give the best results with minimum cost. Therefore, only elements with hexahedral geometry are considered in this study.

In this section properties of C3D8R, C3D20R, C3D20, C3D8I element types are investigated. Naming convention for these elements are as follows: C3D stands for 3D continuum stress/displacement element, number after C3D is the number of nodes of the element, R (optional) means element uses reduced integration scheme, I (optional) means that element is an incompatible mode element. Incompatible mode elements are enhanced versions of linear first order fully integrated elements to decrease the vulnerability of element to shear locking numerical problem explained in this Section 3.3.2.4. Among these element types considering order of shape function, elements with 8 nodes are linear elements and elements with 20 nodes are quadratic elements.

Based on findings in this section, and advices given in Abaqus Documentation (2010), C3D20 and C3D8R element types are dismissed for analyses conducted in this study. C3D20 is eliminated due to availability of C3D20R, which is more accurate and computationally more efficient. C3D8R is eliminated due to its high vulnerability to specific numerical problem called hourglassing. As for the remaining two element types: accuracy of C3D8I is found as sensitive to distortion compared to C3D20R. On the other hand, C3D20R is computationally more expensive then C3D8I. In the end, due to its reliability on yielding acceptable accuracy C3D20R element type is utilized in all 3D analyses of this study. Trapezoidal distortions in mesh designs of 3D analyses have made the major contribution in elimination of C3D8I element type.

3.3.2.1 Element Formulation and Integration

Element types could be grouped according to order of shape function as linear or quadratic, and according to order of integration as reduced or fully integrated. In this study both linear and quadratic elements, with reduced and full integration scheme are evaluated for their adequateness to be employed in analyses.

Order of Element

First order elements utilize linear shape functions, whereas second order elements utilize quadratic shape functions. In order to use second order (quadratic) shape functions, quadratic elements have higher number of nodes than first order elements. In general, second order elements could more accurately approximate the displacements within the element than first order elements. Moreover quadratic elements are more resilient to numerical difficulties discussed in Section 3.3.2.4.

Order of Integration

As mentioned in Section 3.4 internal work done according to nodal displacements is computed via stiffness matrix. Stiffness matrix is obtained by a procedure which involves integration of shape function of elements. This integral could be computed by a numerical integration method called Gauss Quadrature. Gauss Quadrature can find the exact solution for an integral of any polynomial function with degree of $2n - 1$, if the value of this function is available for at least n number of special points within the integral limits. If the value of the function is available only for less data points than n, Gauss Quadrature can still be employed, however it yields an estimate for the integral but not the exact result. Similarly if the data points are not at locations requested by Gauss Quadrature, but at close locations, Gauss quadrature can still be employed, however it again yields an estimate.

According to Abaqus Documentation (2010), fully integrated elements have sufficient number of Gauss points required to integrate the polynomial terms in an element's stiffness matrix exactly, when the element has a regular shape. Reduced integration elements on the other hand have one fewer number of integration points in each direction compared to fully integrated elements. Therefore for fully integrated elements integral used for computing stiffness matrix is exact if element has regular shape, whereas for reduced integration elements stiffness matrix

has error due to integration.

As an example to number of integration points; fully integrated quadrilateral elements use 3 integration points in each direction, whereas reduced integration quadrilateral elements use 2 integration points. Locations of nodes and integration points of linear and quadratic two dimensional elements for both reduced and full integration schemes are shown in Figure 3.3. In this figure integration points are shown with cross symbols, whereas element nodes are symbolized with filled circles.

It is stressed at Abaqus Documentation (2010) that for fully integrated elements integral is only exact for elements having regular shape. The term regular shape means the edges are straight and meet at right angles and that any edge nodes are at the midpoint of the edge. Therefore in general, in addition to the errors due approximation of the displacements within elements according to the displacements of nodes, an error due to integration of these approximated quantities are introduced as well.

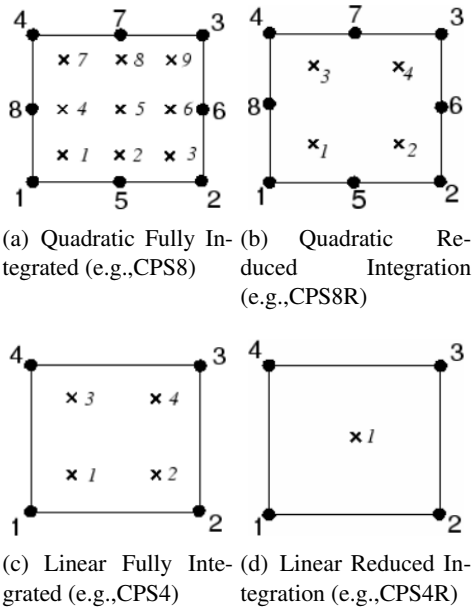

(a) Quadratic Fully Integrated (e.g.,CPS8)

(b) Quadratic Reduced Integration (e.g.,CPS8R)

(c) Linear Fully Integrated (e.g.,CPS4)

(d) Linear Reduced Integration (e.g.,CPS4R)

Figure 3.3: Integration Points at 2D Elements (Abaqus Documentation, 2010)

3.3.2.2 Accuracy of Elements

In order to assess the accuracy of element types, following verification study is conducted.

A linear elastic beam, under cantilever support condition with a point load acting at its free tip, is taken as the analysis subject (Figure 3.4). Verification study is selected as the comparison of deflection of the loading point in the loading direction with the analytical exact solution. This verification study is also reported in Abaqus Documentation (2010).

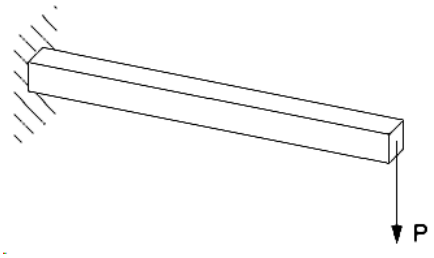

Figure 3.4: Cantilever beam under a point load P at its free end (Abaqus Documentation, 2010)

Equation 3.8 is the precise solution for the vertical displacement at the tip of the beam for an applied load P. In this equation L is the length, E is the Young's modulus and I is the moment of inertia of the beam.

$$\delta_{tip} = \frac{PL^3}{3EI} \tag{3.8}$$

Elastic parameters are selected as, elasticity modulus E = 70GPa, Poisson's ratio ν = 0.0. Dimensions of the beam are selected as 150mm long, 2.5mm wide and 5mm deep. Magnitude of the point load at free end is selected as 5N. Hence, exact solution for vertical deflection of the free tip is found as 3.086mm from Equation 3.8.

Meshes used in element verification analyses are presented in Figure 3.5. Point load acting at the free tip of the beam is applied as 4 point loads with magnitudes P/4 each applied at the four corners of face of the free tip in the model. Hence resultant force would be at the centroid of the face with magnitude of P.

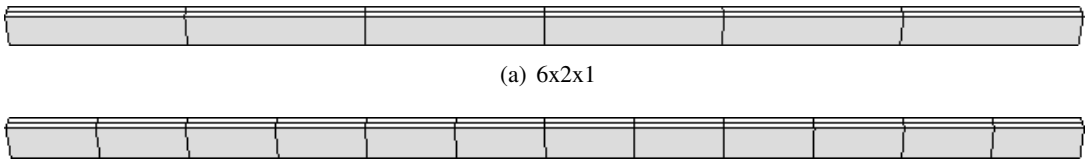

(a) 6x2x1

(b) 12x2x1

Figure 3.5: Meshes used in element verification analyses

Two meshes with different element counts are utilized for each element type in order to see the degree of improvement in solution accuracy with increasing element count. These meshes are presented in Figure 3.5 and are named as 6x2x1, 12x2x1. Naming convention is based on the number of elements through the length, width and height of the beam. For example in 12x2x1 mesh, beam is modeled with 24 elements in such a way that, length of the beam is divided into 12 elements, width of the beam is divided into 2 element and height of the beam is represented by 1 element.

Table 3.1: Error in Analyses Compared to Analytical Solution

Mesh Type	**C3D8R**	**C3D8I**	**C3D20R**	**C3D20**
6x2x1	6922%	0.65%	0.03%	0.45%
12x2x1	6958%	0.13%	0.03%	0.03%

Table 3.1 shows the error level of analyses results with respect to the exact solution for each element and mesh type. Based on the results in this table, it is seen that all elements except C3D8R yields results with less than 1% error. Error in C3D8R elements which is well beyond usable limits is due to the numerical problem called hourglassing effect discussed in Section 3.3.2.4. Closest result to the solution is obtained from analyses utilizing C3D20R elements with error less than 0.1%.

For all mesh types the order of elements yielding closest result to the precise solution does not change. This order, from most accurate to least accurate, is C3D20R - C3D20 - C3D8I - C3D8R. The order of element types from most expensive to the cheapest, from computational cost point of view, is reported by Abaqus Documentation (2010) as C3D20 - C3D20R - C3D8I - C3D8R. Note that although C3D20R is computationally cheaper than C3D20, it provides

better accuracy.

3.3.2.3 Sensitivity of Elements to Distortion

All cases considered up to this point had regular shapes with corner angles of 90°. In this section sensitivity of elements to distortion is investigated by meshing the beam with elements having parallel and trapezoidal distortion with 45° internal corner angle (Figure 3.6). For the investigation 6x2x1 mesh utilized in previous section is employed.

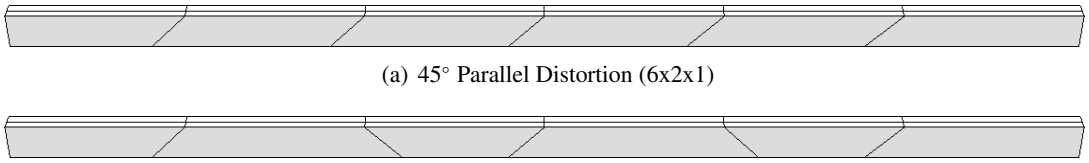

(a) 45° Parallel Distortion (6x2x1)

(b) 45° Trapezoidal Distortion (6x2x1)

Figure 3.6: Meshes used in element verification analyses for distortion vulnerability

Table 3.2: Error in Analyses Compared to Analytical Solution

Element Distortion Type	**C3D8R**	**C3D8I**	**C3D20R**	**C3D20**
45° Parallelogram	226%	33.00%	0.39%	2.11%
45° Trapezoidal	168%	94.65%	2.82%	9.38%

Table 3.2 presents the error level of analysis results with respect to the exact solution for each element and distortion type. It is seen that distortion of elements has significantly unfavorable effect on the accuracy. Among distortion types, trapezoidal distortion causes the highest damage to the accuracy. Most resilient element type to distortion is found as C3D20R, whereas C3D8I is found as the least tolerant. It is notable that although C3D20 element type is more expensive than C3D20R element type, C3D20R performed considerably better.

Seemingly favorable effect of distortion to solution accuracy in analyses with C3D8R elements is because, in previous cases, this element type has suffered from a finite element method instability called hourglassing effect. Distortion introduced in this section has relaxed this numerical problem specifically for the applied loading direction. However this does not

necessarily mean that using deformed C3D8R elements would always yield more accurate results.

3.3.2.4 Numerical Problems Related to Element Types

Numerical problems of elements develop when displacement of the integration points of the elements does not adequately represent the nodal displacements and overall behavior of the element. In this section two major numerical problems, hourglassing and shear locking effects are discussed.

Based on explanations in this section, for quadrilateral and hexahedral elements, it is seen that, linear reduced integration elements are susceptible to hourglassing effect, whereas linear fully integrated elements are vulnerable to shear locking effects. In the end, quadratic elements are found out as resilient to these problems with a note that, although quadratic reduced integration elements can suffer from hourglassing effect in theory, in practice they are considered as resilient to numerical problems by Abaqus Documentation (2010).

Hourglassing Effect

Linear reduced integration elements are vulnerable to this numerical problem which results in unrealistic flexible response of the body under given loads.

Consider a linear, reduced integration element whose integration point and nodes are shown in Figure 3.3(d). Note that this element has only one integration point, which is at the centroid of the element. If this element is subjected to a bending moment M, deformed element shape would be as shown in Figure 3.7.

Figure 3.7: Deformation of a linear reduced integration element subjected to bending moment (Abaqus Documentation, 2010)

As depicted by the dashed visualization lines, location of integration point does not change; hence displacement is zero at that point. Consequently stresses and strains due to bending moment M is zero at the integration point. Since this element has only one integration point,

sum of strain energy within the element due to this deformation would be zero, which is obviously incorrect. Therefore even though the element deforms significantly under the given load, strain energy that is represented with K U term in Equation 3.3 would be zero. Hence the element can not resist these deformations and overall response of the mesh would be an implausibly flexible behavior.

Shear Locking Effect

Linear, fully integrated elements are vulnerable to this numerical problem, the result of which is unrealistic stiff response of the body under given loads.

Consider a linear, fully integrated element whose integration points and nodes are shown in Figure 3.3(c). If this element is subjected to a bending moment M, deformed element shape would be as shown in Figure 3.8.

Figure 3.8: Deformation of a linear fully integrated element subjected to bending moment (Abaqus Documentation, 2010)

As depicted by the dashed visualization lines, horizontal displacements at the location of integration points are as follows. Integration points lying at the tension zone of the element moves further away from each other, indicating tensile behavior with positive σ_{11}, whereas in compression zone the opposite is observed, resulting in negative σ_{11}. As for vertical displacements of integration points, considering small deformations, vertical displacements are zero. These displacements and stresses are in accord with physical phenomena. What should be noticed is the inclination of the originally vertical visualization lines. This indicates shear stresses (σ_{12}) at integration points. This is incorrect, since shear stress is zero under constant moment. This spurious shear stresses results in an extra internal strain energy, which gives additional stiffness against applied loading. Hence the overall response of the mesh would be an implausibly stiff behavior.

3.3.3 Rigid Body Modeling Capability

There are two types of rigid body definitions available in Abaqus. One of them is the analytical rigid body the other is the discrete rigid body. For analytical rigid bodies a reference node must be selected on the part. All loading and boundary conditions must be applied to that reference node only. Surfaces can be defined on the analytical rigid body for its interaction with other parts in the assembly. In the solution process rigid body movement of the analytical rigid part is computed based on the movement of the reference point. One advantage of using analytical rigid body could be its surface accuracy and computation efficiency since it is not meshed. Disadvantage of using analytical rigid body is that loading can only be applied to a single point.

Other rigid body type is the discrete rigid body. Discrete rigid bodies should be meshed. A rigid element type suitable for the analysis is assigned to the rigid body mesh. A reference node must also be selected for discrete rigid bodies and all boundary conditions should be assigned to this node. However unlike analytical rigid bodies, loading could be applied to any node of the discrete rigid body.

This feature is important for horizontal loading cases of this study since there are two loading points on the models. One is center of gravity point where the weight of the model is applied as point load and the other is the loading point where horizontal loading is applied as displacement. Therefore in this study discrete rigid body type is selected for the modeling of foundations of horizontal loading experiments.

3.3.4 Contact Interactions

In a finite element analysis, contact conditions are a special class of discontinuous constraint, allowing forces to be transmitted from one part of the model to another. The constraint is discontinuous because it is applied only when the two surfaces are in contact. When the two surfaces are separate, no constraint is applied. The analysis has to be able to detect when two surfaces are in contact and apply the contact constraints accordingly. Similarly, the analysis must be able to detect when two surfaces separate and remove the contact constraints.

Abaqus provides two distinct approaches for modeling contact interactions: contact pairs and

contact elements. If possible, Abaqus manual recommends use of contact pairs approach. Therefore contact pairs approach is utilized and explained in this study.

In contact pairs approach, surfaces of the bodies that may contact during analysis must be defined as master and slave surfaces. Significance of master slave assignment is that, displacement of the nodes in slave surface depends on the displacement of the master surface.

According to Abaqus Documentation (2010), in reality contact pairs approach also utilizes contact elements, however these elements are not accessible to the user. Abaqus automatically covers the slave surface with this family of contact element types, which construct a measure of overclosure (penetration of the point on the surface of the deforming body into the rigid surface) and means of relative shear sliding.

3.3.4.1 Mechanical Contact Properties

Pressure overclosure relationship and frictional behavior are defined under mechanical contact properties.

Default contact pressure overclosure relationship used in Abaqus is named as ”hard contact” and it implies that; surfaces do not transmit contact pressure if they are not contacting, penetration of master surface into slave surface is not allowed, and there is no limit to the magnitude of contact pressure that could be transmitted between surfaces.

There are other pressure overclosure relationships available in Abaqus, such as softened contact relationship in which the contact pressure is a linear function of the clearance between surfaces. In this study hard contact relationship is utilized.

There are multiple friction formulations available in Abaqus. In this study penalty friction formulation is utilized. Other main friction formulations include rough behavior, and frictionless behavior. Frictionless behavior is the default formulation. For rough behavior, no slip is allowed between surfaces as long as they are in contact.

Penalty friction formulation could be utilized with different parameters. For example, friction coefficient could depend on slip rate and contact pressure, or constant shear stress limit could be utilized. This is possible since Abaqus has an extended version of the classical isotropic Coulomb friction model as explained Abaqus Documentation (2010). In Figure 3.9 slip re-

gions for the coulomb friction model with constant friction coefficient, which is the friction model utilized in this study, is shown.

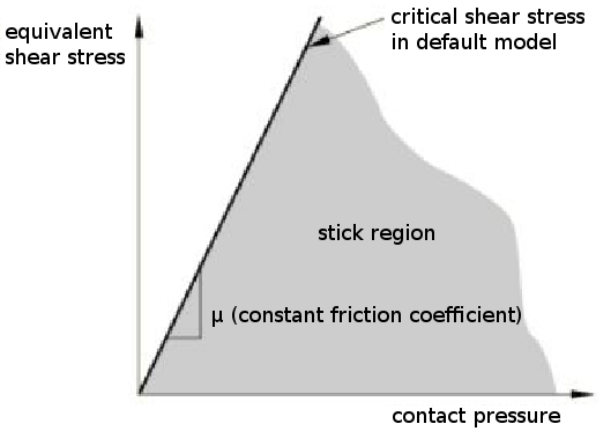

Figure 3.9: Slip regions for the basic Coulomb friction model (Abaqus Documentation, 2010)

Since penalty method is an approximate method as mentioned in Section 3.3.4.4, incremental slip may occur between surfaces even though the friction model determines that the current frictional state is sticking. Figure 3.10 demonstrates this behavior, where κ is the sticking stiffness. Magnitude of the elastic slip could be adjusted, however according to Abaqus Documentation (2010) convergence problems may occur if the elastic slip is chosen very small.

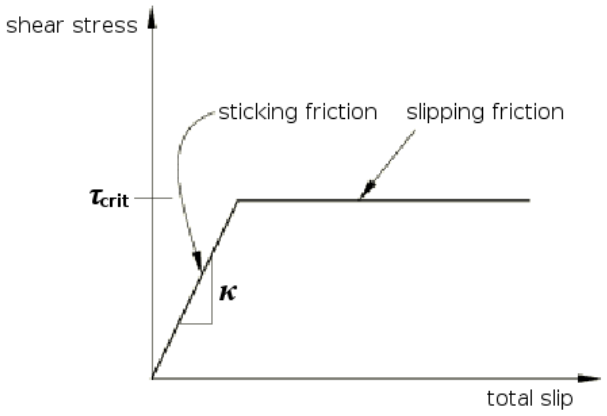

Figure 3.10: Elastic slip versus shear traction relationship for sticking and slipping friction (Abaqus Documentation, 2010)

3.3.4.2 Contact Surface Discretization

Surface discretization defines the locations where the contact constraints are enforced. Such as at individual slave nodes or over regions defined arbitrarily at proximity of slave nodes.

There are two allowed contact discretizations in Abaqus, namely ”node to surface” and ”surface to surface”. In node to surface discretization, slave surface is the set of finite element nodes corresponding to that surface. Displacement of each of these nodes is computed according to the projection of the node on the master surface. Therefore displacement of each slave node depends on average of displacements of a number of master nodes.

Other contact discretization approach is the surface to surface discretization. If this discretization is utilized, contact conditions are enforced in an average sense over regions nearby slave nodes rather than only at individual slave nodes. The averaging regions are approximately centered on slave nodes, so each contact constraint will predominantly consider one slave node but will also consider adjacent slave nodes.

Node to surface discretization simply resists penetrations of slave nodes into the master surface, hence forces tend to concentrate at these slave nodes. This concentration leads to spikes and valleys in the distribution of pressure across the surface; whereas surface to surface discretization resists penetrations in an average sense over finite regions of the slave surface, which has a smoothing effect. Therefore, in general, surface to surface discretization provides more accurate stress results. On the other hand, in surface to surface discretization, penetration of master surface into the slave surface could be observed at a number of nodes, since contact conditions are enforced on slave nodes in an average sense.

According to Abaqus Documentation (2010), calculation cost of both approaches could be considered as same for most applications. Although surface to surface discretization generally involves more nodes per constraint and can therefore increase solution cost.

3.3.4.3 Contact Tracking Approaches

There are two tracking approaches to account for the relative motion of two interacting surfaces in mechanical contact simulations. Namely, finite sliding and small sliding approaches.

For small sliding approach, coupling of slave nodes with their projections on master surface is calculated at the beginning of the analysis and does not change throughout the analysis, whereas for finite sliding approach, this coupling is checked and recalculated throughout the analysis.

Therefore, if small sliding approach is utilized and significant relative tangential motion of the surfaces occurred, than the vertical contact pressure would still act on the nodes of the slave surface which were originally in contact with the master surface whether or not they are still in contact.

3.3.4.4 Contact Enforcement Methods

Contact enforcement method defines how the boundary conditions originating from contact interactions are resolved into the numerical operations of the finite element method. There are three contact enforcement methods in Abaqus. Namely, direct method, penalty method and augmented Lagrange method. Augmented Lagrange method, which is an approximate implementation, is not considered in this study.

Direct method strictly enforces a given pressure-overclosure behavior for each constraint without approximation. According to Abaqus Documentation (2010), because of its strict interpretation of contact constraints, hard contact simulations utilizing the direct enforcement method are susceptible to overconstraint issues, which is a numerical difficulty.

The penalty method approximates hard pressure-overclosure behavior likewise the penalty method remarked in Section 3.2. With this method the contact force is proportional to the penetration distance, so some degree of penetration of master surface into slave surface will occur. Numerical softening associated with the penalty method can mitigate overconstraint issues and reduce the number of iterations required in an analysis. Penalty stiffness could be defined as a constant or as a function depending on the penetration distance. Former is called linear penalty method. In this study linear penalty method is utilized as contact enforcement method, both for frictional and pressure versus overclosure contact behaviors since it is the default method for finite sliding surface to surface contact formulation in Abaqus.

3.3.5 Automatic Stabilization Mechanism

Automatic stabilization is employed for stabilizing instable quasi-static analyses. Instabilities may be of a geometrical nature, such as buckling, or of a material nature, such as material softening. By automatic stabilization, extreme displacements computed during a step are decreased by adding artificial stiffness for the problematic region of the model. This is achieved by modifying the Equation 3.3 as in Equation 3.9 by including artificial stiffness to the problematic nodes where extreme displacements are computed.

$$KU + F_v = P \tag{3.9}$$

Effect of automatic stabilization occurs when the displacement per load increment size computed is very high for any node in the model. In this case the displacement velocity (v) computed for that particular node according to Equation 3.10 increases. In this equation Δu is the displacement of the node in the increment, and Δt is the increment size. And the increase in v results in an increase in the viscous force to be applied to that node F_v, which is calculated according to Equation 3.11. In that equation c is damping factor, M^* is artificial mass matrix computed via unit density of the material.

Finally, since the F_v is subtracted from load vector (P) as shown in Equation 3.9, and effect of automatic stabilization would be an extra (artificial) resistance to displacement for that particular node.

$$v = \frac{\Delta u}{\Delta t} \tag{3.10}$$

$$F_v = cM^*v \tag{3.11}$$

Risk of this technique is that, if the artificial stiffness computed is higher than a suitable value, this procedure can decrease the accuracy of the solution by resulting in overly stiff behavior, thus yielding unrealistically high loads and / or implausibly low displacements. Note that the undesired effect of this technique is on yielding higher load resistances. Effect of automatic stabilization is investigated in Section 3.6.1.

In adaptive automatic stabilization scheme, damping factor (c) computed at the first increment

of the step is modified spatially and with time. Modification depends on the convergence history of the step. If convergence behavior is problematic because of instabilities, damping factor is automatically increased. For example, damping factor may increase if an analysis takes extra equilibrium iteration per increment, or requires time increment cutbacks. On the other hand, damping factor may be reduced if instabilities subside.

In order to limit the artificial stiffness brought, the ratio of the energy dissipated by viscous damping to the total strain energy is defined by the user as a maximum limit.

3.4 General Layout of Finite Element Method Analyses

In order to see the effect of plane strain assumption, both 2D and 3D analyses are conducted. In this section modeling and solution control details of all finite element analyses of test cases are explained.

3.4.1 3D Monotonic Vertical Loading Analyses

Due to symmetry 1/4 of the problem is modeled in order to increase the computational efficiency.

3.4.1.1 Mesh and Element Selection

Dimensions of the soil continuum are selected as 2 m width x 2 m length x 2 m depth. Note that, these are the dimensions of the quarter of the actual problem. Therefore, the actual problem modeled would have the dimensions of 4 m width x 4 m length x 2 m depth. It is aimed to employ the dimensions of the soil tank utilized in experiments by Fukui et al. (2005). Selected mesh boundaries are 1 m wider than the boundaries of the modeled soil tank, which had 4 m width x 3 m length. This modification of boundary size is done, in order to have better sized elements by symmetry, which have internal face corner angles closer to 90 degrees. Depth of the soil layer varied among experiment cases, according to the relative density of the test medium as 2 m and 3 m as mentioned in Section 2.1. Same mesh is employed for both cases Case 1 and Case 2, hence, selected mesh boundary dimensions are 1 m shallower than soil tank boundaries of the experiment case Case 1. Results of two-dimensional analyses

conducted for Case 1, employing material parameters presented in Table 4.1, with meshes of 2 m and 3 m depth, yielded ultimate bearing capacities of 568.2 kPa and 567.6 kPa, respectively. Difference between these results was less than 0.12%, which is considered as negligible.

Mesh design is important for computational efficiency and solution accuracy. It is required to have a mesh which yields most accurate solution for least number of elements. In this study, among many factors, attention is paid to two main factors in mesh selection. First, more elements should be placed where there are rapid changes in stresses and strains, which corresponds to rapid changes in directions of movement (Potts and Zdravkovic, 2001). Second, a mesh of regular shaped elements will give the best result; therefore elements with widely distorted geometries should be avoided (Potts and Zdravkovic, 1999).

Mesh and element type of 3D FEM analysis of monotonic vertical loading cases are based on the study by Zhu and Michalowski (2005). Efficiency of this mesh design is verified with an analysis by comparing it with another design composed of more regular shaped elements. Both meshes were utilizing C3D20R elements and are shown in Figure 3.11. It is seen that mesh design utilized by Zhu and Michalowski (2005) with 725 elements yields practically the same results with a mesh design utilizing 2520 elements for a bearing capacity analysis. It should be noted that both of the analyses were preliminary analyses and according to further mesh refinements it was seen that both meshes were not adequate to achieve required accuracy. Nevertheless considering the mesh used in the analyses in this study, shown in Figure 3.13(b) is composed of 1036 elements which is considerably less than 2520 elements, it could be seen that mesh used by Zhu and Michalowski (2005) is both efficient and accurate compared to the other mesh design which has more regular element shapes.

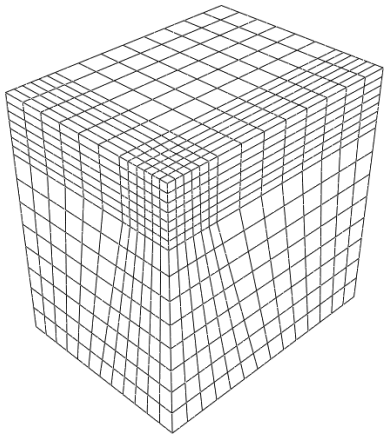

(a) Mesh with 2520 Elements

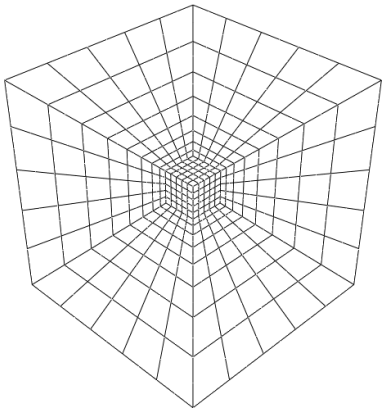

(b) Mesh with 725 Elements

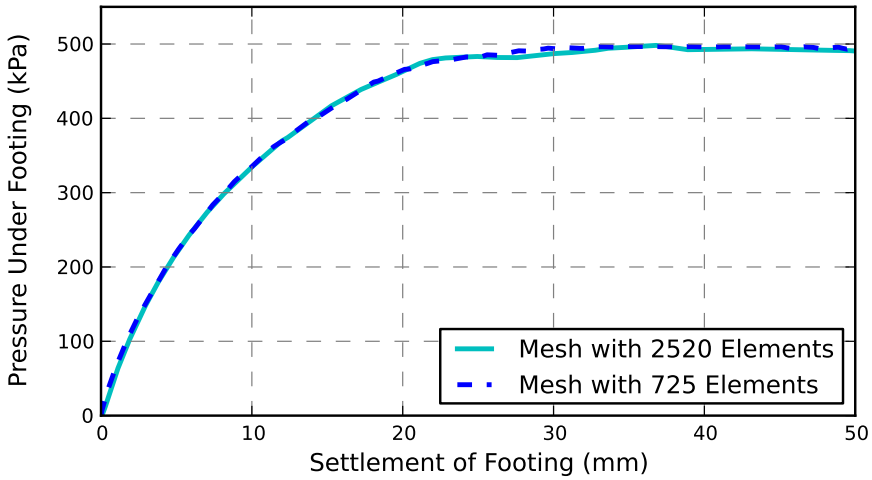

(c) Comparison of Pressure - Displacement Curves

Figure 3.11: Comparison of results of different mesh designs

It is worth to note that advantage of the mesh design utilized by Zhu and Michalowski (2005) is that, areas which are out of interest could be meshed with very little number of elements compared to other mesh types, and number of elements is independent of problem size if any value of aspect ratio and edge size is suitable. Moreover Potts and Zdravkovic (1999) has also shown this type of mesh for 2D as a good mesh example as shown in Figure 3.12. Disadvantage of this mesh design is that most elements have trapezoidal shapes from the beginning. This is not preferable as shown in Section 3.3.2.3. However by increasing the number of elements, angles between the edges of elements close to foundation area can be set as close to ideal as desired. Nonetheless this type of meshing would not be preferable for elements, such as incompatible mode elements (C3D8I), that are too sensitive to distortion as shown in Section 3.3.2.3. Hence C3D20R elements are used in analyses, especially for its tolerance to distortion and resistance to numerical problems as discussed in Section 3.3.2.4.

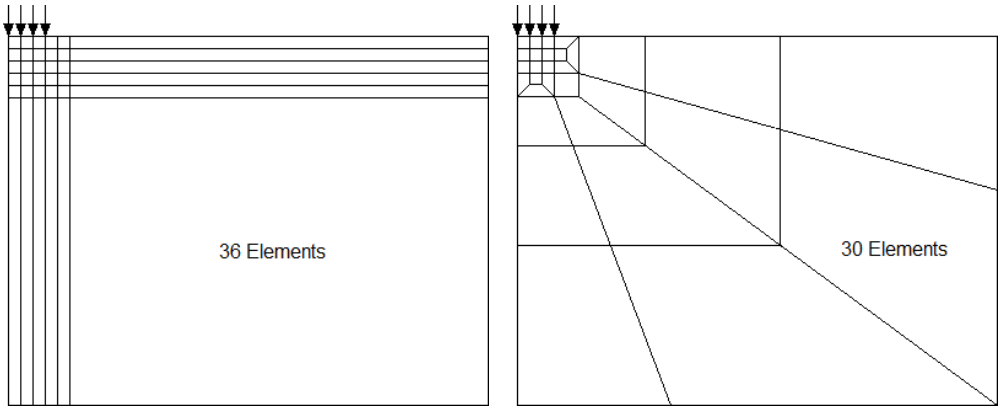

(a) Ill-conditioned mesh (b) Well conditioned mesh

Figure 3.12: Examples of good and bad meshes after Potts and Zdravkovic (2001)

Boundary conditions do not allow normal displacements on the boundaries of the model, but allow tangential displacements. Loukidis and Salgado (2009) states that based on preliminary analyses, fixing both degrees of freedom or fixing only the horizontal one at the lateral boundary nodes does not affect the resulting collapse load as long as the lateral boundaries are placed far enough from the developing collapse mechanism. Base of the model does not allow either tangential or normal displacements. Planes of symmetry are constrained with symmetric boundary conditions which only restrain normal displacement. These conditions are in accord with the study by Zhu and Michalowski (2005).

Two different meshes are used in bearing capacity analyses, these meshes are shown in Figure 3.13. For associated flow rule conditions coarse mesh, composed of 1036 elements is used, whereas for unassociated flow rule conditions fine mesh, composed of 8640 elements is used. Using the coarse mesh in analyses utilizing unassociated flow rule, results in very small increment sizes.

This observation might be explained by a comment from Abaqus Documentation (2010). ”In plasticity applications as the solution approaches the limit load, discontinuities occur in the solution such as slip lines. In order to reasonably model the discontinuities in the gradient field of the solution, locations at which discontinuities could be modeled should be plenty. These locations are the element edges.”

From this comment it is understood that, the finer the mesh, the better the discontinuities are modeled. In general, refining the mesh increases the solution accuracy since as the element size gets smaller, errors due to strain approximation within the element decreases. However for this specific case, aim is to increase the surface area of the elements so that discontinuities such as slip could be better modeled. Slip could be modeled at element surfaces such that nodes of the top surface of an element moves in an opposite direction to the nodes at bottom surface of the element.

In this context, Abaqus Documentation (2010) continues and advises to use first order elements, since for a given number of nodes these elements provide the most locations at which some component of the gradient of the solution can be discontinuous.

As an explanation to this comment, note that in first order three dimensional elements there are 4 nodes per element face, whereas in second order elements there are 8 nodes per element face. Second order elements are computationally more expensive. Therefore this comment could be considered as an advice from computational efficiency point of view.

Abaqus Documentation (2010) adds that incompatible mode elements, which are fully integrated first order elements that have been enhanced by incompatible modes to improve the bending behavior to eliminate the parasitic shear stresses that causes locking instability, are able to represent strain localizations such as the ones occur in shear bands. Comment ends with a warning that defining shear localization better increases the strain magnitude, therefore tends to increase the number of increment and iterations required for the analysis.

Based on the advices of Abaqus Documentation (2010) it could be concluded that manual advises the use of incompatible mode elements for plasticity limit analyses. Reason of this might be that, these elements, as being first order elements, are computationally cheaper than all second order elements and do not have the finite element instabilities of shear and volumetric locking, to which first order elements are vulnerable.

In the end, choice of not using first order elements may have inversely affected the computational efficiency of the analyses particularly for unassociated bearing capacity solutions. Nonetheless these comments and advices do not imply that analyses using a fine mesh of second order elements might not be suitable from solution accuracy point of view.

Employment of second order elements in analyses employing unassociated flow rule could be supported by the studies by Loukidis and Salgado (2009) and Loukidis et al. (2008) which favored employment of second order elements. Difference of these studies from this study should be noted that these studies were employing triangular elements with plane strain assumption. Loukidis et al. (2008) commented that triangular elements provides flexibility in element arrangement and size. Study of plastic limit loads of shallow foundations lying on cohesionless soils that obey Mohr Coulomb yield criterion is common among the studies. Loukidis and Salgado (2009) utilized second order elements for finite element analyses of ultimate bearing capacity of foundation subjected to vertical load without eccentricity or inclination, where dilation angles were chosen to model unassociated flow rule. Loukidis et al. (2008) studied foundation subjected to combined loading by considering eccentricity and inclination of the foundation load. They commented that use of second order elements provided superior numerical performance than first order elements for analyses employing unassociated flow rule, due to better performance of second order elements in intense strain localization. They utilized coarser mesh with second order elements for analyses with unassociated flow rule, and finer mesh composed of first order elements for associated flow rule. They added that selection of first order or second order elements does not affect the analysis results when associated flow rule is employed.

In order to ensure that selected meshes are adequately fine, a mesh convergence study is conducted. For this purpose mesh shown in Figure 3.13(b) is compared with a finer mesh shown in Figure 3.13(a). For Case 2 analysis with material parameters of $\phi = 39.9°$, $\psi = 30°$, and c = 0.1 kPa, ultimate bearing capacity obtained from selected mesh and convergence

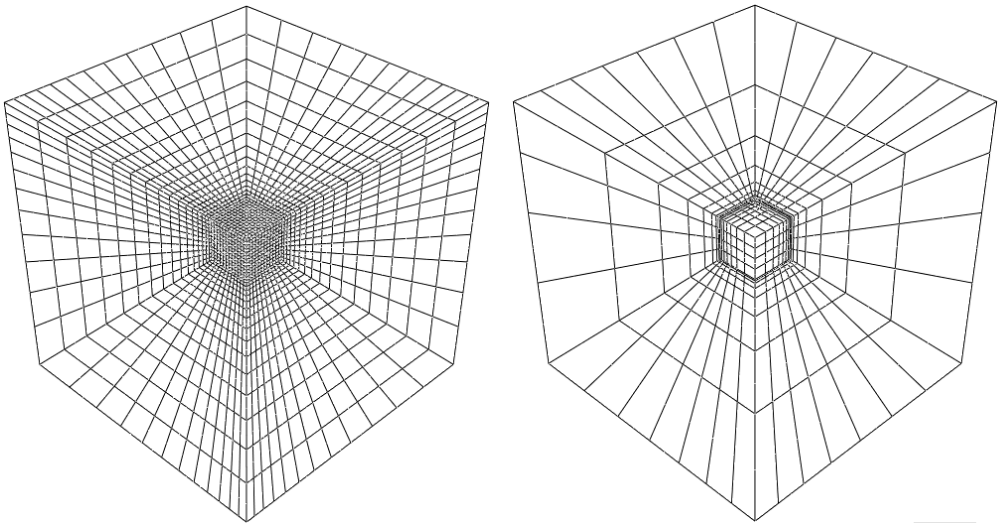

(a) Fine (b) Coarse

Figure 3.13: Meshes used in 3D monotonic vertical loading analyses

study mesh are 480.64 kPa and 478.40 kPa respectively. There is 0.47% difference between results. This level of difference is considered as acceptable.

3.4.1.2 Application of Loads

Analyses are performed under displacement control. Foundation is modeled as rough and rigid with uniform downward displacement at the nodal points applied at the element nodes which lie immediately beneath the footing. Rough footing is modeled by not allowing horizontal displacements for these nodes. Modeling rough and rigid foundation in this manner is both consistent with Zhu and Michalowski (2005) and Potts and Zdravkovic (2001).

3.4.1.3 Analysis Procedure

Each analysis consists of 2 main steps.

1. Calculation of free-field stresses: This step simulates stress distribution in the free field. (ie. before foundation placement). In this step, gravity loading is applied to the elements modeling the soil medium according to the defined soil density, and then the initial conditions for the lateral pressures are enforced according to the defined lateral earth pressure at rest

coefficient (Ko). In this thesis lateral earth pressure at rest coefficient is computed according to Jaky's (1948) formula.

2. Application of foundation load: Vertical displacement modeling the foundation load is applied at this step. A maximum value of 50 mm of vertical displacement is found to be appropriate to reach the limit load for the modeled cases.

3.4.1.4 Output Requests and Evaluation of Results

Vertical components of reaction forces, and vertical displacements at the nodes which lie directly below the foundation are recorded for each increment throughout the analysis. Bearing pressure is calculated as the sum of the vertical components of the reaction forces at the nodal points where the vertical displacement is applied divided by the foundation area. Settlement of the foundation is computed from the vertical displacement of these nodes. Unlike Zhu and Michalowski (2005) study, sizes of the neighboring elements are not considered in the area of foundation in calculation of the bearing pressure.

At the end of free-field stress calculation stage, although very small compared to given foundation displacement at the foundation load step, vertical displacements occur throughout the soil medium. These unwanted displacements at nodes directly under the foundation are deducted from the total displacements of the foundation load application step.

3.4.1.5 Solution Strategy and Control Parameters

In this section solution control parameters, increment size selection, solution technique are explained. These parameters are selected both for increasing the computational efficiency of the analyses, and avoiding convergence difficulties.

Increment Size Selection

Automatic increment size selection algorithm is employed. Maximum number of allowed increments is selected as 1 million, in order to have practically unlimited number of increments. Initial increment size is set as 0.01%, which is observed to be a suitable initial increment size. Minimum increment size is selected among $1x10^{-6}$%, $1x10^{-7}$% and $1x10^{-10}$% depending on the convergence behavior. Among the calculation parameters, minimum increment size pa-

rameter is defined as the limiting parameter that decides whether the analysis will continue or terminate. Selection of a large value for this parameter may result in early termination of the analysis; however, selection of a very small value may result in continuation of analysis with very small increment sizes. Since automatic stabilization effect is increased by the algorithm as minimum increment size is approached.

Maximum increment size is set as 1% to obtain smooth displacement versus pressure graphs and prohibit algorithm from selecting high increment sizes and subsequently have convergence problems and waste of processor time.

Solution Control Parameters

Only calculation parameters of the foundation load step are modified from their default values.

If automatic increment size selection algorithm decides that the selected increment size is too large, increment is terminated by identifying it as unconverged and another attempt is made with a smaller increment size starting from the last successful increment. Basically an increment size is considered as too large, if the increment could not converge to a solution within allowable number of iterations. However Abaqus also utilizes another set of rules which may identify the increment as diverging and terminate it before reaching the maximum allowed number of iterations. One such rule is the increase of residuals in 2 subsequent iterations. However as stated by Abaqus Documentation (2010) this and similar convergence rate checks may not be appropriate for some material models and could be deactivated by modifying time incrementation parameters I_O and I_R that define the number of increments after these checks are started. By assigning very high values (such as $1x10^{10}$) to these parameters those checks are disabled.

Increment size selection algorithm decides that an analysis should terminate after a certain number of subsequent increment size degradations. This certain number is defined by I_A parameter and default value of it is 5. Based on observation this value is found as too small, therefore I_A parameter, which controls the maximum number of successive unconverged attempts within a step is set to 100. Therefore early termination of analyses due to this parameter is avoided.

Line search algorithm is activated by specifying maximum number of searches as 10 and error contingency for line search as 0.01. According to Abaqus Documentation (2010) pur-

pose of the line search is to improve the robustness of the Newton or quasi-Newton methods. This algorithm helps to prevent divergence in strongly nonlinear problems, and increases the efficiency of problems involving high coefficient of friction, since by automatic step size selection algorithm smaller the number of unconverged cases, larger the step size. Since test medium has high internal friction angles, line search algorithm is employed.

Moreover automatic stabilization is activated since it is observed to help solving the convergence difficulties. Automatic stabilization method is chosen to be applied by specifying dissipated energy fraction as 0.0002 and using adaptive stabilization with maximum ratio to stabilization to strain energy as 0.01. Default value for maximum ratio to stabilization energy to strain energy was 0.05, however using this value resulted in decrease of solution accuracy as elaborated in Section 3.6.1.

Solution Technique

Full Newton solution technique is used as it performed better than Quasi-Newton method. Quasi-Newton method might have been utilized if only recalculation of stiffness matrix could have been avoided throughout the analyses. This technique was utilized by Loukidis and Salgado (2009) in order not to suffer from numerical difficulties in analyses using strongly non-associated flow rule. Unable to follow this technique, numerical difficulties are avoided by utilizing automatic stabilization method with Full Newton solution technique in this study.

Unsymmetrical matrix storage is selected based on advice in Abaqus Documentation (2010) for analyses using Mohr-Coulomb yield criterion, as it increases analysis speed. Direct equation solver is utilized as iterative equation solver is feasible for models composed of higher number of elements.

3.4.2 2D Monotonic Vertical Loading Analyses

These analyses, utilizing plane strain assumption, are conducted with an aim to compare with 3D analyses in order to assess the effect of plane strain assumption on analyses results. Therefore 2D analyses are conducted with same modeling preferences as 3D analyses, which are described in Section 3.4.1, except mesh, element type and output evaluation procedures, to which modifications were inevitable due to change in modeling dimension.

Due to symmetry 1/2 of the problem is modeled to increase the computational efficiency. For this purpose half of the foundation breadth is modeled.

3.4.2.1 Mesh and Element Selection

Dimensions of the soil model are selected as 4 m wide x 1.5 m long x 2 m deep. Note that these are the dimensions of the half of the actual problem. Therefore the actual problem modeled would be 3 m wide x 2 m deep. This is 1 m shallower than the boundaries of the soil tank modeled, which was 4 m long x 3 m wide x 2 m deep. This modification is done in order to be consistent with the 3D bearing capacity analyses presented in Section 3.4.1.1.

Although mesh design is important for computational efficiency and solution accuracy, since 2D analyses are computationally cheaper than 3D analyses, greater tolerance to increase in number of elements are given in order to have better proportioned elements. Mesh used in analyses, composed of 1432 elements, and are shown in Figure 3.14(a). Element type is selected as CPE8R which is a second order reduced integration element for plane strain analyses, analoguos to C3D20R for 3D analyses.

In order to ensure that selected mesh shown in Figure 3.14(a) is adequately fine, a mesh convergence study is conducted. For this purpose an analysis to be used as a mesh convergence study is conducted with a finer mesh, which is presented in Figure 3.14(b). Monotonic vertical loading analysis with material parameters of $\phi = 39.9°$, $\psi = 37°$, and c = 0.1kPa is conducted. Ultimate bearing capacities obtained from the selected convergence study meshes are 358.36kPa and 352.82kPa respectively. There is 1.57% difference between the results. This level of difference is considered as acceptable.

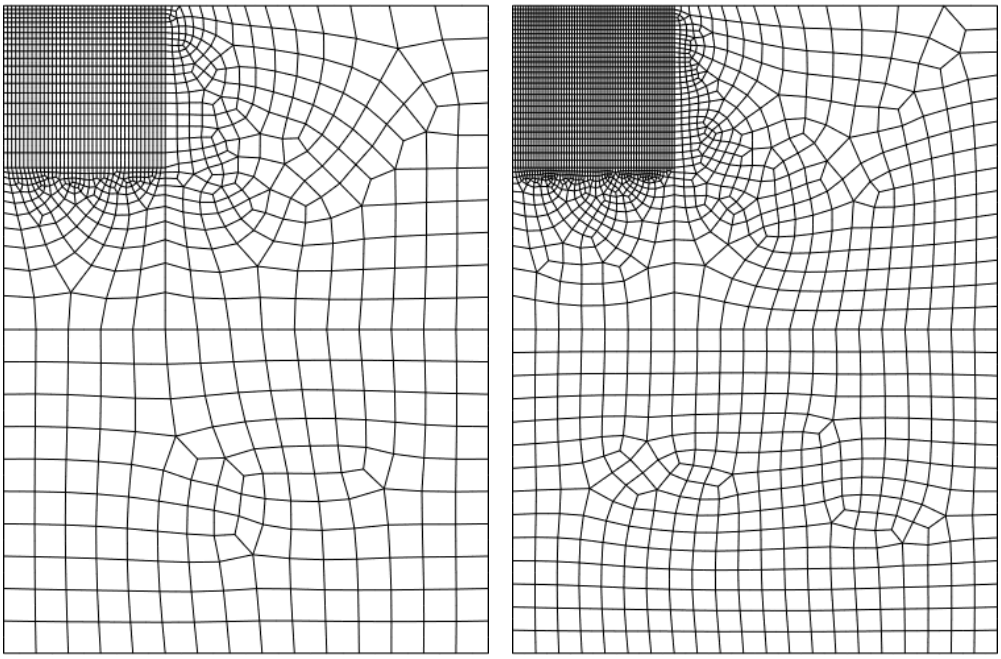

(a) Mesh used in analyses (b) Mesh used in mesh convergence study

Figure 3.14: Meshes used in 2D monotonic vertical loading analyses

3.4.2.2 Output Requests and Evaluation of Results

At the end of free-field stress calculation stage, although very small compared to given foundation displacement at the foundation load step, vertical displacements occur throughout the soil medium. These unwanted displacements at the nodes directly under the foundation are deducted from the total displacements of the foundation load application step.

Bearing pressure is calculated as the sum of the vertical components of the reaction forces at the nodal points where the vertical displacement is applied divided by the foundation area.

Since this is a plane strain analysis foundation length is assumed as 1m. Therefore instead of the actual foundation area which is 0.50m x 0.50m, an area of 0.25m x 1m should be used, considering half of the breadth of the footing is modeled due to symmetry, for calculating the pressure under footing. Note that unlike Zhu and Michalowski (2005), size of the neighboring elements are not considered for the calculation of the bearing pressure.

Settlement of the foundation is computed from the vertical displacement of the nodes directly

under foundation, which settle uniformly according to the prescribed boundary condition.

3.4.3 3D Monotonic Horizontal Loading Analyses

In this section modeling details of 3D monotonic horizontal loading analyses are explained. Due to symmetry, half of the problem is modeled in order to increase the computational efficiency.

3.4.3.1 Mesh and Element Selection

Mesh design is selected as similar to the mesh used in monotonic vertical loading analyses explained in Section 3.4.1.1. Selected mesh, presented in Figure 3.15(a), is composed of 3520 elements where 96 elements are placed directly below the footing.

Soil medium is modeled by 20 node reduced integration quadratic (C3D20R) elements. As explained in Section 3.3.2 two element types, namely C3D20R and C3D8I, are considered as usable in this study. C3D20R is chosen over C3D8I because of its tolerance to distortion, considering most of the elements have trapezoidal distortion in the selected mesh.

Dimensions of the soil model are selected as 4 m wide x 1.5 m long x 2 m deep. Note that these are the dimensions of the half of actual problem. Therefore the actual problem would have the dimensions of 4 m width x 3 m length x 2 m depth. This is 1 m shallower than the soil boundaries of the soil tank modeled, which was 4 m wide x 3 m long x 3 m deep.

Boundary conditions do not allow normal displacements on the boundaries of the model, but allow tangential displacements. Base of the model allows neither tangential nor normal displacements. Plane of symmetry is constrained with symmetric boundary conditions which only restrains normal displacement.

In order to ensure that selected mesh is adequately fine, a mesh convergence study is conducted. For this purpose, mesh shown in Figure 3.15(a) is compared with a finer mesh, composed of 4416 elements shown in Figure 3.15(b). 144 elements are placed directly below the footing in this finer mesh. For Case 9 analysis with material parameters of $\psi = 37^{\circ}$, $\phi = 39.9^{\circ}$ and c = 0.05 kPa, maximum horizontal load carrying capacities obtained from selected mesh and convergence study mesh are 6.27 kPa and 6.24 kPa, respectively. There is

0.48% difference between the results. This level of difference is considered as acceptable.

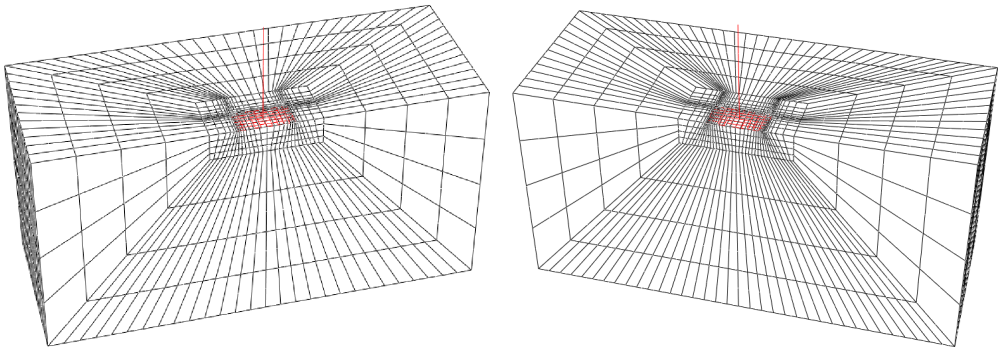

(a) Mesh used in analyses (b) Mesh used in mesh convergence study

Figure 3.15: Meshes used in 3D monotonic horizontal loading analyses shown with low pier foundation model

3.4.3.2 Foundation Model and Interaction with Soil

Foundation model is idealized to consist of a rigid shell, representing the foundation base, and a rigid wire monolithically connected to the foundation base representing the pier. Foundation is modeled as a rigid body, utilizing discrete rigid body type, as explained in Section 3.3.3.

Foundation base is a rectangle with dimensions of 0.25 m x 0.5 m. Note that these dimensions are the dimensions of the half of actual foundation. Therefore, the actual foundation base modeled is a square with 0.5 m edge length. Pier is positioned at the middle of the half-footing base as shown in Figure 3.15(a) so that together with the symmetric counterpart, the resultant force applied to the pier would act exactly at the center of the full foundation model.

Reference node of the foundation model is selected as the top of the pier. This selection was a requirement in order to apply the horizontal load with displacement control, since all boundary conditions assigned to the rigid body are moved to the reference node. Significance of reference node was discussed in Section 3.3.3.

Symmetric boundary condition is assigned to the rigid body for the direction perpendicular to the horizontal load application axis, in order to restrain the movement of the foundation perpendicular to the symmetry plane due to accumulated small numerical errors in analyses. It is worth to note that these displacements, since very small, do not affect the results even if they are allowed.

One approach for modeling soil structure interaction in finite element method, as employed by Yılmaz (2004), is binding all degree of freedoms of foundation nodes to the soil nodes that lie directly below the foundation and then use the tension cut-off feature of the soil material to prevent the undesirable sticking of the soil to the foundation bottom during uplift. However due to the observed convergence difficulties when tension-cutoff feature of Mohr-Coulomb failure criterion is utilized in Abaqus, this method could not be employed. Instead, contact interaction is utilized for modeling the interface between soil and foundation for horizontal loading cases since uplift of foundation is expected.

Foundation-soil interface is modeled with contact pairs approach of Abaqus. Interacting surfaces are selected as the bottom of footing and the soil surface immediately below the footing. It was desired to include a portion of the soil surface near foundation edges into the contact interaction, however due to the observed convergence difficulties, this was not achieved. According to the analysis results, significant vertical deformations of the elements directly near the foundation edge prohibit surface contact at these element faces. Moreover, forward edge of the footing embeds into the soil due to rotation. However, since sliding of the foundation is not at the soil surface as could be seen from this description, this situation did not have considerable effect on analysis results.

Finite sliding contact tracking approach is utilized since sliding of the foundation is expected. However, overall sliding of the foundation was observed to be mostly due to the plastic surface developing within the soil medium according to the analysis results. This observation suggests that utilization of finite sliding formulation was redundant and instead small sliding formulation could have been selected. Small sliding formulation is referred as a subset of finite sliding formulation in Abaqus Documentation (2010). As explained in Section 3.3.4.3 finite sliding formulation performs additional calculations compared to small sliding formulation. Therefore this redundancy may have increased computational cost of the analyses.

Surface to surface contact discretization is utilized due to observed computational efficiency. This efficiency could be explained by the comment from Abaqus Documentation (2010) stating that for finite-sliding contact interactions surface to surface contact tends to converge in fewer iterations than node-to-surface contact discretization since surface-to-surface contact has more continuous behavior upon sliding.

Hard contact pressure-overclosure relationship is utilized. Therefore contact pressures are

directly transferred to soil medium.

Frictional behavior is modeled by using Coulomb friction model with constant friction coefficient equal to the tangent of internal friction angle of the soil. Since Mohr-Coulomb yield criterion, if not considering cohesion, reduces to Coulomb friction model under the footing on the surface of the soil. Rough footing is modeled since sand papers were glued at the bottom of the actual footing.

Note that instead of utilizing Coulomb friction model, frictional forces could have directly been trasferred to the soil continuum elements by utilizing rough friction formulation. This method is not chosen due to faster convergence rate with utilization of the penalty method and observed finer accuracy with less number of elements under the footing.

Penalty contact enforcement is utilized for both frictional and pressure overclosure behavior. Therefore certain magnitude of undesired elastic sliding, and penetration to the soil continuum of the foundation is observed. Magnitudes of these undesired effects are investigated with the verification studies presented in Section 3.5.2 and are considered as negligible.

State based contact tracking algorithm is used due to observed faster convergence to solution with this algorithm.

3.4.3.3 Application of Loads

Weight of the model is applied as a point load, at the center of gravity, which lies on the pier at a certain height from the foundation bottom. Since half of the foundation is modeled, half of the weight of the actual model is utilized. Application of the model self weight at certain height above ground level, has enabled consideration of the additional eccentricity due to self weight (P - Δ effect) to be taken into account. For this purpose consideration of non-linear effects of nodal displacements are included for all steps of the analysis.

Horizontal test load is applied as a prescribed displacement at the top of the pier of the foundation model. 40 mm of horizontal displacement is observed as adequate both for reaching the peak capacity and establishing the decrease in load horizontal load carrying capacity. Therefore analysis is a displacement controlled analysis. This is necessary to model the decrease in horizontal load after reaching the peak capacity observed in the experiment results. This

reduction in horizontal load carrying capacity is expected due to two reasons. First reason is, as indicated by Fukui et al. (2005), that submergence of the forward tip of the foundation into the soil results in decrease in horizontal load carrying capacity of the foundation. And the second reason is, with increasing tilt angle of the foundation, second order moments would increase with a consequence of decrease in horizontal load capacity of the foundation as indicated by analytical solutions such as Paolucci and Pecker (1997). These aspects could be considered through implementation of geometric nonlinearities.

3.4.3.4 Analysis Procedure

Each analysis consists of three main steps. Figure 3.16 demonstrates these steps. In this figure g and w represent the gravitational acceleration and weight of foundation respectively. Whereas Δx represents the horizontal force applied in a displacement controlled manner.

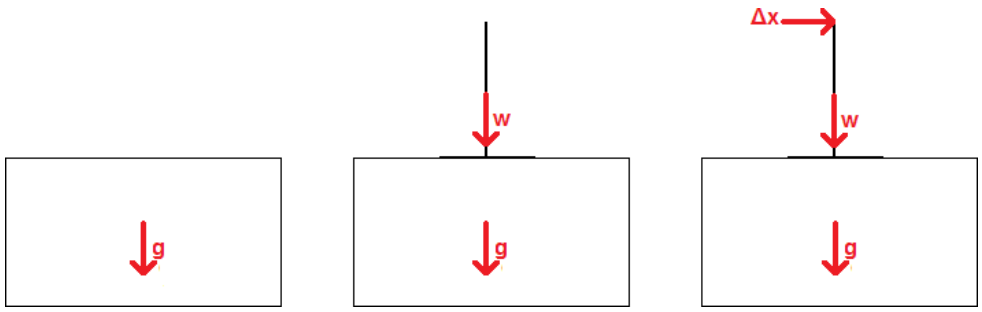

Figure 3.16: Demonstration of Load Steps of Monotonic Horizontal Loading Analyses

1. Calculation of free-field stresses: This step simulates stress distribution in the free field. (ie. before foundation placement). In this step, gravity loading is applied to the elements modeling the soil medium according to the defined soil density, than the initial conditions for the lateral pressures are enforced according to the defined lateral earth pressure at rest coefficient (K_o).

2. Application of model self weight: In this step foundation model is placed on the soil surface by activating the interaction between foundation and soil, and applying the self weight of the foundation model to its center of gravity.

3. Application of the test loading: In this step, horizontal test load is applied at the horizontal

loading point of the foundation model.

3.4.3.5 Output Requests and Evaluation of Results

Vertical and horizontal components of reaction forces at the side and bottom boundaries of the soil mesh, horizontal and vertical displacements of the loading point, backward edge and forward edge of the foundation are recorded for each increment throughout the analyses.

At the end of free-field stress calculation stage, although very small compared to given foundation displacement at the foundation load step, vertical displacements occur throughout the soil medium. These displacements at the nodes directly beneath the foundation are deducted from the total displacements of the later steps of the analyses.

Horizontal force acting at the loading point of the foundation model is calculated as the sum of the horizontal components of the reaction forces at the nodal points of outer boundaries of soil mesh. Since half of the foundation is modeled, this value is multiplied by two in order to reach the actual capacity of the experiments.

Tilt angle and sliding of the foundation are computed from the vertical and horizontal displacements of the backward and forward edges of the foundation.

3.4.3.6 Solution Strategy and Control Parameters

Solution Technique

Full Newton solution strategy is employed. Note that using Riks nonlinear problem solution strategy (Abaqus Documentation, 2010) with load controlled analyses instead of Newton method might also capture the decrease in horizontal load carrying capacity. But utilizing displacement controlled analysis with Newton solution strategy is believed to be a more efficient choice, due to its simplicity and less number of unknowns compared to Riks solution strategy.

Unsymmetrical matrix storage is selected based on advice in Abaqus Documentation (2010) for analysis using Mohr-Coulomb yield criterion; as it increases analysis speed. Direct equation solver is utilized as iterative equation solver is feasible for models composed of higher number of elements.

In order to consider second order moments nonlinear geometry analysis is enabled for all steps of the analysis.

Solution Control Parameters

Solution control parameters of steps coming after calculation of free field stresses are modified as described in Section 3.4.1.5.

Increment Size Selection

In free-field stress calculation step fixed increment size with 100% is utilized. This configuration is the suggested configuration in Abaqus Documentation (2010). Since the requested free field stresses would not be considerably different than the original stress configuration this step is advised to complete in a single load increment.

In self weight application step, automatic increment size selection algorithm is utilized with 1% as the first increment size, 100% as the maximum increment size and $1x10^{-8}$% as the minimum allowable increment size. 1% increment size is a high value for the first increment; however, considering the model self weight is not close to the bearing capacity of the foundation, it is found as adequate.

In test loading application step, automatic increment selection algorithm is used. First increment size is selected as 0.01%, and 100% as the maximum increment size and $1x10^{-9}$% as the minimum increment size.

3.4.4 2D Monotonic Horizontal Loading Analyses

These analyses, utilizing plane strain assumption, are conducted with an aim to compare with 3D analyses in order to assess the effect of plane strain assumption on analyses results. Therefore, these analyses are conducted with same modeling preferences as 3D analyses described in Section 3.4.3 except mesh, element type, evaluation of results and load application procedures, to which modifications are required due to change in problem dimension.

3.4.4.1 Mesh and Element Selection

Meshes used in analyses, composed of 1711 CPE8R elements, are shown in Figure 3.17(a). Element type is selected as CPE8R which is a second order reduced integration element for plane strain analyses, analogous to C3D20R which is for 3D analyses.

Dimensions of the soil model are selected as 3 m wide x 2 m deep. This is 1m shallower than the boundaries of the soil tank modeled, which was 4 m long x 3 m wide x 2 m deep. This modification is done in order to be consistent with the 3D bearing capacity analyses presented in Section 3.4.3.1.

Boundary conditions are set to not allow normal displacements on the boundaries of the model, but allow tangential displacements. Base of the model does not allow neither tangential nor normal displacements.

In order to ensure that selected mesh shown in Figure 3.14(a) is fine enough, a mesh convergence study is conducted. For this purpose an analysis to be used as a mesh convergence study is conducted with a finer mesh composed of 3458 elements, which is presented in Figure 3.17(b). Monotonic horizontal loading analysis with material parameters of $\psi = 37°$, $\phi = 39.9°$ and c = 0.05kPa is conducted. Maximum horizontal load carrying capacities obtained from selected mesh and convergence study mesh are 5.78 kPa and 5.70 kPa, respectively. There is 1.40% difference between the results. This level of difference is considered as acceptable.

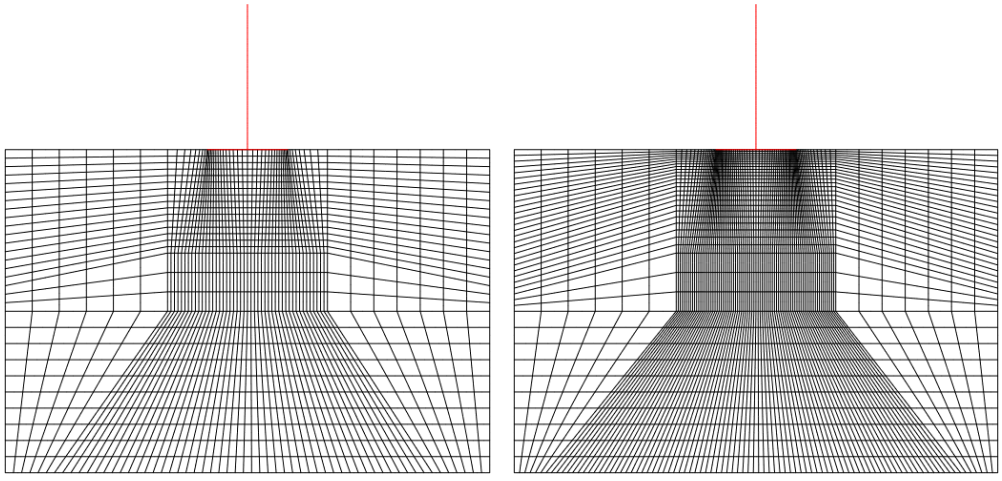

(a) Mesh used in analyses (b) Mesh used in mesh convergence study

Figure 3.17: Meshes used in 2D monotonic horizontal loading analyses

3.4.4.2 Application of Loads

Due to plane strain assumption, foundation is modeled as strip foundation with breadth 0.5 m and unit length (1 m). Since the actual length of the foundation was 0.5 m, in order to apply same pressure on the soil, two times the actual weight of the foundation is applied on the model. Compare this with the 3D analyses, which exploits the symmetry of the loading conditions, half of the footing was modeled, consequently half of the actual weight of the foundation was applied on the model. This was necessary since for plasticity, yield is defined in terms of pressure.

3.4.4.3 Output Request and Evaluation of Results

Vertical and horizontal components of reaction forces at the side and bottom boundaries of the soil mesh, horizontal and vertical displacements of the loading point, backward edge and forward edge of the foundation are recorded for each increment throughout the analyses.

At the end of free-field stress calculation stage, although very small compared to the given foundation displacement at the foundation load step, vertical displacements occur throughout the soil medium. These unwanted displacements at nodes directly under the foundation are deducted from the total displacements of the later steps of the analyses.

Horizontal force acting at the loading point of the foundation model is calculated as the sum of the horizontal components of the reaction forces at the nodal points of outer boundaries of soil mesh. Since plane strain analysis is conducted with imaginary length dimension of 1 m, this value is divided by two in order to reach the actual capacity of the experiments conducted with foundation length of 0.5 m.

Tilt angle, and sliding of the foundation is computed from the vertical and horizontal displacements of the backward and forward edges of the foundation.

3.5 Verification of Modeling Approaches

In this section, suitability of the modeling choices made in Section 3.4 is verified with available theoretical solutions.

3.5.1 Verification Studies for Monotonic Vertical Loading Analyses

3.5.1.1 Verification of 3D Analyses with Exact Solution by Cox (1962)

In order to verify the solution method, a circular foundation bearing capacity problem, whose solution is found by Cox (1962) is modeled. Cox (1962) has shown that for smooth circular shallow foundation with radius (R) lying on a soil with cohesion (c), internal friction angle (ϕ), unit weight (γ) satisfying Equations 3.12a and 3.12b; solution for the ultimate bearing capacity (q_{ult}) of this foundation could be found by Equation 3.12c.

$$\frac{\gamma R}{c} = 10 \tag{3.12a}$$

$$\phi = 30^{\circ} \tag{3.12b}$$

$$q_{ult} = 141c \tag{3.12c}$$

Following the modeling layout described in Section 3.4.1, a finite element model is constructed with R = 0.25m, γ = 16kN/m^3, c = 0.4kPa. Since these parameters and analysis satisfies the conditions of the Cox (1962) solution, it is expected to find ultimate bearing capacity of 56.4kPa from the finite element model.

As a result, 57.8 kPa is found from the finite element analysis with a mesh composed of 2821 elements. Therefore, the exact solution is approached from above with less than 2.50% error. This analysis verifies that selected element type, boundary conditions, application of symmetry, application of vertical displacement on the nodes lying directly below the foundation as loading, reading the vertical components of reaction forces at these nodes as the result, modifications done to the default solution control parameters, are adequate for modeling the bearing capacity problem.

3.5.1.2 Verification of 2D Analyses with Exact Solution by Prandtl (1920)

In order to verify the solution method, bearing capacity of a strip foundation lying over a cohesive soil, to which exact solution is found by Prandtl (1920) is modeled. Prandtl (1920) has shown that for smooth strip shallow foundation lying on a soil with cohesion (c), internal friction angle (ϕ) satisfying Equation 3.13a; exact solution for the ultimate bearing capacity (q_{ult}) of this foundation could be found by Equation 3.13b.

$$\phi = 0^{\circ} \tag{3.13a}$$

$$q_{ult} = (\pi + 2)c \tag{3.13b}$$

Following the modeling layout described in Section 3.4.2, a finite element model is constructed with $\phi = 0^{\circ}$, c = 100kPa. Since these parameters and analysis satisfies the conditions of the Prandtl (1920) solution, it is expected to find ultimate bearing capacity of 514.16kPa from the finite element analysis.

As a result 516.32kPa is found from the finite element analysis with mesh composed of 1234 elements. Therefore the exact solution is approached from above with 0.42% error. This analysis verifies that selected element type, boundary conditions, application of symmetry, application of vertical displacement on the nodes lying directly below the foundation as loading, reading the vertical components of reaction forces at these nodes as the result, modifications done to the default solution control parameters, are proper approaches for modeling the bearing capacity problem.

3.5.2 Verification Studies For Monotonic Horizontal Loading Analyses

These analyses utilize the same element type and boundary conditions with monotonic vertical loading analyses which were verified in Section 3.5.1. The main difference introduced in modeling the monotonic horizontal loading analyses is the modeling of the foundation as a rigid body and the contact interaction defined between rigid body and the soil.

In this section, chosen contact simulation technique for soil foundation interface modeling is

verified in three steps. First, tangential contact behavior will be verified for its compliance with Coulomb Friction Model described in Abaqus Documentation (2010). Then, capability of normal contact behavior to model uplift behavior is assessed. Finally, it is verified that the analyses take second order moments into account, which are due to rotational deformation of the foundation model.

3.5.2.1 Verification of Frictional Contact Behavior with Coulomb Friction Rule

Frictional contact behavior between soil and foundation defines the relative sliding of foundation with respect to the soil and the amount of shear the soil - foundation interface can support.

Frictional contact behavior is modeled to obey the Coulomb Friction Rule which enforces absolutely no relative sliding up to a defined maximum shear resistance calculated according to Equation 3.14 between soil and foundation. Once the ultimate shear capacity is reached, the foundation is expected to slide indefinitely under this shear resistance.

$$F_f = \mu F_n \tag{3.14}$$

In Equation 3.14, F_f is the maximum shear resistance, μ is the friction coefficient and F_n is the normal force acting on the soil - foundation interface.

Note that in this formulation friction coefficient is of constant value which does not depend on any other variable such as, strain magnitude or magnitude of F_n. Therefore, modeling soil - foundation interface in this manner is not physically exact, since friction coefficient generally depends on these parameters. Nonetheless, this formulation is selected for its simplicity, and unknown parameters to define the more rigorous sliding models.

A foundation, with weight V, sustaining a horizontal load H, overlying a linear elastic continuum is taken as the analysis subject for investigation. Contact interaction is defined between bottom surface of foundation and whole top surface of the elastic continuum. Verification study is selected as the comparison of the maximum horizontal load the foundation can carry and sliding amount at the instant immediately before the onset of this maximum horizontal load with theoretical solution.

Horizontal force is applied at the base of the foundation in order not to create eccentric loading. Weight of the foundation and friction coefficient are chosen to be equal to parameters used in Case 9 analysis as 4.364kN and 0.83613, respectively. Weight of the foundation is applied at the center of gravity of the foundation as a point load. General view of the analysis showing loads and support conditions is presented in Figure 3.18.

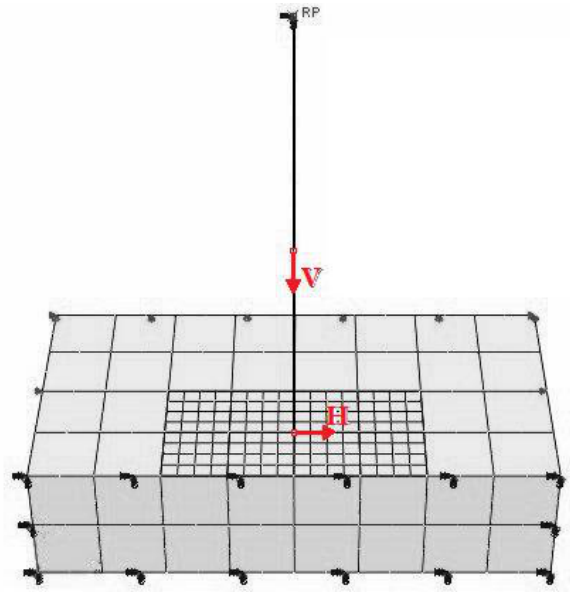

Figure 3.18: General view of frictional contact behavior verification analyses

Load steps are defined as described in Section 3.4.3.

Under these conditions slip is expected to occur for a horizontal load magnitude of $F_f = 3.649kN$ according to Equation 3.14.

Table 3.3 presents the amount of sliding (Δx) and horizontal force (F_f) at the onset of sliding. Analyses have successfully provided the sliding load with less than 0.1% error, whereas there is an amount of unexpected sliding before this point.

Table 3.3: Comparison of the results of finite element analysis and analytical solution

Slip Tolerance	**Expected F_f (kN)**	**Analysis F_f (kN)**	**Expected Δx (mm)**	**Analysis Δx (mm)**
Default	3.649	3.648	0.00	0.93
Stricter	3.649	3.648	0.00	0.64

Figure 3.19 shows the horizontal force versus horizontal displacement curves of these analyses. It is seen that the chosen method yielded the same value for sliding. However there is a region in this figure showing behavior analogous to elastic behavior. This is due to a trade-off between computational cost and solution accuracy as explained in Section 3.3.4.1. Magnitude of allowed elastic slip can be adjusted by the user. In the analyses of this study default parameter controlling the allowed elastic slip which is as fraction of characteristic surface dimension is chosen as 10 times lower than its predefined value of 0.005. As an alternative, a single value could have been selected for allowed slip distance instead of modifying this parameter.

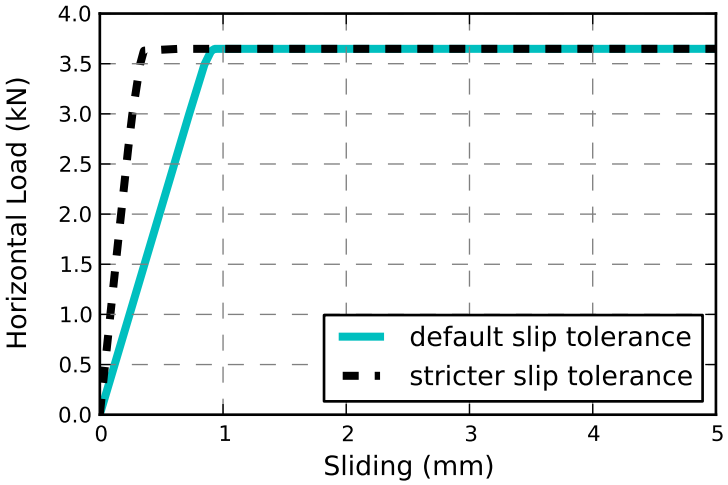

Figure 3.19: Variation of force versus sliding of frictional contact behavior in verification analyses

3.5.2.2 Verification of Pressure - Overclosure Contact Behavior for Uplift

Pressure overclosure contact behavior ensures that penetration of one surface into another is resisted as described by Abaqus Documentation (2010). Therefore normal contact behavior between soil and foundation assures that normal displacement of the soil nodes yield adequate resistance in normal direction, to the forces applied on foundation.

For verification of the technique used for modeling pressure - overclosure contact and uplift behavior between soil and foundation model, a finite element model utilizing linear elastic beam-column behavior is constructed with C3D20R elements. In the model, foundation is placed on top of a linear elastic continuum as shown in Figure 3.20. First an axial load which

results in compression of the beam-column is applied on the foundation. In the next step, a moment is applied on the foundation.

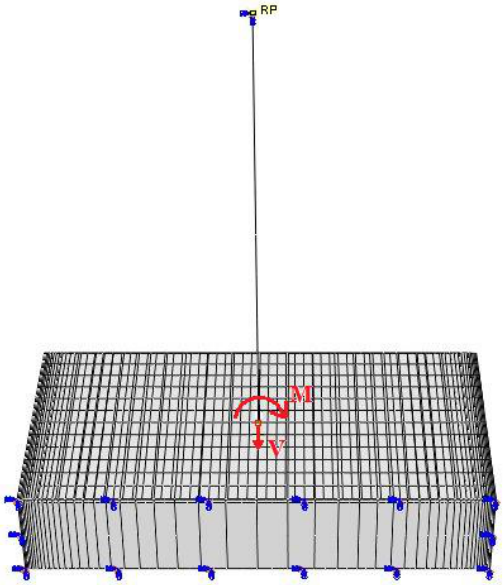

Figure 3.20: General view of the model used for pressure - overclosure contact verification analysis

Since the continuum would behave as an elastic beam column under the given loading conditions, an analytical solution shown in Equation 3.15 based on small displacement assumption is available for stress at the continuum under the tension edge of the foundation under the vertical load and applied moment. According to this solution, moment required to establish zero stress at the tension edge of the beam can be computed. At this magnitude of moment, finite element model is expected to yield zero contact pressure at the tension edge of the beam. Additionally, beyond this point uplift of the footing is expected.

$$\sigma = \frac{P}{A} - \frac{Mc}{I} \tag{3.15}$$

In Equation 3.15 σ is the foundation pressure at the tension edge of the foundation, P is the vertical load, A is the foundation area, M is the applied moment and I is the moment of inertia of the footing computed with respect to middle of the footing.

Contact pressure and contact opening at the foundation edge that is over the tension fiber of the beam are monitored throughout the analysis.

Foundation is placed on top of a beam column with 0.1 m height, 0.25 m width, 0.5 m length. Elasticity modulus and Poisson's ratio of the continuum are selected as 10.000 MPa and 0.0, respectively. Small displacement condition is achieved by utilizing such a high elasticity modulus compared to magnitude of applied loading.

Vertical load and moment are applied at the pier base of the foundation model. In first step, a vertical load of 12.5 kN is applied.

Frictional coefficient between soil and foundation base is selected as 0.80. Note that for this load configuration, development of shear stresses between foundation and the beam is not expected. However, for the sake of faster convergence to the solution with large increment sizes, frictional behavior is defined. After the analysis, total shear between foundation and the beam is found as close to zero, as expected.

Results are compared in Table 3.4. In order to obtain the error between analytical and finite element solutions with the desired accuracy, moment is applied with 0.001 kNm load increments after reaching 1.0 kNm. Instead of the exact solution, which is 1.0417 kNm, zero stress is achieved one load step later for 1.043 kNm moment magnitude. And uplift was expected one more step later, for 1.044 kNm; however, it is encountered at 1.046 kNm.

Table 3.4: Comparison of the moment results of finite element analysis and analytical solution

Analytical Solution (kN m)	**Finite Element Result (kN m)**	**Uplift Moment (kN m)**
1.042	1.043	1.046

From Table 3.4 it can be seen that finite element model computes the zero stress moment with 0.43% error, compared to the analytical solution. Moreover, uplift of the foundation is encountered for moment which is greater than the zero stress moment, as expected. These errors could be attributed to the use of penalty method as the contact enforcement method, as explained in Section 3.3.4.4

3.5.2.3 Verification of Capability to Model P-Delta Moment Effect

In order to verify that second order moments developing due to rotation of the foundation, a finite element model utilizing linear elastic beam column behavior is constructed. In the

model, foundation is placed on top of a linear elastic continuum as shown in Figure 3.21. First an axial load which results in compression of the beam-column is applied on the foundation at the pier top. In the next step, a moment is applied on the foundation.

Foundation is placed on top of a beam column with 1m height, 0.25m width, 0.5m length. Elasticity modulus and Poisson's ratio of the continuum are selected as 10 MPa and 0.0, respectively. Vertical load is applied at the top of the pier, and moment is applied at the pier base of the foundation model. In the first step a vertical load of 12.5kN is applied. Then in the next step, a moment of 1kNm is applied on the foundation.

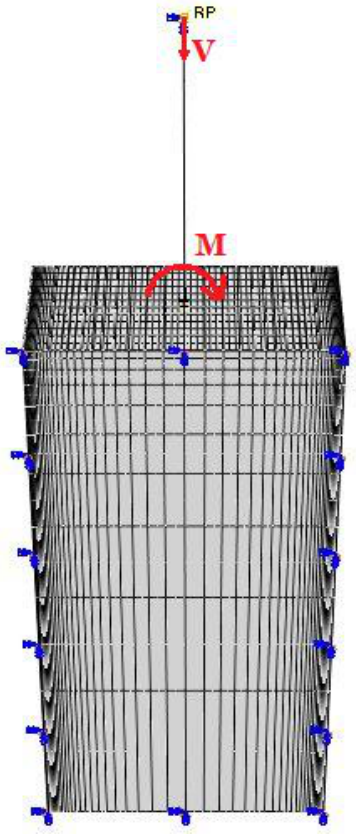

Figure 3.21: General view of P-Delta effect verification analysis

Due to high beam length and low elasticity modulus of the beam-column, bending of the beam-column and significant second order moments were expected.

Reaction forces at the base of the beam column are monitored throughout the analysis. Under the given vertical force and moment, beam-column is expected to show considerable bending

deformation, which would yield additional, second order moments due to horizontal displacement of the vertical load application point with respect to the centroid of the base support area of the beam. Therefore although the sum of the vertical reaction forces are expected to be equal to the vertical load applied, moment of vertical components of reaction forces with respect to center of base of the beam column is expected to be equal to the sum of applied moment and second order moment.

Results of the analysis are shown in Table 3.5. It is seen that the second order moments are taken into account. If it were not, the reaction moments would be equal to the applied moment. However, considering the deformed shape of the model, additional moment was included in the solution and it yielded the expected moment with less than 0.3% error.

Table 3.5: Comparison of the results of finite element analysis with the expected solution

Applied Loads		**Analysis Results**			
V. Force (kN)	**Moment (kNm)**	Δx_V **(cm)**	**V. Force (kN)**	**Moment (kNm)**	**Exp. Moment (kNm)**
12.50	1.00	6.652	12.50	1.837	1.832

3.6 Evaluation of Measures Taken to Resolve Convergence Difficulties

3.6.1 Effect of Automatic Stabilization on Results

It is observed that, the automatic stabilization technique has potential to increase the plastic limit loads of the analyses significantly, which is detrimental to accuracy of analyses results. In this section, this influence together with step taken to reduce it is discussed with an example analysis.

Example analysis models the monotonic vertical loading of soil that is meshed with 21523 C3D8I elements. This mesh and element combination, without automatic stabilization, could provide the solution of verification case studied in Section 3.5.1.1 with 6.7% error. When the material properties defining plasticity of the analysis are changed as $\psi = 10°$, $\phi = 39.9°$, c = 0.1 kPa, and rough footing is modeled by prohibiting horizontal displacements of the nodes placed directly below the foundation, this analysis terminates as a result of failing to achieve

minimum step size criterion specified, due to a number of successive diverging increments. In order to remedy this issue two additional analyses which employ automatic stabilization mechanism are conducted.

Figure 3.22 presents the foundation pressure - settlement variation of these three analyses. In Figure 3.22 curve with label ”no stabilization” belongs to the analysis, that does not employ the automatic stabilization mechanism. It is seen for this analysis that, last load increments show an unexpected sharp deviation from the almost linear trend, which was expected continue until the limit load is approached. The other two analyses were identical to this analysis, with the exception of making use of the automatic stabilization mechanism in order to overcome the divergence from solution issue. Difference between the analyses employing automatic stabilization technique shown in Figure 3.22 is the ratio of stabilization to strain energy (allsdtol).

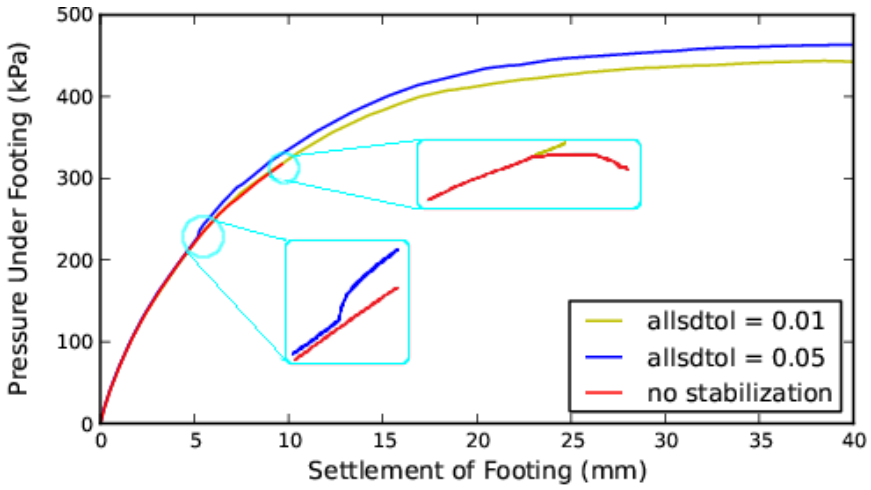

Figure 3.22: Effect of Automatic Stabilization on Analysis Results

In order to overcome the divergence from solution issue, analysis was conducted again by enabling automatic stabilization and employing the default value of 5% for the ratio of stabilization to strain energy. In that case, analysis completed successfully, despite an unexpected asymptotic jump in pressure - displacement curve as shown in Figure 3.22. Note that, this asymptotic jump might be considered as originated from a sudden increase in stiffness of the overall response of soil mesh, and according to the explanation in Section 3.3.5 it could be inferred that this is due to the introduced high artificial stiffness by the automatic stabilization method. For automatic stabilization technique, ratio of the energy dissipated by viscous

damping to the total strain energy is calculated to control the introduced artificial stiffness . This ratio is named as the ratio of stabilization to strain energy (allsdtol). A maximum limit is defined by the user to this energy in order to limit the artificial stiffness brought. Based on observation, it is seen that another consequence of decreasing this value is the decrease of initial damping factor utilized for automatic stabilization. Decreasing this value directly results in decrease in artificial stiffness introduced. Considering this observation, as an attempt to see if the analysis would still converge with less amount of artificial stiffness, this ratio is decreased to 1% from the original value of 5%. For this magnitude, the sudden asymptotic jump disappeared, and analysis yielded a considerably lower plastic limit. Therefore ratio of 1% is utilized for all analyses as stated in Section 3.4.

From analyses utilizing 5% ratio, with different meshes composed of C3D20R elements, it is observed that aspect ratio of elements might have significant effect on sudden increases in overall stiffness. Three meshes and foundation stress - settlement curves of the monotonic vertical loading analysis using these meshes are shown in Figure 3.23. In this Figure, elements with aspect ratios greater than 10 are highlighted. Note that the abnormal increase in stiffness occurs earlier if the elements with high aspect ratio are closer to the load application area.

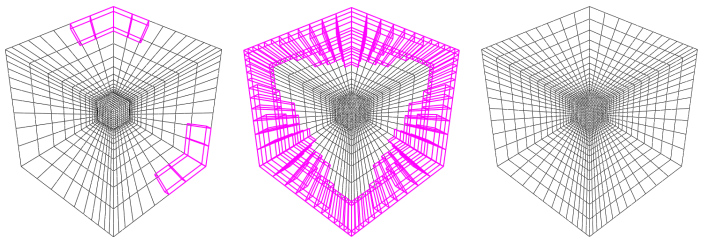

(a) Mesh A (b) Mesh B (c) Mesh C

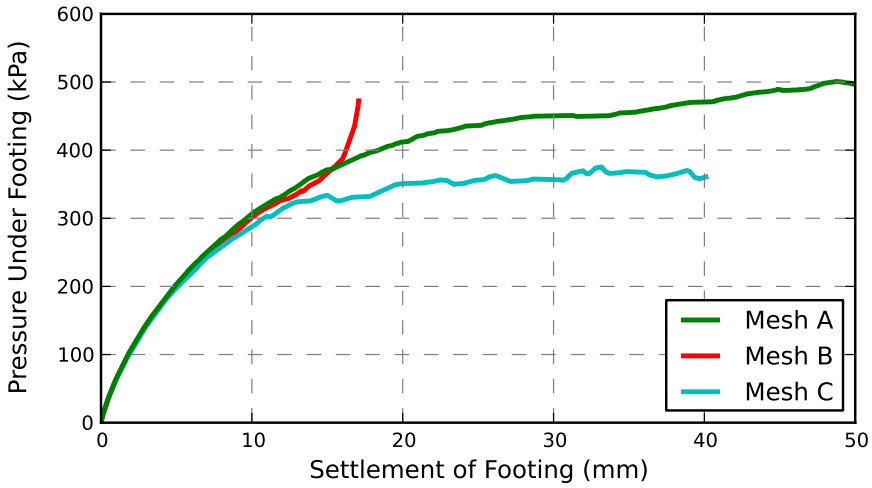

(d) Comparison of Pressure - Displacement Curves

Figure 3.23: Effect of High Magnitude of Automatic Stabilization on Different Meshes

3.6.2 Effect of Artificial Cohesion on Results

Cohesion is observed to have favourable effect on completion speed of analyses, and improvement of the convergence difficulties. Based on works in literature such as Zhu and Michalowki (2005) and Loukidis and Salgado (2009) which model cohesionless materials, it is seen that inclusion of a small cohesion value in material parameters in order to prevent convergence difficulties is common practice. In this section effect of defining artificial cohesion to the purely frictional material for bearing capacity analyses and elimination of this effect is discussed.

For analytical bearing capacity solutions, contribution of cohesion to the bearing capacity is defined by cN_c. Where c is the cohesion magnitude, and N_c is the bearing capacity factor for cohesion which depends on the internal friction angle of the soil. Figure 3.24 shows N_c value with respect to internal friction angle, according to Meyerhof's proposal. It is seen

that N_c factor increases with increasing rate with internal friction angle. Therefore for high internal friction angles such as for the sand modeled in this study, effect of addition of a small cohesion value might not be negligible. In contrast inclusion of cohesion is most needed for high internal friction angles.

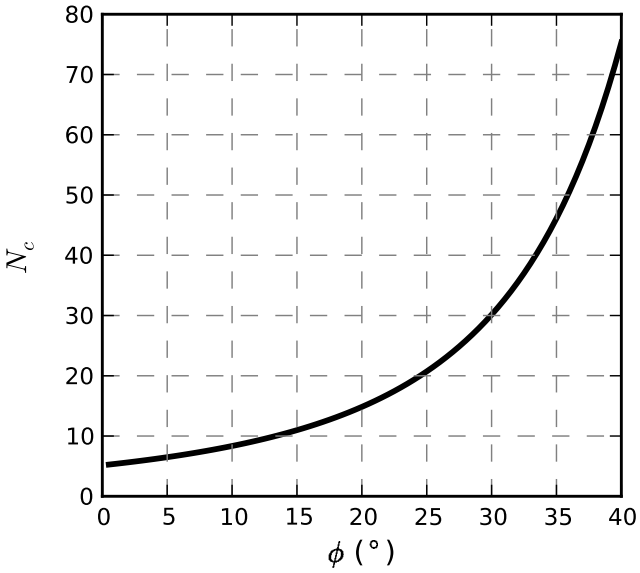

Figure 3.24: Bearing capacity factor N_c (Meyerhof, 1963)

Possibly considering that the cohesion effect is not negligible, Zhu and Michalowski (2005) chose to deduct the effect of cohesion from the result of finite element analyses with artificial cohesion by subtracting the cN_cf_{sc} (cN_cs_c) term of Equation 1.2 from the ultimate bearing capacity found from the analysis.

They chose to obtain the magnitude of N_cs_c factor from a finite element analysis which models weightless soil ($\gamma = 0$) and no overburden (q=0). By this means, bearing capacity equation reduces to Equation 3.16. And from this equation, N_cs_c term could be found, by the known values of given cohesion, and bearing capacity found from analysis. Then this N_cs_c term is multiplied with the small cohesion used in the analysis and deducted from the ultimate bearing capacity. Hence the error due to cohesion is removed from the ultimate bearing capacity by removing the contribution of the artificial cohesion. Note that the analysis conducted for finding the N_c value does not necessarily have the same cohesion as the analysis where the effect of the cohesion is deducted.

$$q_{ult} = cN_c s_c \tag{3.16}$$

In order to observe the effect of added artificial cohesion, and the sufficiency of the procedure practiced by Zhu and Michalowski (2005) , 6 analyses with different cohesion values of 0.2, 0.5, 1.5, 2.0, 3.0, 4.0 kPa are conducted for $\phi = 39.9°, \psi = 30°$. Among these analyses cohesion was the only variable.

Ultimate bearing capacity of each analysis (q_{ult}) and resulting bearing capacity after deducting the effect of cohesion with above described procedure is shown in Figure 3.25.

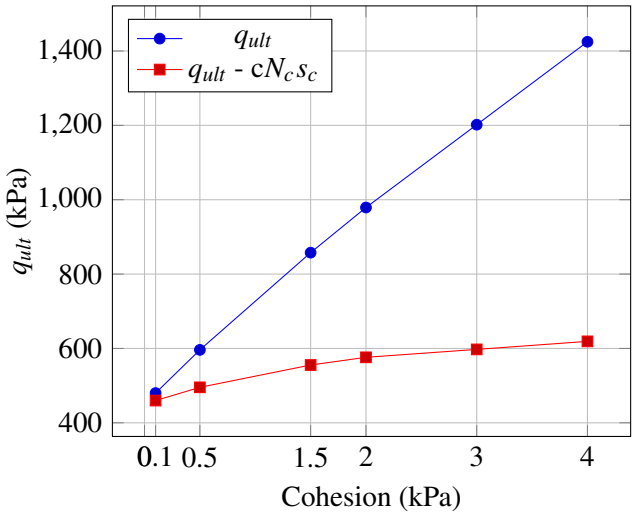

Figure 3.25: Effect of cohesion on results

It is seen from this figure that unlike as expected from Equation 1.1, bearing capacity is considerably different for each analysis although the effect of added cohesion is deducted. Based solely on this figure and Equation 1.1 it could be concluded that some of the factors in this equation increase for increasing cohesion value. This phenomenon can be explained according to the fact that N_c and N_γ factors also depend on $c/\gamma B$ ratio which is stated by Michalowski (1997). Therefore it could be stated that N_c and N_γ factors depend on the magnitude of the selected cohesion range for the analysis in this study.

It could be seen from the $q_{ult} - cN_c s_c$ curve in Figure 3.25 that effect of cohesion on ultimate bearing capacity is almost linear in 0.1 kPa - 1.5 kPa cohesion range. This could mean that rate

of change in magnitude of N_c and N_γ is linear within this range. Exploiting this observation, in order to remove the effect of added cohesion, two analyses can be performed with cohesion values of 0.5 kPa and 1.5 kPa respectively. Then $N_c s_c$ factor could be found from these two analyses according to Equation 1.2, by assuming N_γ is constant and $N_c s_c$ is changing linearly with c. Afterwards the $cN_c s_c$ could be computed for 0.5 kPa and deducted from the 0.5 kPa analysis. Note that this suggested method for deducting the effect of cohesion is not strictly correct and is based solely on observation. Therefore considerable magnitude of artificial cohesion is not employed in this study. Maximum artificial cohesion is limited to 0.1 kPa in this study.

Figure 3.26 shows pressure - settlement curves of analyses with $\phi = 42.1°, \psi = 39°$ and cohesion values of 1.5 kPa, 0.5 kPa and 0.1 kPa. In this figure an approximation for zero cohesion, computed based on results of the two analyses with cohesion of 0.5 kPa and 1.5 kPa is also shown. It is seen that the method provides a reasonable estimate. It should be mentioned that analysis with cohesion of 0.1 kPa progressed with very small increment sizes and took considerably more time than the two analyses. Average increment sizes of analyses with cohesion of 0.1 kPa, 0.5 kPa, and 1.5 kPa were $3x10^{-6}$, $2x10^{-5}$ and $1x10^{-4}$, respectively. This could be interpreted as analysis with 0.1 kPa cohesion progressed 7 and 33 times slower than the analyses with 0.5 kPa and 1.5 kPa cohesion respectively.

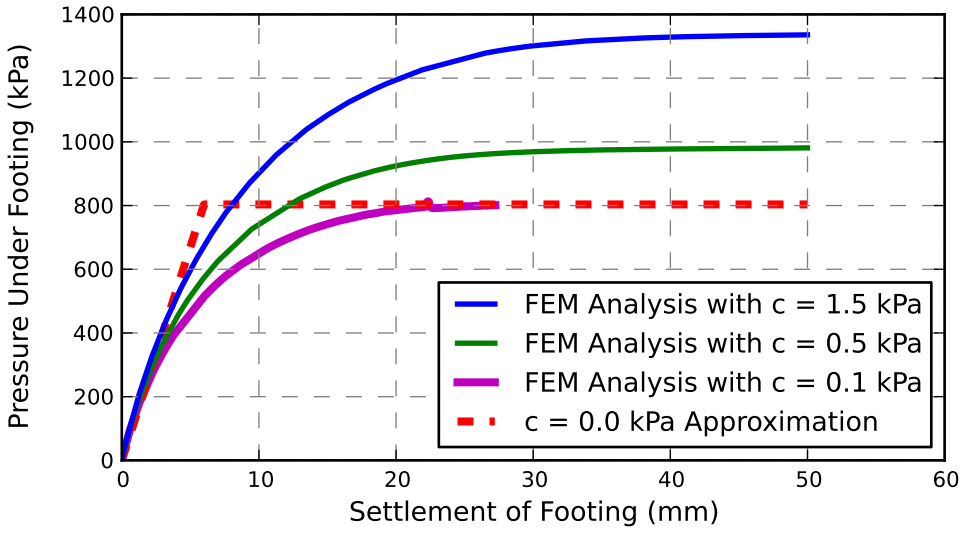

Figure 3.26: Deduction of effect of artificial cohesion

Figure 3.27 shows pressure - settlement variation of analyses the results of which were pre-

sented in Figure 3.25. It is seen from this figure that increase in cohesion does not change the initial inclination of the curve.

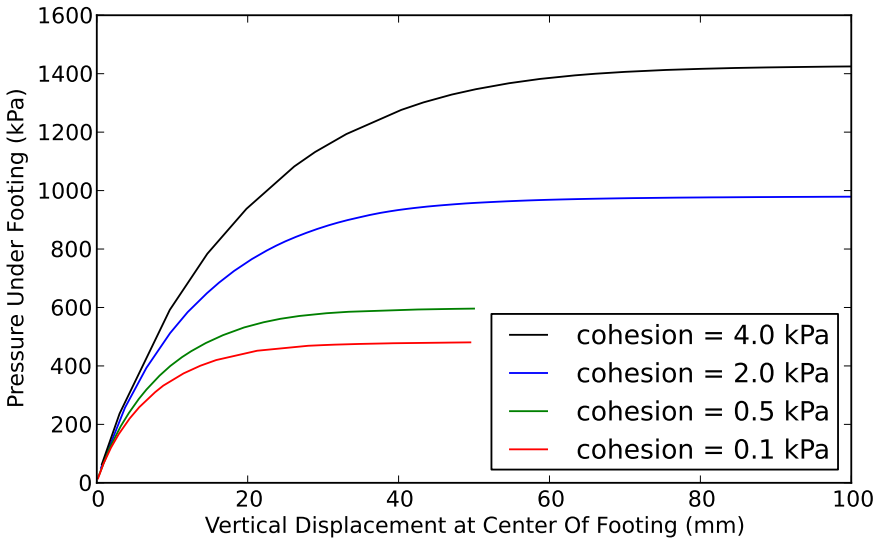

Figure 3.27: Effect of cohesion on pressure - displacement curve

3.7 Material Parameters Used In Analyses

3.7.1 Parameters Controlling Elasticity

3.7.1.1 Poisson's Ratio

As summarized in Das (2007), Trautmann and Kulhavy (1987) provided the approximation presented in Equation 3.17 for drained Poisson's ratio as a function of drained friction angle in the triaxial compression test.

$$\nu = 0.1 + 0.3\left(\frac{\phi_t - 25^\circ}{45^\circ - 25^\circ}\right) \tag{3.17}$$

Moreover, Krizek and Corotis (1975) showed that although the magnitude of Poisson's ratio depends on the confining pressure and the level of major principal stress, the range of variation of Poisson's ratio for these parameters for a given soil is rather narrow. Therefore, for simplicity, effect of variance of Poisson's ratio with depth is not taken into account.

In this study, Poisson's ratio is selected according to Equation 3.17 for the given internal friction angles experiment manual, which are presented in Section 2.6. Obtained values for Poisson's ratio from Equation 3.17 are presented in description of each analysis in Chapter 5.

3.7.1.2 Modulus of Elasticity

Modulus of elasticity is found according to Hooke's law of isotropic elasticity (Das, 1997) via its relationship between Poisson's ratio and shear modulus presented in Equation 3.18 .

$$E = \frac{2G}{1+\nu} \tag{3.18}$$

Elasticity modulus is obtained via shear modulus since vast amount of relationships are found in literature, which considers effects of relative density, confining pressure, and strain magnitude for shear modulus. A number of these relationships are summarized by Ishihara (1996).

3.7.1.3 Shear Modulus

Ishihara (1996) has summarized a number of relationships for shear modulus in literature which consider effects of relative density, confining pressure, and strain magnitude.

Small Strain Shear Modulus

Among relationships summarized by Ishihara (1996), relationship by Kokusho (1980) is selected for finding small strain stiffness in this study, since it is based on tests conducted on Toyoura sand. Kokusho (1980) conducted cyclic triaxial tests on saturated Toyoura sand with various void ratios and confining pressures and measured shear modulus. As a result of conducted tests for shear strain magnitude of 10^{-6}, Kokusho (1980) has obtained relationship presented in Equation 3.19 for shear modulus, depending on void ratio and confining pressure. In this equation $G_\circ$ is the small strain shear modulus, e is the void ratio and σ_c is the confining pressure. Void ratio to be used in this equation is found from its relationship with minimum and maximum dry densities ($\delta_{min}, \delta_{max}$), specific gravity of solid particles (G_s) and relative density (RD) provided by experiment manual. These relationships are presented in Equation 3.20.

$$G_\circ = 840\frac{(2.17-e)^2}{1+e}(\sigma_c')^{1/2} \tag{3.19}$$

$$e = e_{max} - RD(e_{max} - e_{min}) \tag{3.20a}$$

$$\delta_{max} = \frac{G_s}{1+e_{min}} \tag{3.20b}$$

$$\delta_{min} = \frac{G_s}{1+e_{max}} \tag{3.20c}$$

Based on Figure 3.28 by Wicaksono et al. (2008), which shows normalized small strain shear modulus with respect to a pressure index on log-log scale for triaxial tests run on dry and saturated samples, it is concluded that saturation has small effect on small strain shear modulus. Therefore, although soil medium modeled in this study is air-dried and Equation 3.19 is obtained from tests on saturated specimens, Equation 3.19 is employed for finding small strain shear modulus in this study.

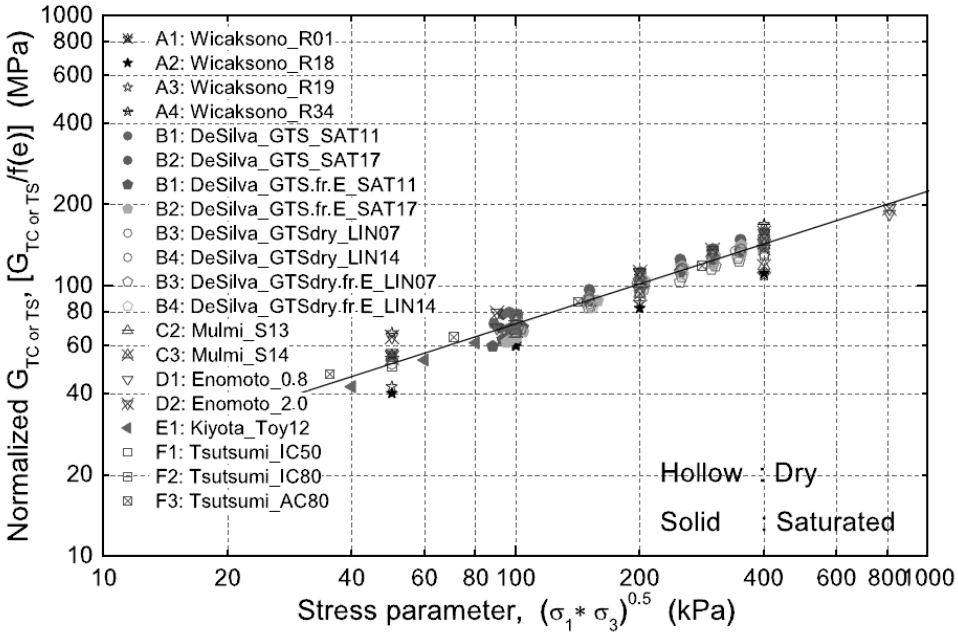

Figure 3.28: Effect of saturation on small strain stiffness, after Wicaksono et al. (2008)

As seen from Equation 3.19 shear modulus tends to increase with confining pressure. And it is mentioned in Plaxis Reference Manual (2002) that when using a constant stiffness modulus to represent soil behaviour, it is advised to choose a value that is consistent with the stress level and expected stress path. In order to achieve this, while determining the confining pressure which will be utilized for obtaining the small strain shear modulus, not only the free-field stresses, which increases linearly with depth, but also stresses due to foundation load are considered as well. Considering the effect of foundation load together with free-field stresses on confining pressure which will be experienced by the region under certain depth of the loading area, Equation 3.21 is used in obtaining σ_c for Equation 3.19.

$$\sigma_c = \left(\frac{qBL}{(B + 2z\tan 45°)(L + 2z\tan 45°)} + \gamma z \right) \frac{1 + 2K_\circ}{3} \tag{3.21}$$

Secant Shear Modulus

According to Plaxis Reference Manual (2002), using secant modulus at 50% strength is more appropriate in soil mechanics for sand compared to using initial slope. Therefore small strain shear modulus is converted to secant shear modulus by utilizing the given modulus degradation curve in the experiment manual.

Strain level for the degradation of small strain shear modulus to secant shear modulus is obtained from finite element analyses conducted with an estimated elasticity modulus. It is selected based on the average of vertical strain components of elements lying directly below the foundation at a selected load level during analysis.

Separate load levels are selected for horizontal loading analyses and vertical loading analyses. For monotonic vertical loading cases load level is selected as the load where the applied load is 50% of the ultimate bearing capacity of the soil. For monotonic horizontal loading analyses load level is selected as the instant where soil carries the full weight of the foundation model but immediately before the application of horizontal load.

Under the above mentioned conditions for all loading cases it is seen that the order of magnitude of strain level is $1\text{x}10^{-3}$. Therefore this value is used for determining secant shear modulus in all analyses cases.

3.7.2 Coefficient of At-Rest Earth Pressure

For normally consolidated soils, an approximate relationship of earth pressure at rest ($K_\circ$) with internal friction angle (ϕ) is defined by Jaky (1944) as in Equation 3.22.

$$K_\circ = 1 - sin\phi' \tag{3.22}$$

In this study coefficient of at rest earth pressure is calculated according to Jaky's formula presented in Equation 3.22.

There are a number of more recent studies in literature that questions the accuracy and suitability of Equation 3.22, such as Zhu and Michalowski (2005) which concludes that its meaningful results are coincidental. Additionally study by Guo (2010) concludes that Jaky's equation may still be considered as a reasonable representation for $K_\circ$ for granular soils statistically, even though it may not be able to reproduce the experimental data of a specific soil.

However since it is shown by Potts and Zdravkovic (2001) and Yılmaz (2004) that the coefficient of lateral earth pressure at rest has little effect on the bearing capacity of soil obtained from finite element models, Equation 3.22 is justified as suitable for this study since it is one of the most commonly used method of estimation for $K_\circ$.

3.7.3 Parameters Controlling Plasticity

3.7.3.1 Cohesion Intercept

According to given material properties in the experiment manual, soil medium is cohesionless. Therefore cohesion should not be included in the analysis. However due to the observed beneficial effect of cohesion on solving convergence problems, a small amount of cohesion, which is not more than 0.1 kPa, is added to the models. Effect of this artificial cohesion on analysis results is investigated in Section 3.6.2.

3.7.3.2 Angle of Internal Friction

Angle of internal friction values are given for the soil in the experiment manual by Fukui et al. (2005) as listed in Table 2.5. These given values are used in analyses without any modification.

For a mean effective stress of 98 kPa, Sun et al. (2008) found peak internal friction angle for Toyoura Sand with 80% relative density as 40.5°. For Toyoura sand with 80% relative density, experiment manual (Fukui et al., 2005) provides internal friction angle value as 42.1°. Therefore, it is most probable that internal friction angle values given in the test manual are the peak internal friction angles.

Loukidis and Salgado (2009) states that angle of internal friction depends on relative density, level of mean effective stress, relative magnitude of the intermediate principal stress and the direction of the principal effective stresses relative to the axis of sand deposition. The difference in values of internal friction angle between experiment manual and Sun et al.(2008) might therefore be attributed to mean effective stress magnitude the tests were conducted.

3.7.3.3 Angle of Dilation

Magnitude of this parameter is not available in the experiment manual (Fukui et al., 2005). Yılmaz (2004) has shown that the angle of dilation has significant effect on bearing capacity. Plaxis Manual (2002) states that angle of dilation is approximately 30° less than internal friction angle for quartz sands.

Analyses, the results of which are presented in Chapter 4, target associated flow rule with employment of dilation angles very close to the internal friction angle of the soil in order to be able to obtain comparable results with solutions in literature. Influence of dilation angle on analysis results is separately sought by conducting analyses aiming unassociated flow rule presented in Section 6.2.

CHAPTER 4

RESULTS AND COMPARISONS

4.1 Introduction

In this section, limit loads obtained from finite element method analyses, experiment cases of Fukui et al. (2005), and selected solutions from literature are presented. These results are compared and discussed in Section 4.5 and Section 4.6 respectively.

Before presentation of the findings, properties of the finite element analyses not mentioned in Section 3.4 such as magnitudes of material properties are presented in Section 4.2.

4.2 Details of Analyses

For all cases at least one 2D and one 3D analysis results are presented which employs the material properties presented in Table 4.1. In these analyses, although associated flow rule is aimed, angle of dilation is selected slightly lower than internal friction angle of the soil according to advice of Abaqus Documentation (2010) based on convergence considerations. Moreover, although the analysis medium is cohesionless, a magnitude of cohesion of 0.1 kPa and 0.05 kPa is introduced to monotonic vertical and horizontal cases, respectively, for easier convergence as discussed in Section 3.6.2.

For monotonic vertical loading experiments, Case 1 and Case 2, elasticity modulus is obtained from Equation 3.21 by considering the magnitude of confining pressure at 0.25 m below the foundation for vertical load corresponding to the 50% of the ultimate bearing capacity. For monotonic horizontal loading experiments, Case 3, 6 and 9, elasticity modulus is computed from the same equation for the confining pressure immediately below the foundation before

application of horizontal loading. Poisson's ratio and coefficient of at rest earth pressure for all analyses are selected as described in Section 3.7.

Table 4.1: Material Properties Employed in Analyses

Experiment	ϕ	ψ	c	γ	E	ν	$K_\circ$
Case 1	42.1°	39°	0.1kPa	16.02kN/m^3	65,831.45kPa	0.3565	0.330
Case 2	39.9°	37°	0.1kPa	15.39kN/m^3	41,641.6kPa	0.3235	0.359
Case 3	42.1°	39°	0.05kPa	16.02kN/m^3	34,629.1kPa	0.357	0.330
Case 6	42.1°	39°	0.05kPa	16.02kN/m^3	34,246.7kPa	0.357	0.330
Case 9	39.9°	37°	0.05kPa	15.39kN/m^3	29,783.2kPa	0.324	0.359

Table 4.2 presents height of center of gravity and loading point from foundation base, together with the model weight employed in analyses. Center of gravity and horizontal load application points of low pier model lie 427 mm and 900 mm above foundation base, respectively. Actual model weight is 8.728 kN. In 3D analyses which employs low pier model, since half of the foundation is modeled due to symmetry, 4.364 kN is employed as model weight. In 2D analyses since foundation length is assumed as 1 m which is double of the actual length, 17.456 kN is employed as model weight. Similarly, center of gravity and horizontal load application points of high pier model lie 700 mm and 1300 mm above foundation base respectively. Actual model weight is 8.924 kN. In 3D analyses since half of the foundation is modeled due to symmetry, 4.462 kN is employed as model weight. In 2D analyses since foundation length is assumed as 1 m which is double of the actual length, 17.848 kN is employed as model weight.

Table 4.2: Model Weights Employed in Monotonic Horizontal Loading Analyses

Experiment	Dimension	Model Type	H_{CoG}	H_{LP}	Model Weight
Case 3	3D	High Pier	700mm	1300mm	4.462kN
Case 3	2D	High Pier	700mm	1300mm	17.848kN
Case 6	3D	Low Pier	427mm	900mm	4.364kN
Case 6	2D	Low Pier	427mm	900mm	17.456kN
Case 9	3D	Low Pier	427mm	900mm	4.364kN
Case 9	2D	Low Pier	427mm	900mm	17.456kN

H_{CoG}, H_{LP}: Height of center of gravity and horizontal load application points of foundation models with respect to foundation base

Table 4.3 presents friction coefficients employed in analyses, for the contact interaction be-

tween foundation and soil. Frictional behavior of the interface is modeled to obey Coulomb friction law as described in 3.3.4.1. Rough interface is modeled by setting the friction coefficient equal to tangent of internal friction angle of the soil, considering the bottom surfaces of the actual foundation models were covered with sand paper.

Table 4.3: Friction Coefficients Employed for Soil Foundation Interface in Monotonic Horizontal Loading Analyses

Experiment	ϕ	μ
Case 3	42.1°	0.90357
Case 6	42.1°	0.90357
Case 9	39.9°	0.83613

4.3 Results of Experiments

4.3.1 Monotonic Centered Vertical Loading Cases

Figure 4.1 presents the results of centered vertical loading experiments Case 1 and Case 2 by Fukui et al. (2005).

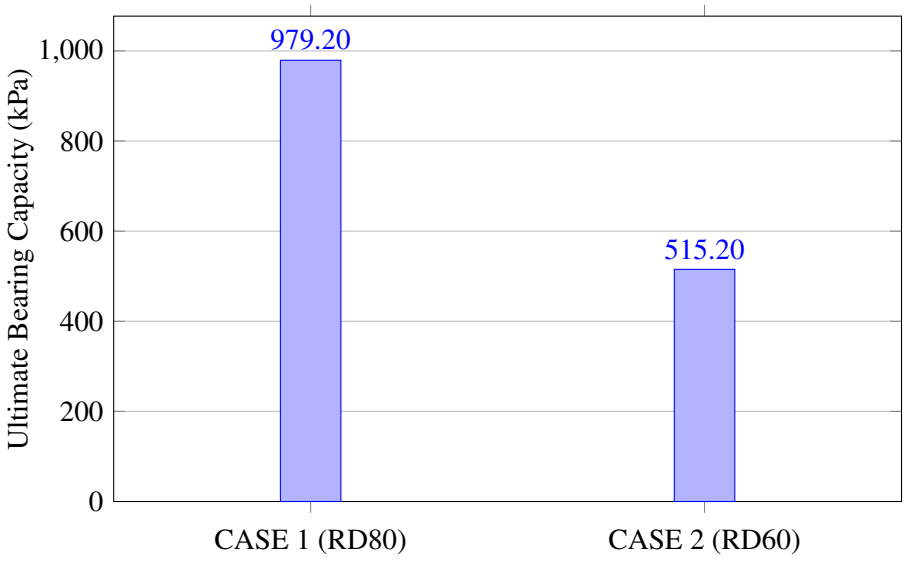

Figure 4.1: Results of Monotonic Vertical Loading Experiments

4.3.2 Monotonic Horizontal Loading Cases

4.3.2.1 Tilt Angle and Sliding

From the test recordings for vertical displacement of the foundation tilt angles are calculated for each data point. Then the horizontal displacement of the loading point is calculated according to the found tilt angle. Afterwards the difference of recorded displacement of loading point and calculated displacement is found, and named as the sliding of the model.

Among obtained tilt angles, tilt angle corresponding to maximum pressure is named as tilt angle at maximum pressure. From tilt angle at maximum pressure, horizontal displacement of the center of gravity is calculated, which is employed in calculation of second order moments. These values for monotonic horizontal loading analyses are presented in Table 4.4 and Table 4.5.

Table 4.4: Tilt Angle and Sliding of the Models At Ultimate Load Capacity and At The End of Loading

	Tilt Angle (°)		**Sliding (mm)**	
Test Name	**At Maximum Pressure**	**Maximum Tilt Angle**	**At Maximum Pressure**	**Maximum Sliding**
Case 3	1.04	3.98	1.30	7.40
Case 6	0.84	5.28	1.83	17.90
Case 9	0.89	4.85	14.02	76.41

Table 4.5: Sway of Center of Gravity at Maximum Test Load, and at Maximum Tilt Angle

	Sway of Center of Gravity (mm)	
Test Name	**At Maximum Pressure**	**At Maximum Tilt Angle**
Case 3	12.78	49.00
Case 6	6.31	39.90
Case 9	6.66	36.33

4.3.2.2 Ultimate Loads

Figure 4.3.2.2 presents the results of horizontal loading experiment cases Case 3, Case 6 and Case 9 by Fukui et al. (2005).

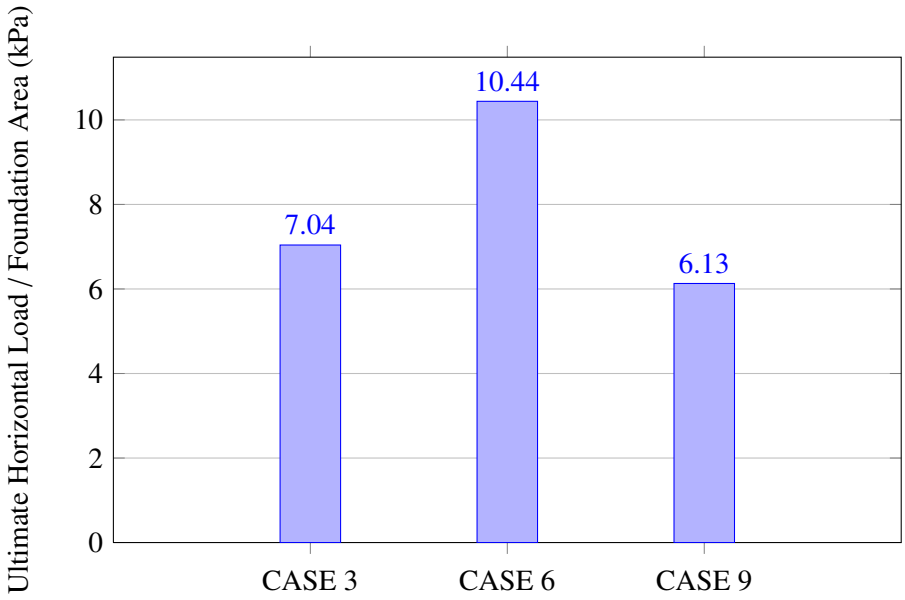

Figure 4.2: Results of Monotonic Horizontal Loading Experiments

4.4 Results of Selected Solutions in Literature

In this section, estimates to the plastic limit loads by solutions in literature are presented for the monotonic experiment cases conducted by Fukui et al. (2005). Results of selected solutions are presented in order to compare with analyses results of this study together with the experimental findings of Fukui et al. (2005).

4.4.1 Monotonic Vertical Loading Cases

Solutions for the ultimate vertical load of monotonic vertical loading experiments could be obtained from bearing capacity equations available in literature. In this section, equations proposed by Terzaghi (1943), Meyerhof (1961) and Vesic (1973) will be utilized. Additionally shape factors for square foundations proposed in studies by Zhu and Michalowski (2005) and

Lyamin et al. (2007) will be employed with the exact bearing capacity factor calculated by Martin (2005) for rough and strip foundation.

Table 4.6 shows the parameters supplied to analytical solutions for obtaining the results presented in this section. In this table B, L and D are the foundation dimensions of breadth, length and depth, respectively; ϕ and c are the Mohr-Coulomb model parameters, angle of internal friction and cohesion; finally, γ is the unit weight of the soil.

Table 4.6: Input parameters supplied to solutions in literature

Experiment	**B**	**L**	**D**	$\boldsymbol{\phi}$	**c**	$\boldsymbol{\gamma}$
Case	**(m)**	**(m)**	**(m)**	**(°)**	**(kPa)**	$\boldsymbol{kN/m^3}$
Case 1	0.50	0.50	0.0	42.1°	0.0	16.02
Case 2	0.50	0.50	0.0	39.9°	0.0	15.39

Figure 4.3 and Table 4.7 presents results of available solutions in literature. Figure 4.4 and Table 4.8 presents results only for studies among these solutions which propose shape factor s_γ greater than unity for square shaped foundations.

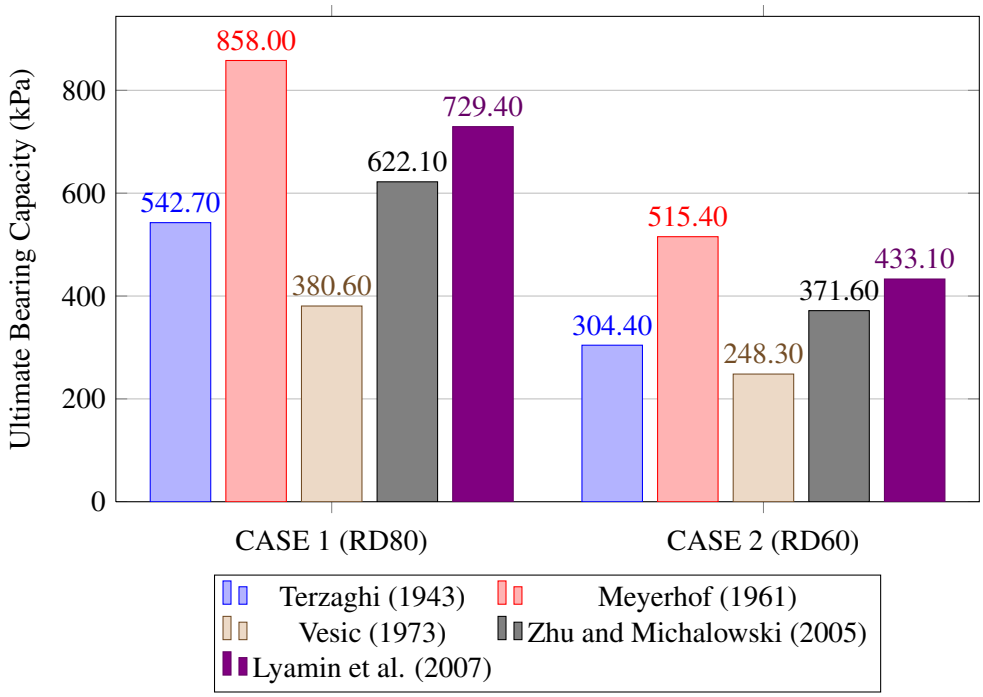

Figure 4.3: Results of Solutions In Literature for Monotonic Centered Vertical Loading Cases

Table 4.7: Results of Solutions in Literature for Monotonic Centered Vertical Loading Cases

Solution	**Case 1**			**Case 2**		
	N_γ	s_γ	q_{ult}	N_γ	s_γ	q_{ult}
Terzaghi (1943)	169.4	0.80	542.7	98.9	0.80	304.4
Meyerhof (1961)	142.2	1.51	858.0	91.9	1.45	515.4
Vesic (1973)	158.4	0.60	380.6	107.5	0.60	248.3
Zhu and Michalowski (2005)	128.7	1.21	622.1	83.96	1.15	371.6
Lyamin et al. (2007)	128.7	1.41	729.4	83.96	1.34	433.1
Average	145.5	1.11	626.6	93.24	1.07	374.6
Standard Deviation	18.12	0.39	181.45	10.12	0.36	105.04

For Zhu and Michalowski (2005) and Lyamin et al. (2007) exact value of N_γ by Martin (2005) is employed.

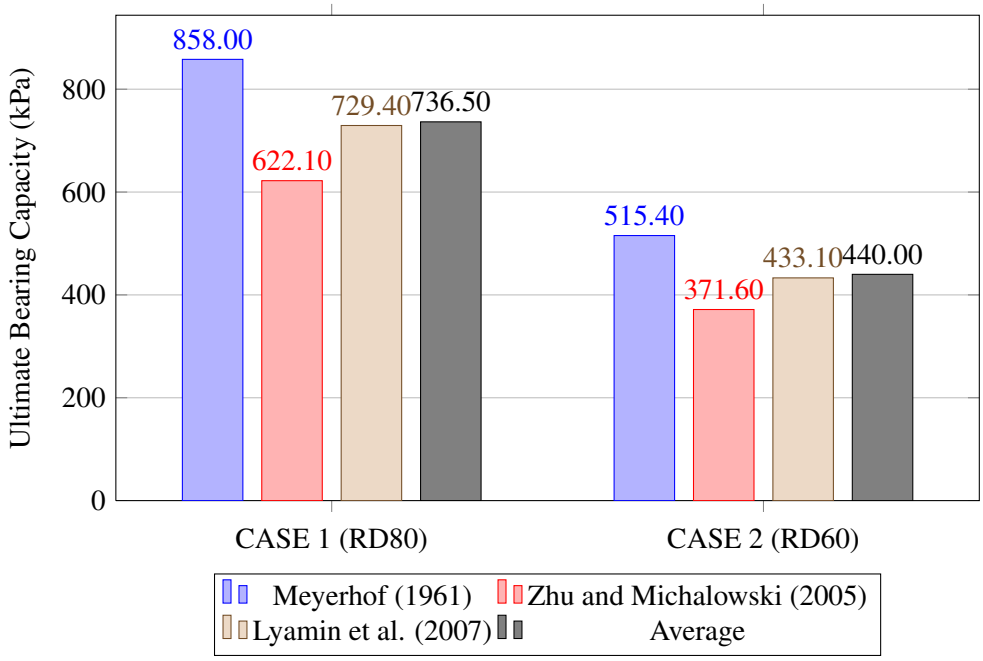

Figure 4.4: Results of solutions in literature for monotonic centered vertical loading cases with shape factor greater than unity

Table 4.8: Results of solutions in literature for monotonic centered vertical loading cases with shape factor greater than unity

Solution	**Case 1**			**Case 2**		
	N_γ	s_γ	q_{ult}	N_γ	s_γ	q_{ult}
Meyerhof (1961)	142.2	1.51	858.0	91.9	1.45	515.4
Zhu and Michalowski (2005)	128.7	1.21	622.1	83.96	1.15	371.6
Lyamin et al. (2007)	128.7	1.41	729.4	83.96	1.34	433.1
Average	133.2	1.38	736.5	86.61	1.3	440.0
Standard Deviation	7.8	0.15	118.1	4.58	0.2	72.2

For Zhu and Michalowski (2005) and Lyamin et al. (2007) exact value of N_γ by Martin (2005) is employed.

It is seen from Figure 4.3 that Meyerhof (1961), Zhu and Michalowski(2005), Lyamin et al. (2007) provides considerably higher results than Terzaghi (1943) and Vesic (1973). Major reason of this is the significant difference between shape factors employed in the equations. For example, shape factors provided for square foundations of Terzaghi's and Vesic's bearing capacity equations are given as constants with values of 0.8 and 0.6, respectively; whereas according to Meyerhof this value depends on the internal friction angle of soil and is 1.51 and 1.45 for internal friction angles of Case 1 and Case 2 respectively. In this case, Meyerhof's proposal indicates that bearing capacity of square foundations are higher compared to strip foundations, whereas Terzaghi's and Vesic's proposals indicate the opposite.

Zhu and Michalowski (2005) commented on this issue and stated that, these proposals for the shape factors are based on empirical or semiempirical considerations leading to conflicting results. As summarized by Zhu and Michalowski (2005), shape factors proposed by Terzaghi (1943) for square footings were based on the tests of Golder (1941) together with some unpublished data. As stated by Zhu and Michalowski (2005), the results of Golder (1941) had a large scatter, and Terzaghi disregarded the scatter and took only the most unfavorable test result as a basis for establishing a provisional equation. Zhu and Michalowski (2005) continued that based on the very same experiments, Golder (1941) concluded that the footing length does not influence the bearing capacity.

On the other hand, Loukidis and Salgado (2009) commented on this issue as well, by stating that, although in reality the bearing capacity of square and circular footings with zero embedment is smaller than the bearing capacity of strip footings, theoretical methods assuming simple Mohr Coulomb failure criterion suggests the opposite, with reasoning that, as pointed out by Meyerhof and discussed by other studies, peak friction angle of sand is lower in near triaxial conditions (square and circular footings), than in plane strain conditions (strip footings). Loukidis and Salgado (2009) further reminds the suggestion of Meyerhof, on internal friction angle to be used for bearing capacity calculation of strip foundations, that internal angle of friction should be increased by 10% if it is obtained under triaxial loading conditions.

Considering the experiment results of Fukui et al. (2005), and analyses of this study, only the results of equations providing shape factor s_γ greater than unity are included in the comparison presented in Section 4.5.

4.4.2 Monotonic Horizontal Loading Cases

Solution for the ultimate horizontal load of monotonic horizontal loading experiments conducted by Fukui et al. (2005) could be obtained from combined vertical loading equations for shallow foundations, and from seismic bearing capacity equations by neglecting inertia effects. Four studies are selected from literature for the comparison: Meyerhof (1951, 1963) is the conventional solution based on effective width rule and inclination factor; Paolucci and Pecker (1997) is an analytical upper bound solution based on kinematic approach of yield design theory; Loukidis et al. (2008) is a numerical study based on finite element method; and finally, Butterfield and Gottardi (1994) is an experimental study conducted on scaled laboratory models.

Input parameters supplied to studies are presented in Table 4.9. In this table V_{ult} is ultimate monotonic vertical load bearing capacity of foundation obtained from Case 1 and Case 2 test results of Fukui et al. (2005), V is the weight of the foundation model - which was the only vertical load acting on the foundation, Δx_{CoG} is the component of horizontal displacement of the center of gravity due to tilt obtained from Table 4.5, M_{arm} is signifying the moment arm which is the height of horizontal load application point from foundation base, B is the foundation breadth, and finally Φ, c and γ are the angle of internal friction, cohesion intercept and unit weight of the soil respectively. Moment acting on foundation (M) is calculated according to Equation 4.1 which considers moment due to applied horizontal test loading (H) and second order moments developed due to tilt of the foundation. Table 4.10 and Figure 4.5 presents the results obtained from these studies.

Table 4.9: Input parameters supplied to solutions in literature

Experiment	V_{ult}	V	Δx_{CoG}	M_{arm}	**B**	ϕ	**c**	γ
Case	**(kN)**	**(kN)**	**(cm)**	**(m)**	**(m)**	**(°)**	**(kPa)**	kN/m^3
Case 3	244.8	8.924	1.28	1.3	0.5	42.1	0.0	16.02
Case 6	244.8	8.728	0.63	0.9	0.5	42.1	0.0	16.02
Case 9	128.8	8.728	0.67	0.9	0.5	39.9	0.0	15.39

$$M = HM_{arm} + V\Delta x_{CoG} \tag{4.1}$$

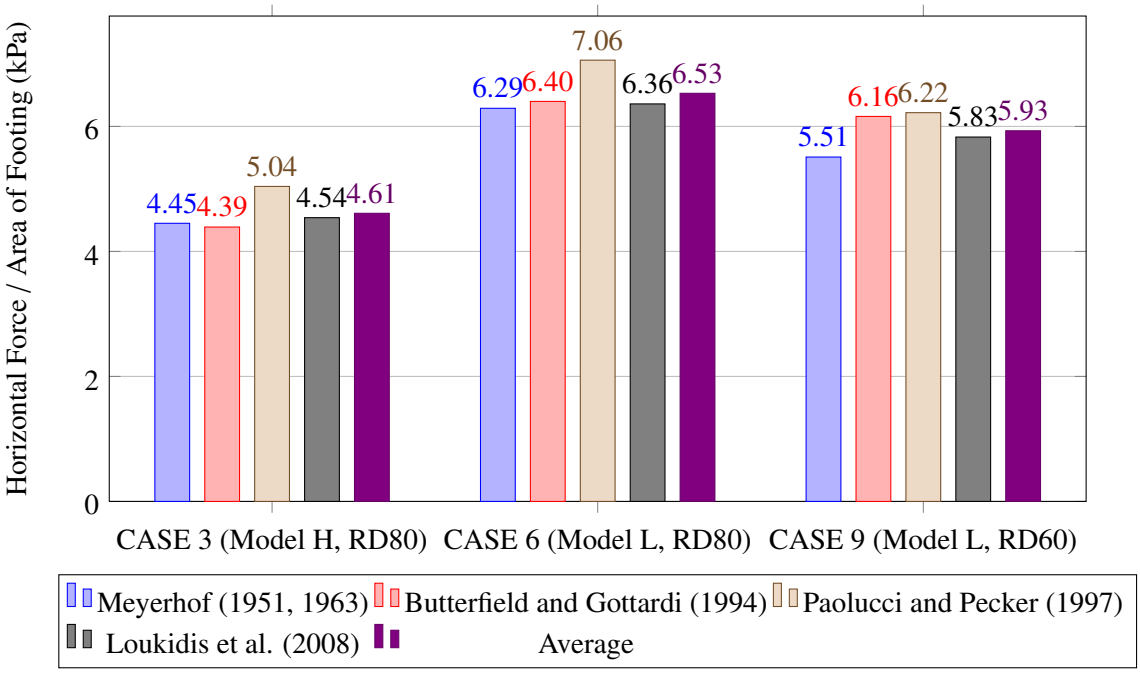

Figure 4.5: Results of Solutions in Literature for Monotonic Horizontal Loading Cases

Table 4.10: Results of Solutions in Literature for Monotonic Horizontal Loading Cases

Solution	**Case 3 (kPa)**	**Case 6 (kPa)**	**Case 9 (kPa)**
Meyerhof (1951, 1963)	4.45	6.29	5.51
Butterfield and Gottardi (1994)	4.39	6.40	6.16
Paolucci and Pecker (1997)	5.04	7.06	6.22
Loukidis et al. (2008)	4.54	6.36	5.83
Average	4.61	6.53	5.93
Standard Deviation	0.30	0.36	0.33

4.5 Results of Analyses and Comparisons

In this section, results of three dimensional analyses of this study are presented in a comparative manner with the experimental findings of Fukui et al. (2005) and average of solutions in literature; both of which were previously presented in Section 4.3 and Section 4.4, respectively.

Only three-dimensional finite element analysis results of this study are included in this comparison, considering they simulate the experiment conditions more realistically than the 2D analyses, whereas 2D and 3D analysis results are compared in Section 6.3.

4.5.1 Monotonic Vertical Loading Cases

Figure 4.5.1 presents the limit plastic loads obtained from three dimensional analyses of this study with the mean of selected solutions in literature and experimental findings of Fukui et al. (2005). In Table 4.11 normalized magnitudes of analyses results, and results of solutions in literature with respect to experimental findings are presented.

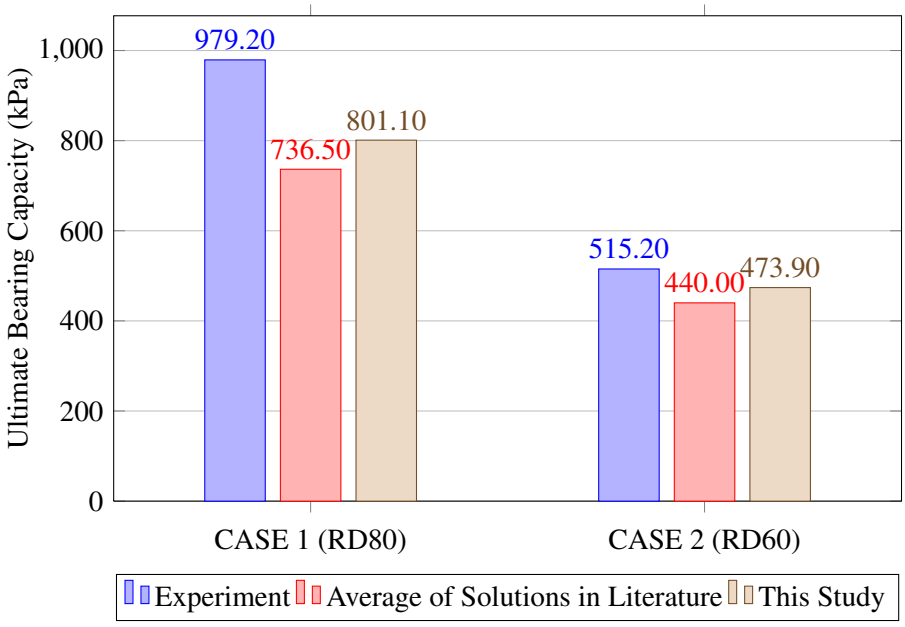

Figure 4.6: Comparison of Monotonic Vertical Loading Results

Table 4.11: Ultimate bearing capacities provided by monotonic vertical loading tests by Fukui et al. (2005), solutions in literature and 3D FEM analyses

Experiment Case	Exp. (kPa)	Lit. (kPa)	T.S. (kPa)	Lit. / Exp.	T.S. / Exp.
Case 1	979.2	736.5	801.1	0.75	0.82
Case 2	515.2	440.0	473.9	0.85	0.92

Exp.: Experiment by Fukui et al. (2005)
T.S.: This Study
Lit.: Average of solutions in literature with shape factor greater than unity, calculated in Section 4.4.1

4.5.2 Monotonic Horizontal Loading

4.5.2.1 Ultimate Loads

Figure 4.5.2.1 and Table 4.12 presents the limit plastic loads obtained from three dimensional analyses of this study in a comparative manner with the mean of solutions in literature and experimental findings of Fukui et al. (2005).

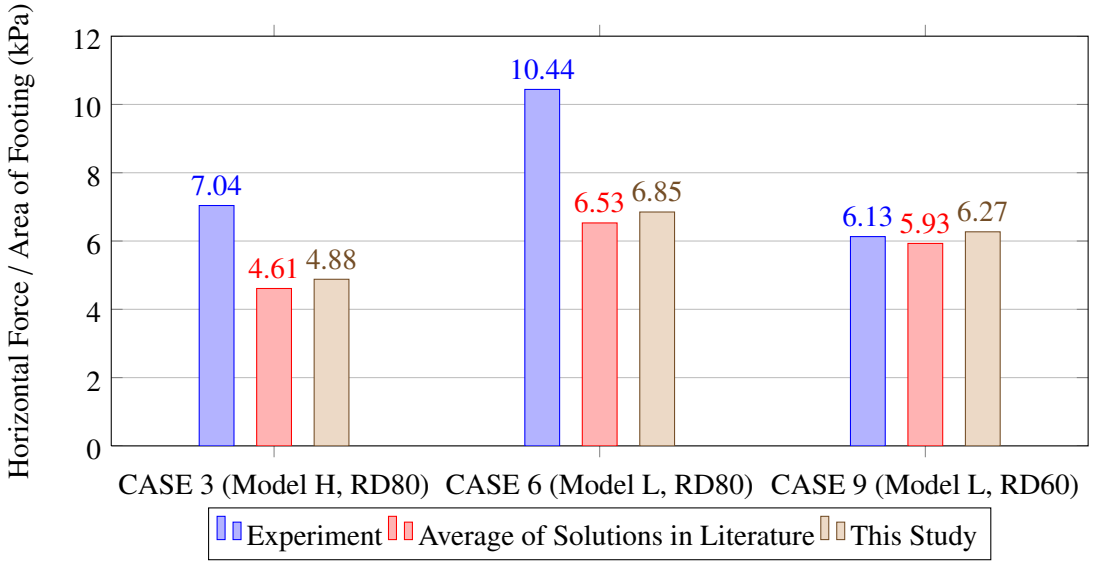

Figure 4.7: Comparison of Monotonic Horizontal Loading Results

Table 4.12: Comparison of Monotonic Horizontal Loading Results

Experiment Case	Exp. (kPa)	Lit. (kPa)	T.S. (kPa)	Lit. / Exp.	T.S. / Exp.
Case 3	7.04	4.61	4.88	0.65	0.69
Case 6	10.44	6.53	6.85	0.63	0.66
Case 9	6.13	5.93	6.27	0.97	1.02

Exp.: Experiment by Fukui et al. (2005)
T.S.: This Study
Lit.: Average of solutions in literature calculated in 4.4.2

4.6 Discussion of Results

4.6.1 Monotonic Vertical Loading

Finite element method analyses of monotonic centered vertical loading experiment cases Case 1 and Case 2, carried on by Fukui et al. (2005), are conducted; and results of selected solutions in literature for the ultimate loads of these experiment cases are calculated. Analyses provided lower bearing capacities than experiment measurements. There are 18% and 8% difference between analysis and experiment results of Case 1 and Case 2 experiments cases respectively. These cases differ only in the relative density of the Toyoura sand employed as foundation soil. Such that, for Case 1 80% relative density is employed, whereas for the Case 2 foundation soil had 60% relative density.

It is known that finite element method analyses for vertical bearing capacity problems approach true solution from above, hence smaller and more accurate solutions for bearing capacity problems are achieved with increasing mesh refinement (Zhu and Michalowski, 2005). Therefore, further increase in mesh refinement would not contribute to closing the gap between analysis and experiment results.

There are a number of simplifications and assumptions employed in construction of finite element method models of this study. By excluding the items concerning material model, these points could be listed as follows: i) rough soil - foundation interface idealization, ii) employment of dilation angle close to internal friction angle, iii) taking gravitational acceleration as 10 m/s^2 instead of its actual value (9.8 m/s^2) in unit weight calculation of the soil iv)

employment of artificial cohesion for computational efficiency, v) employment of automatic stabilization mechanism for computational efficiency.

Considering (i), Potts and Zdravkovic (2001) showed that for finite element analyses of strip foundation, employment of rough footing idealization results in significantly higher bearing capacities (almost 100% greater for the case presented by them) than the smooth footing idealization. Even though sand paper was glued at foundation base for the experiment cases (Fukui et al., 2005) it is unlikely that this idealization is fully achieved in experiments, hence this idealization is expected to introduce an error, on the side of increasing the analysis results.

Considering (ii), it is well known that dilation angle of frictional soils is significantly lower than internal friction angle (Randolph et al. 2004; Loukidis et al. 2008). As presented in Section 6.2.1 for analyses conducted in this study, as dilation angle increases ultimate bearing capacity obtained from analyses increases. Significance of dilation angle on limit loads provided by finite element method analyses on vertical bearing capacity problems is recognized by Yılmaz (2004) and Loukidis and Salgado (2009) as well. Although it is considered as less significant by Potts and Zdravkovic (2001) and Randolph et al. (2004), there is consensus on the increase in bearing capacity with the increase in dilation angle. Since employed dilation angle values are higher than their true value in the simulations conducted in this study, this point is expected to introduce an error on the side of increasing the analysis results. Hence, employment of dilation angles more representative of the actual experiment conditions would not contribute to closing the gap between analysis and experiment results.

Considering (iii), it is well known that bearing capacity increases as the unit weight increases for frictional soils. By employing gravitational acceleration higher than its precise value, obtained unit weight from unit density is higher than its actual value. Therefore introduced error is on the side of increasing the analysis results.

As for (iv) and (v), effect of these points were studied in Section 3.6 and it is concluded that these points introduce errors on the side of increasing the analysis results.

It is seen that these listed assumptions and simplifications have provided errors that lie on the side of increasing the results of the analyses. Accordingly, it would normally be expected that the analysis results should have been higher than the experiment results. Since analysis results are lower than the experiment results, by considering that the analysis approach has

been verified with solution by Cox (1962) as presented in Section 3.5.1, it could be inferred that the only point which could be responsible for the difference should be connected to the material model, and material parameters employed for defining plasticity.

Loukidis and Salgado (2009) states that there are certain aspects of bearing capacity problem, which are not considered by traditional approaches, that stem mainly from dependence of the internal friction angle on a number of factors. Factors influencing the magnitude of internal friction angle, within the context of bearing capacity problems, are stated as follows: "ϕ depends on a number of variables that evolve continuously during the footing loading process: the relative density, D_R, the level of mean effective stress p, the relative magnitude of the intermediate principal effective stress (stress induced anisotropy) and the direction of the principal effective stresses relative to the axis of sand deposition (fabric induced anisotropy)."

Siddiquee (2001), regarding the limitations of traditional approaches, states the following factors as well: highly non-linear strain-hardening and softening stress-strain behavior, shear banding with a specific shear band width as a function of the particle size of the test material.

Employed linear elastic perfectly plastic material model with Mohr Coulomb failure criterion in the simulations of this study, being a simple model which only requires internal friction angle, cohesion intercept and dilation angle as the parameters to define behavior of plasticity, does not take into account any of these conditions listed by Loukidis and Salgado (2009) and Siddiquee (2001).

Employment of a more advanced material model in simulations to consider these phenomena may provide closer results to the experiments. Alternatively, better results could be obtained by employing a higher internal friction angle considering that the majority of the phenomena listed by Loukidis and Salgado (2009), influence the magnitude of internal friction angle. Since the results of experiments are higher than analysis results of this study, it could be judged that internal friction angles employed in analyses were lower than their representative values for the experiment conditions of these listed phenomena. This suggestion would justify the significant difference between the error levels for Case 1 and Case 2, with reasoning that internal friction angle for Case 2 is better selected than that for Case 1 in the analyses. Solutions in literature support this condition as well, such that, Case 2 result is better predicted than Case 1 result, with error levels of 15% and 25% respectively.

4.6.2 Monotonic Horizontal Loading

4.6.2.1 Ultimate Loads

Finite element method analyses of monotonic horizontal loading experiment cases Case 3, Case 6 and Case 9, carried on by Fukui et al. (2005), are conducted; and results of selected solutions in literature for the ultimate loads of these experiment cases are calculated. For all experiment cases, results obtained from solutions in literature are in good agreement among themselves and with finite element method analyses conducted in this study. It is worth to note that selected solutions in literature include the solution by Butterfield and Gottardi (1994) which is based on laboratory model experiment results similar to the experiments modeled in this study. Among all experiment cases, there is at most 6% difference between analysis results and the arithmetic mean of the selected solutions from literature. Likewise, for all cases there is at most 9% difference between an individual solution and arithmetic mean of solutions.

Three experiment cases, namely Case 3, Case 6 and Case 9 were conducted as monotonic horizontal loading experiments. Relative density of the foundation soil (80% or 60%) and the foundation model employed (high pier or low pier model) are the differences among these cases.

Relative density of soil on which the experiments were conducted is found to have a high effect on conformation of experiment results with analysis results. For example, Case 3 and Case 6 are conducted on sand with 80% relative density and experiment results for these cases are 31% and 34% higher than the analysis results, respectively. Case 9 is conducted on sand with 60% relative density and experiment result is 2% lower than the analysis result. In contrast, foundation model type does not have significant effect on conformation of the experiment results with analysis results. For instance, while Case 3 and Case 6 are conducted on sand with the same relative density, Case 3 employed high pier model and Case 6 employed low pier model. Analyses of both of these cases have provided similar performance regarding conformation with experiment results. This indifference between error levels with respect to employed foundation model, at a first glance, might be considered to indicate that analyses had successfully captured the influence of moment to base shear ratio difference introduced in experiments due to employment of different foundation models.

In order to reason the strong relationship between relative density of foundation soil and conformation of analysis results with experiment results, centered vertical loading cases Case 1 and Case 2 could be considered. Although not as significant as observed for the monotonic horizontal loading cases, the relationship between relative density and conformation of analysis results with experiment results has been seen for monotonic vertical loading experiment cases as well. Such as, centered vertical loading cases, Case 1 and Case 2 were conducted on 80% and 60% relative density sand respectively. Experiment result of Case 1 and Case 2 were 18% and 8% higher than the analysis result respectively. There is an additional similarity, considering centered vertical and horizontal loading analyses, all experiment cases on foundation soil with 60% relative density has better conformation with analysis results than the experiment cases on sand with 80% relative density.

These similarities are significant since the same yield criterion, flow rule and magnitudes of internal friction and dilation angles are employed in both horizontal and vertical loading analyses. Additionally, while discussing the results of monotonic centered vertical loading analyses, difference of experiment and analysis results were concluded as connected to material model and employed parameters; more specifically, selection of internal friction angle representative for the factors of which were not considered by the employed material model in analyses. Therefore, it may be expected that a similar condition would govern the error levels in monotonic horizontal loading cases as well. Mentioned observed similarity of better conformance of analysis results with experiment cases on 60% relative density foundation soil encourages this expectation.

On the other hand, assuming that internal friction angles presented in experiment manual (employed in analyses as well) are measured under identical conditions, such as under same mean effective stress, it is unlikely that an unaccounted phenomenon in analyses to increase the errors in results of cases on sand with 80% relative density (Case 3 and Case 6), and diminish the errors for case on sand with 60% relative density (Case 9). Moreover, increase of error level of horizontal loading cases with respect to centered vertical loading case (from -18% to -31%) for cases on 80% relative density, whereas decrease of error level of horizontal loading case with respect to centered vertical loading case (from -8% to +2%) for 60% relative density questions this logic as well, since overall influence of the unaccounted factors are not expected to change side for the experiments which have similar stress levels such as Case 6 and Case 9.

Additionally, studies in literature are in very good agreement with each other and analyses conducted in this study. It should be emphasized that experiment results are not in harmony with results from Butterfield and Gottardi (1994) as well. This is significant since, that study is based on laboratory experiment data; therefore, does not share the same shortcomings discussed in Section 4.6.1, which are common for the analysis of this study and the rest of the selected studies in literature based on method of characteristics or plasticity limit solutions that inherently employ Mohr-Coulomb failure criterion with associated flow rule. Furthermore, Butterfield and Gottardi (1994) does not depend on the internal friction angle of the soil; instead, it provides results according to the centered vertical bearing capacity of foundation. Therefore, phenomena listed in Section 4.6.1 or adequateness of selected internal friction angle are not likely the factors that govern the difference between analysis and experiment results.

Although it is expected to have certain difference between the experiment and analysis results, especially due to the employed simple material model; high magnitude of the difference between the analysis and experiment results, and broad variation of this difference among experiment cases could not be reasoned in this section. Therefore, it is possible that an unconsidered factor is governing the difference between experiment and analysis results. Hence, good agreement of Case 9 with analysis results, or observation made on insignificance of employed foundation model on conformation of experiment and analysis results might not have value. Finally, conditions that might be responsible for this difference are investigated in Chapter 5.

CHAPTER 5

ASSESSMENT OF DIFFERENCES IN RESULTS

5.1 Introduction

In Section 4.6.2.1 it is stated that there might be another factor, which could not be explained with the results presented in Chapter 4, influencing the errors in analyses with respect to experiment results of monotonic horizontal loading cases. Reason of inferring such a condition could loosely be restated as the significant difference between error levels of Case 9 with respect to Case 3 and Case 6. As shown in Figure 4.5.2.1, Case 3 and Case 6 experiment results are significantly higher than the analysis results and results of solutions in literature, whereas experiment result of Case 9 is in very good agreement with both.

Two possible conditions are evaluated in this chapter to explain this observation. First condition considers the difference is connected to possible contribution of side face of the foundation in horizontal load bearing as the result of significant rotation. Considering Case 3 and Case 6 experiments were conducted on denser sand than that of Case 9, higher horizontal load capacities are obtained from these experiments. Consequently, higher angles of rotations, as the result of higher horizontal load capacities together with higher resistance to deformation, are expected to occur for these cases. Validity of this condition is evaluated in Section 5.2.

The other condition is connected to the note by Fukui et al. (2005) that vertical load readings of load cells placed under the footing base indicate eccentric application of model weight on sand even before the beginning of horizontal load application. Direction of the reported eccentricity has the opposite sign with eccentricity introduced with horizontal load application in Case 3 and Case 6, whereas it has same sign for Case 9. Therefore, side of the eccentricity is adequate for all experiments such that it could explain the high experiment results for Case

3 and Case 6. Reason of this initial eccentricity and its influence on experiment results are investigated in Section 5.3.

5.2 Contribution of Foundation Side Face to Load Bearing As a Result of Significant Rotation

Ultimate horizontal load capacities provided by experiments conducted by Fukui et al. (2005) for Case 3 and Case 6 analyses are considerably higher than results obtained from analyses in this study or solutions in literature. One explanation of this difference might be the contribution of side face of the foundation in load bearing. This condition is investigated in this section, for the instant where maximum horizontal load is applied to the foundation model. Shear force recorded by load cells attached to the bottom face of the footing is compared with the expected base shear according to the horizontal load applied at loading point of the model, and tilt angle of the foundation at that instant. It is concluded that side face of the foundation has not made noticeable contribution to load bearing, since recorded base shear is not lower than the shear expected according to the applied horizontal load.

Figure 5.1 shows base shear recorded throughout the experiments with applied horizontal test loading for monotonic horizontal loading cases of Case 3, Case 6 and Case 9. In these figures, portion of the curves corresponding to the loading zone is shown with different color to indicate where the loading starts. It is seen from this figure that the base shear is not zero before beginning of the experiment. After employing zero compensation procedure, described by Fukui et al. (2005) to correct this error (i.e., deducting a value from all data points to set initial data point equal to zero), values of base shear corresponding to maximum test loading is found as in Table 5.1.

In addition to the horizontal force applied at loading point of the foundation model, base shear additionally depends on the weight and the angle of rotation of the foundation. This is demonstrated with the free body diagram of the foundation model presented in Figure 5.2. Equilibrium equations that satisfy the conditions of rigid body equilibrium for this free body is presented in Equations 5.1. In this figure and equations, H is the shear force at the foundation base, W is the weight of the foundation model, θ is the rotation angle of the foundation model, M is the moment, N is the normal component of force acting on centroid of the foundation

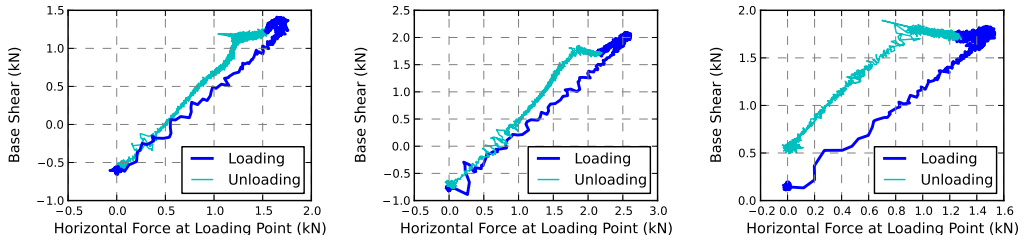

(a) Case 3 (b) Case 6 (c) Case 9

Figure 5.1: Base Shear versus Horizontal Test Load According To Test Measurements by Fukui et al. (2005)

base; finally, h and L are the height of the center of gravity, and horizontal load application point with respect to foundation base, respectively.

Expected resultant shear force under foundation is found as shown in Table 5.1, according to Equation 5.1 and tilt angles calculated at ultimate horizontal load presented in Table 4.4. Then, this expected base shear is compared with measured shear force by eleven load cells placed under the foundation shown in Table 5.1. Measured shear forces at the foundation base are found as at most 5% greater than their expected values. This may be considered as within the error tolerances of the load cells, details of which were presented in Section 2.4.1.

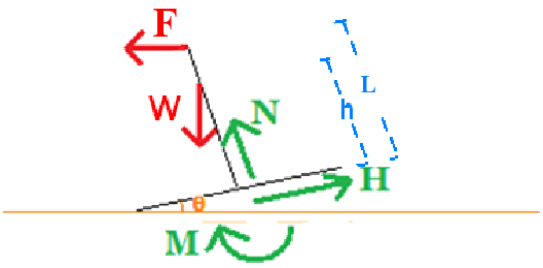

Figure 5.2: Free body diagram for the tilt of the foundation model

$$H\cos\theta - N\sin\theta = F \tag{5.1a}$$

$$N\cos\theta + H\sin\theta = W \tag{5.1b}$$

$$L\cos(\theta)F + h\sin(\theta)W = M \tag{5.1c}$$

Table 5.1: Comparison of Expected Base Shear with Recorded Base Shear

Test Name	Expected (kN)	Recorded (kN)	Difference (%)
Case 3	1.92	2.03	5%
Case 6	2.74	2.87	4%
Case 9	1.67	1.53	4%

It is seen that magnitude of base shear is not considerably lower than the test loading, in fact it is higher than test loading; hence it could be concluded that side face of the foundation did not bear horizontal load. This conclusion is supported by the shape of the curves in Figure 5.1 where base shear versus horizontal load curve follows a linear path in loading region without showing a change in curve shape with the increase in load and consequent rotations. Therefore, difference of horizontal load carrying capacity obtained from experiments and solutions in literature or finite element analyses in this study may not be explained with this hypothesis.

5.3 Initial Eccentricity

5.3.1 Introduction

It is stated in the experiment manual (Fukui et al., 2005) that, based on the recordings of load cells attached to foundation base, weight of the foundation is applied in an eccentric fashion to the soil before application of the horizontal experiment loading on models as shown in Figure 5.3.2.

However, the origin of this eccentricity is not mentioned, which is significant for this study in order to introduce the eccentricity to the solutions in literature and analyses in a correct fashion. This initial eccentricity might be due to inclined placement of the foundation models or due to unbalanced weight of the foundation models.

In this section, the origin of this initial eccentricity and its influence on ultimate horizontal loads provided by experiments are sought. Based on reasoning in this section, it is inferred that the eccentricity is mainly due to unbalanced weight of the foundation models. According to

the solutions in literature, and result of an analysis of this study, influence of this eccentricity is reasoned to have significant influence on ultimate horizontal loads of the experiments.

5.3.2 Experiment Results

Figure 5.3.2 presents the pressure distribution under footing, according to the load cells placed beneath foundation, before application of horizontal experiment loading, for monotonic horizontal loading experiment cases, Case 3, Case 6 and Case 9. Direction of the eccentricity is different among experiments and could be seen from Figure 5.3.2 shown as points "a", "d", "i" for Case 3, Case 6, and Case 9 experiments cases respectively. In this figure moment is calculated according to vertical loads recorded at eleven load cells placed under the footing by multiplying the load of each cell with its distance to centroid of the foundation. Magnitude of the initial moments calculated by this means are presented in Table 5.2. In Table 5.2 presented base shear is obtained by the summation of horizontal force measured by each load cell.

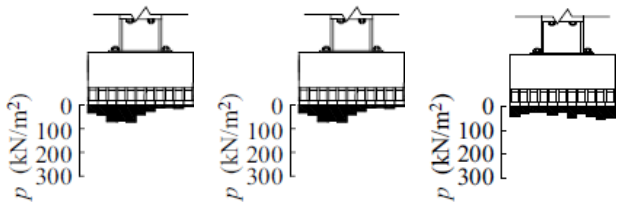

(a) Case 3 (b) Case 6 (c) Case 9

Figure 5.3: Distibution of contact pressure before application of horizontal loading (Fukui et al., 2005)

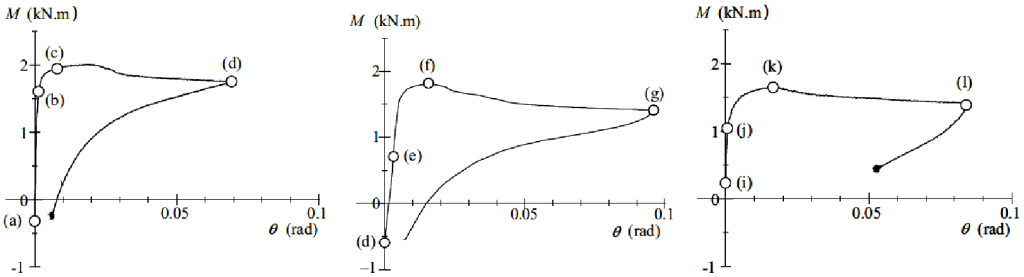

(a) Case 3 (b) Case 6 (c) Case 9

Figure 5.4: Moment versus rotation curves of test data (Fukui et al., 2005)

Table 5.2: Moment and shear force measured by load cells placed at bottom of foundation model, before application of horizontal experiment load

Experiment Case	Moment(kNm)	Base Shear (kN)
Case 3	-0.316	-0.606
Case 6	-0.595	-0.759
Case 9	0.241	0.142

5.3.3 Reason of Initial Eccentricity

5.3.3.1 Introduction

Initial eccentricity may be due to placement of the model on soil surface with an inclination, or due to center of gravity of the model not lying on the vertical axis passing through the geometric center of the foundation area. For the first condition, a resultant shear force under footing is expected to satisfy static equilibrium equations presented in Equation 5.2, whereas for the second condition, base shear is expected to be equal to zero.

5.3.3.2 First Alternative

Figure 5.5 presents the free body diagram of the foundation model at the instant before application of the horizontal experiment load according to the assumption that model is placed on soil surface in an inclined manner. In this figure W is the weight of the model acting on center of gravity which is at h magnitude above the foundation base; N, H, M are the normal, shear and moment reaction forces acting on the foundation base, and finally, θ is the angle of inclination of the model. Equation 5.2 presents the equations of equilibrium for this free body diagram.

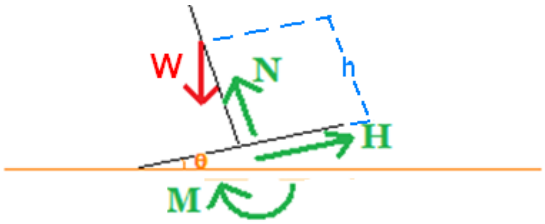

Figure 5.5: Free body diagram for the inclined placement of the foundation model on soil surface

$$H = W \sin\theta \tag{5.2a}$$

$$M = Hh \tag{5.2b}$$

$$N = W \cos\theta \tag{5.2c}$$

Table 5.3 shows magnitudes of measured moments before beginning of the horizontal experiment loading, together with the tilt angle and base shear values calculated according to Equation 5.2 to conform to these moments. In Equation 5.2 base shear is the resultant shear force at the foundation base before application of the horizontal test loading. It is obtained by summation of the shear loads measured by the eleven load cells placed under the foundation base.

Table 5.3: Base shear and tilt angle computed in order to satisfy equilibrium equations for measured moment

Experiment Case	**Measured Moment (kNm)**	**Base Shear (kN)**	**Tilt Angle (°)**
Case 3	-0.316	-0.451	-2.9°
Case 6	-0.595	-1.393	-9.2°
Case 9	0.241	0.564	3.7°

Table 5.4: Comparison of measured and computed base shear according to first alternative

Experiment Case	Measured (kN)	Computed (kN)	Computed / Measured
Case 3	-0.606	-0.451	0.74
Case 6	-0.759	-1.393	1.84
Case 9	0.142	0.564	3.97

Table 5.4 presents the comparison of the measured base shear introduced in Table 5.2 with the computed base shear given in Table 5.3 in order to assess the validity of assumption stating the inclined placement of foundation on soil surface.

5.3.3.3 Second Alternative

Figure 5.6 presents the free body diagram of the foundation model for the moment before application of the horizontal experiment load, with the assumption that center of gravity of the foundation model not lying on the vertical axis passing through the centroid of the foundation area. In this figure W is the weight of the model, M is the moment, and finally e is the eccentricity. Equation 5.3 presents the equation for the magnitude of moment that satisfies the static equilibrium conditions of this free body diagram.

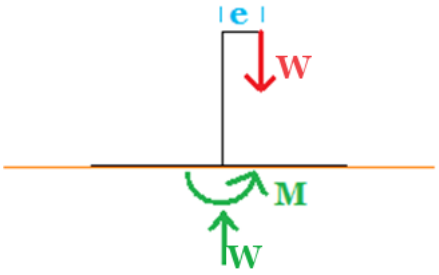

Figure 5.6: Free body diagram for the application of model weight eccentrically

$$M = We \tag{5.3}$$

Table 5.5 presents the magnitudes of measured moments before application of the horizontal experiment load, together with the eccentricity values calculated according to Equation 5.3 to conform with these moments.

Table 5.5: Eccentricity computed in order to satisfy the equilibrium equations for measured moment

Experiment Case	Measured Moment (kNm)	Eccentricity (cm)
Case 3	-0.316	-3.54
Case 6	-0.595	-6.81
Case 9	0.241	2.76

Figure 5.7 for Case 6 experiment, depicts the location of center of gravity with a red dot, as deviating from geometric centroid with 6.81cm in horizontal, as indicated in Table 5.5. Case 6 is given as the example since it has the highest eccentricity among the cases presented in Table 5.5.

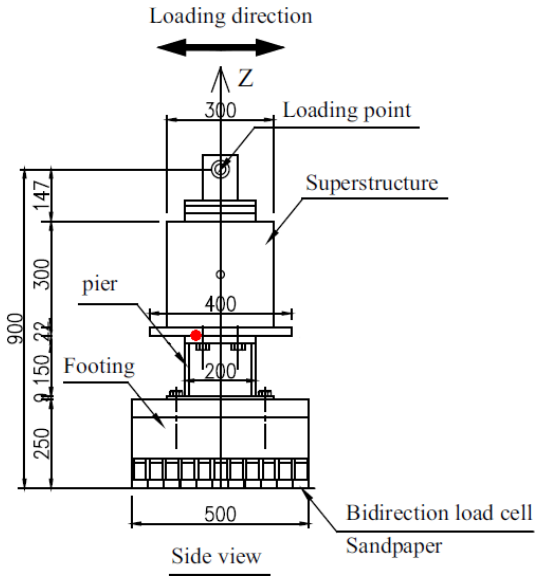

Figure 5.7: Location of center of gravity for Case 6 experiment considering initial eccentricity

5.3.3.4 Discussion

Two potential alternatives were considered to explain the eccentric application of model weight on sand before the application of horizontal experiment load. These alternatives were

(i) placement of the model on soil surface in an inclined fashion, and (ii) center of gravity of the model not lying on the vertical axis passing through geometric center of the foundation area, respectively. Existence of the measured shear force under foundation base is the distinction between these alternatives. For the first alternative, a resultant shear force under footing is expected, in order to satisfy static equilibrium equations presented in Equation 5.2, whereas for the second alternative, base shear is expected to be equal to zero.

As shown in Table 5.2 considerable magnitude of base shear is measured by the load cells placed beneath the foundation for all monotonic horizontal experiment cases before the application of horizontal experiment load. Moreover, as shown in Table 5.4 for all experiment cases, direction of these shear forces are in accord with the measured moments. However, magnitudes of these shear forces are significantly different from the calculated shear forces according to the measured moments as presented in Table 5.4. Furthermore, these differences show high variation among experiment cases.

What is more, inclination angles computed to support the measured moment and presented in Table 5.3 are considerably above probable values. Breadth of the foundation is 50 cm; therefore, it could be computed that for a 1° inclination, 0.87 cm elevation difference should exists between the edges of the foundation. Considering the vertical displacements are measured with gauges that have precision even below one millimeter, existences of such high and unnoticed inclinations are not probable.

Then again, measured shear forces are large to be considered as due to measurement errors. Shear load interference is checked by Fukui et al. (2005) by verifying each load cell with a universal testing machine, applying vertical load, and recording the shear force measured by the bidirectional load cell. In this configuration shear force is expected to be zero. Hence, the shear load interference is defined by the measured shear force per applied vertical load. Based on verification data by Fukui et al. (2005) it could be calculated that for each individual load cell, this value is in range between -3% and +5%. For Case 6 experiment where the highest base inclination is found among cases, weight of the foundation is 8.728 kN, and base shear is measured as 0.759kN. Shear load interference should be $0.759/8.728 = 8.7\%$ for the inclination to be considered as zero. This interference is relatively higher than measures by Fukui et al. (2005). Therefore, measured shear forces are not likely to be completely due to measurement errors. Conformation of direction of these shear forces with the directions of

measured moments supports this suggestion.

Nevertheless, high inclination angles suggested by the first alternative are not likely to have occurred. This indicates that the first alternative could not be the governing factor for the explanation of the measured moments. Therefore, for simplicity, first alternative will be neglected.

Considering the second alternative explanation, calculated eccentricity magnitudes are presented in Table 5.5. Location of center of gravity is demonstrated in Figure 5.7 for the Case 6 experiment case where highest eccentricity is calculated. Deviation of center of gravity in such manner is more likely to have occurred than the demanding tilt angles of first alternative. Hence in this chapter eccentricity is considered to be explained by the placement of center of gravity of the models with a horizontal distance from the geometric center of the foundation models with the eccentricity magnitudes presented in Table 5.5.

5.3.4 Results of Selected Solutions in Literature

In Section 5.3.3.4 it is reasoned that the reported eccentric application of model weight to soil surface by Fukui et al. (2005) is originating from unbalanced placement of model weight. Eccentricities calculated to conform to this condition is presented in Table 5.5. Table 5.6 presents these initial eccentricities, together with the eccentricities due to rotation of foundation at the instant corresponding to attainment of ultimate horizontal load in experiment presented in Table 4.4. Total eccentricity presented in this table is obtained by summation of these two eccentricities.

Parameters supplied to solutions in literature in this section follow the description presented in Section 4.4.2. Only parameter that has changed in magnitude in this section compared to Table 4.9 is the Δx_{CoG}, for which total eccentricity presented in Table 5.6 is employed in this section.

Table 5.7 and Figure 5.8 present the results of solutions in literature which consider the initial eccentric placement of the model self weight on soil surface.

Table 5.6: Eccentricity at maximum horizontal load considering initial eccentricity

Test Name	Initial Eccentricity (cm)	Eccentricity Due to Rotation (cm)	Total Eccentricity (cm)
Case 3	-3.54	1.28	-2.26
Case 6	-6.81	0.63	-6.18
Case 9	2.76	0.67	3.43

Table 5.7: Estimates of collapse load by studies in literature (considering both initial and second order moments)

Solution	Case 3	Case 6	Case 9
Meyerhof (1951, 1963)	5.33	8.53	4.61
Butterfield and Gottardi (1994)	5.34	8.82	5.13
Paolucci and Pecker (1997)	5.92	9.26	5.34
Loukidis et al. (2008)	5.42	8.56	4.93
Average	5.51	8.79	5.00
Standard Deviation	0.28	0.34	0.31

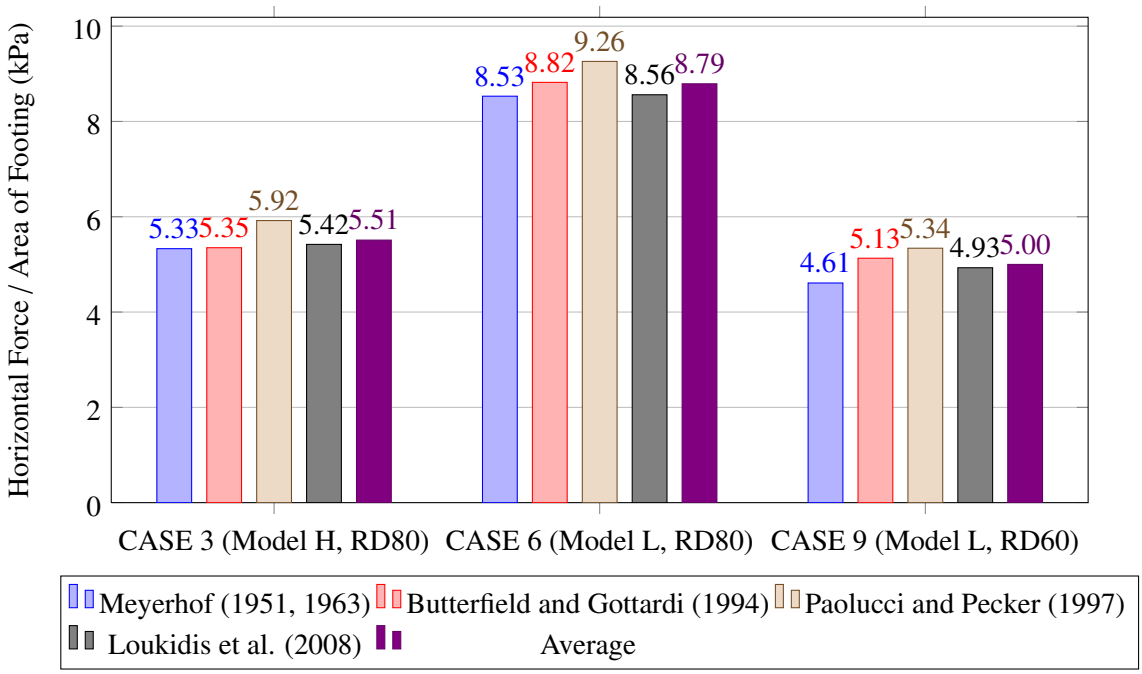

Figure 5.8: Results of Solutions in Literature for Monotonic Horizontal Loading Cases by Considering Initial and Second order Moments

5.3.5 Analyses Results and Comparisons

Results of the analyses conducted in the manner to account for the initial eccentricities are presented in Table 5.8 and Figure 5.3.5 together with experiment results and average of solutions in literature presented in Section 5.3.4. All aspects of these analyses are identical to those analyses, the results of which were presented in Section 4.5.2.1, with the exception that weight of the model is applied in the manner as shown in Figure 5.6, with the eccentricities presented in Table 5.5 to account for the initial moments.

Table 5.8: Comparison of Monotonic Horizontal Loading Results Considering Initial Eccentricity

Experiment	**Exp. (kPa)**	**Lit. (kPa)**	**T.S.**	**Lit. / Exp.**	**T.S. / Exp.**
Case 3	7.04	5.51	5.86	0.78	0.83
Case 6	10.44	8.79	9.30	0.84	0.89
Case 9	6.13	5.00	5.27	0.82	0.86

Exp.: Experiment by Fukui et al. (2005)
T.S.: Results of analyses of this study
Lit.: Average of Solutions in Literature Calculated in Section 5.3.4

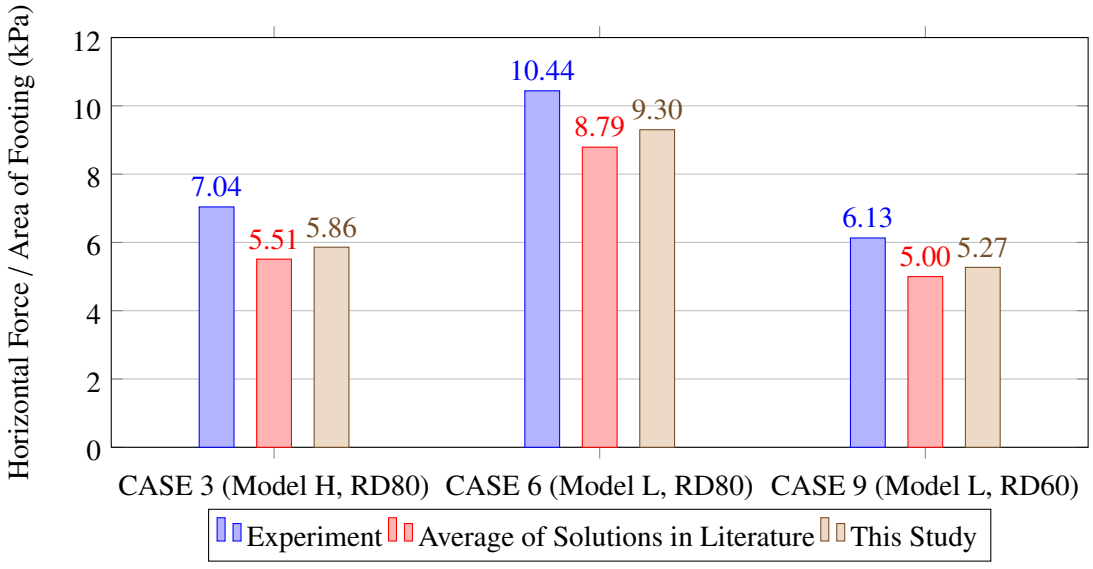

Figure 5.9: Comparison of Monotonic Horizontal Loading Results Considering Initial Eccentricity

5.3.6 Discussions

In Section 4.6.2.1, for monotonic horizontal loading cases, possibility of an unconsidered factor that governs the difference between experiment and analyses results was mentioned based on large magnitude of the difference and variation of the differences among experiment cases, which could not be reasoned at that section.

It is seen that, based on comment by Fukui et al. (2005) on measurements of eleven load cells placed under foundation base to record horizontal and vertical forces, model self weight is applied in an eccentric manner to the soil medium before beginning of experiments. In Section 5.3.3.4 it is reasoned out that this condition could be modeled by relocation of center of gravity of the foundation models according to the measured eccentricity. Note that, modeling in this manner would not account for the significant resultant base shear measured by the load cells.

In Section 5.3.5 results from experiment, analyses, and selected solutions from literature are compared by considering this initial eccentricity. It is seen that analyses results and mean of results of selected solutions in literature are in good agreement with at most 6% difference. By comparison of these results with those presented in Section 4.5.2.1 it is seen that not only the overall difference between experiments and analyses have decreased, but also the variance of the difference among experiment cases has been decreased as well. Since eccentric application of model weight is seen to have significant influence on the results, it would not be proper to neglect this condition in analyses or solutions in literature. Therefore comparison in Section 5.3.5 is more representative for the validation of analyses and solutions in literature than the comparison in Section 4.5.2.1.

Simplifications and assumptions listed for monotonic centered vertical loading cases are valid for monotonic horizontal loading cases as well. Each of these points provides errors that lie on the side that increase the analysis results as discussed in Section 4.6.1. Furthermore, it is observed that increasing the mesh refinement leads to lower results, similar to monotonic vertical loading analyses. Therefore it is expected to obtain higher results from analyses than the precise solution. Slightly higher results obtained from finite element method analyses compared to mean of solutions in literature for all monotonic horizontal loading cases, whether considering initial eccentricity or not, is in agreement with this condition.

In spite of the expectation, finite element method analyses conducted in this study have provided lower bearing capacities than experiment measurements for all experiment cases, ranging between 11% and 17%. This condition is observed for the monotonic vertical loading cases as well. The factors listed in Section 4.6.1 for monotonic centered vertical loading cases which are not considered in analyses and studies in literature based on analytical solutions are likewise valid for monotonic horizontal loading cases. Therefore, it could be reasoned that these unaccounted factors are likely the major source of the difference between experiment and analyses results. Additionally, for monotonic horizontal loading cases, modeling the initial eccentricity without considering the measured base shear might have certain contribution to the difference.

Similar to monotonic vertical loading cases, employment of a more advanced material model in simulations to consider these factors, may provide closer results to the experiments. Alternatively, better results could be obtained by employing a higher internal friction angle considering the majority of the phenomena are influencing the magnitude of internal friction angle as discussed in Section 4.6.1.

5.4 Sensitivity Study for Internal Angle of Friction

In order to evaluate the influence of the uncertainties involved in the magnitude of internal friction angle on analyses results of monotonic horizontal loading experiment cases, that consider the initial eccentricity as described in Section 5.3.3.3, a sensitivity study is conducted for Case 6 and Case 9. Since it is suggested in Section 5.3.6 that, employment of higher internal friction angles may decrease the gap between experimental findings and analysis results, only a set of internal friction angles, presented in Table 5.9 which are composed of magnitudes higher than the values presented in the experiment manual (Fukui et al., 2005) were considered in sensitivity analyses.

Table 5.9: Employed internal friction angles in sensitivity analyses

Experiment Case	Relative Density of Sand	Presented Value in Experiment Manual	Magnitudes Employed in Sensitivity Analyses
Case 6	80%	42.1°	43.1°, 45.0°
Case 9	60%	39.9°	40.9°, 45.0°

5.4.1 Results of Solutions in Literature

In order to observe the sensitivity of solutions in literature to the variation of internal friction angle, and compare this observation with sensitivity analyses of this study, results of solutions in literature were calculated, with the internal angle of friction values presented in Table 5.9 as well. Parameters supplied to solutions in literature in this section follow the description presented in Section 5.3.4. The only parameter that has changed in magnitude in this section is the angle of internal friction.

Figure 5.10 presents the obtained results according to internal friction angles presented in Table 5.9 together with the results that were presented in Section 5.3.5 and obtained according to the internal angle of friction magnitudes provided in experiment manual (Fukui et al., 2005). As can be seen from Figure 5.10, except Meyerhof (1951, 1963), results obtained from literature do not change considerably with the internal friction angle. The reason of this is that, all of the selected solutions, except Meyerhof (1951, 1963), require ultimate bearing capacity under centered vertical conditions as input, to which experiment results of Case 1

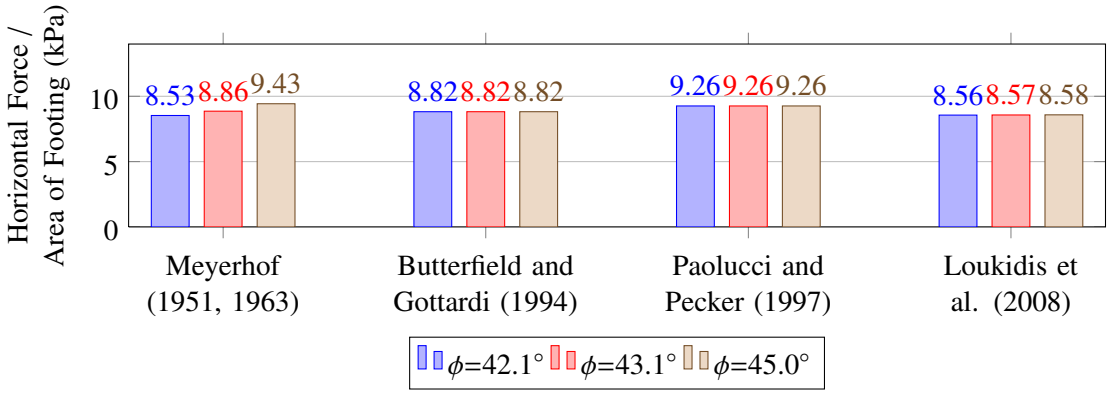

(a) Case 6

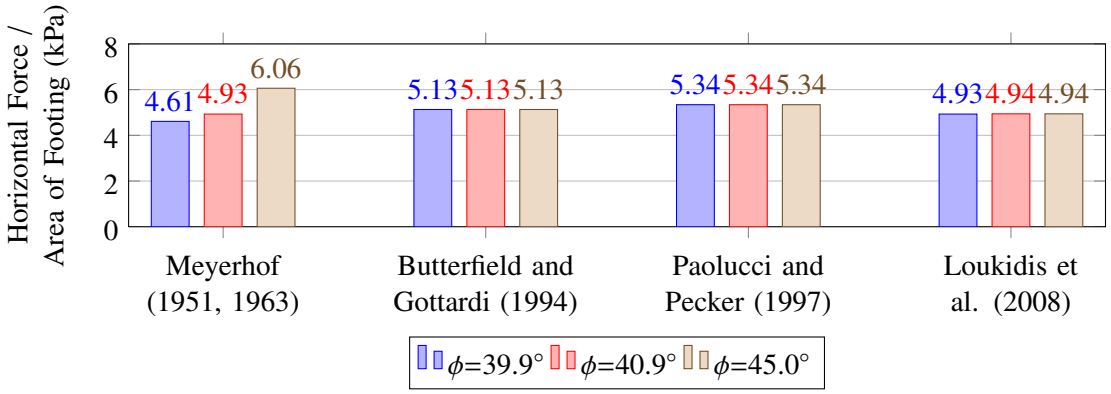

(b) Case 9

Figure 5.10: Results obtained from solutions in literature for varying internal friction angle magnitudes

and Case 2, were provided as input as described in Section 5.3.4. Note that, ultimate bearing capacity under centered vertical loading conditions depend significantly on internal friction angle for cohesionless soils.

According to Figure 5.10 it could be stated that most of the selected solutions from literature are insensitive to the variation of internal angle of friction. This insensitivity is beneficial in terms of comparison with experimental findings. On the other hand, one other aim of calculation of the results of solutions in literature was to compare with analyses results. For this purpose, it could be considered that, results presented in Figure 5.10 does not thoroughly account for the variation of internal angle of friction, since the same ultimate bearing capacity magnitudes are provided as input for different internal angle of friction values. Therefore, in order to obtain more adequate results from selected solutions, and to compare with the sensi-

tivity analyses, influence of increase in internal friction angle to the ultimate centered bearing capacity could be calculated and introduced to the solutions for monotonic horizontal loading experiments. Based on the comparison presented in Section 4.4.1 it is seen that Meyerhof's proposal, among the selected studies in literature for monotonic vertical loading experiment cases, provides the closest results to the experiments. Therefore, ultimate bearing capacity obtained from the Meyerhofs proposal for the centered vertical loading is employed as the input to the studies in this section for the internal friction angles employed in sensitivity analyses. Magnitude of parameters supplied to Meyerhofs proposal and obtained bearing capacities are presented in Table 5.10. Table 5.11 presents the magnitudes of input parameters supplied to solutions in literature with this approach. Results of solutions in literature for the sensitivity to magnitude of internal friction angle are presented in Figure 5.11 and Table 5.12 for Case 6 and in Figure 5.12 and Table 5.13 for Case 9.

Table 5.10: Parameters supplied to Meyerhof (1963) and obtained bearing capacities

Experiment Case	**B (m)**	**L (m)**	**D (m)**	ϕ (°)	**c (kPa)**	γ (kN / m^3)	q_{ult} (kPa)	V_{ult} (kN)
Case 6	0.5	0.5	0.0	43.1	0.0	16.02	1071.84	276.96
Case 6	0.5	0.5	0.0	45.0	0.0	16.02	1665.60	416.40
Case 9	0.5	0.5	0.0	40.9	0.0	15.39	636.03	159.01
Case 9	0.5	0.5	0.0	43.1	0.0	15.39	1600.10	400.02

Table 5.11: Parameters supplied to solutions in literature

Experiment Case	V_{ult} (kN)	**V (kN)**	Δx_{CoG} (cm)	M_{arm} (m)	**B (m)**	ϕ (°)	**c (kPa)**	γ (kN / m^3)
Case 6	267.96	8.728	-6.18	0.9	0.5	43.1	0.0	16.02
Case 6	416.40	8.728	-6.18	0.9	0.5	45.0	0.0	16.02
Case 9	159.01	8.728	3.43	0.9	0.5	40.9	0.0	15.39
Case 9	267.96	8.728	3.43	0.9	0.5	45.0	0.0	15.39

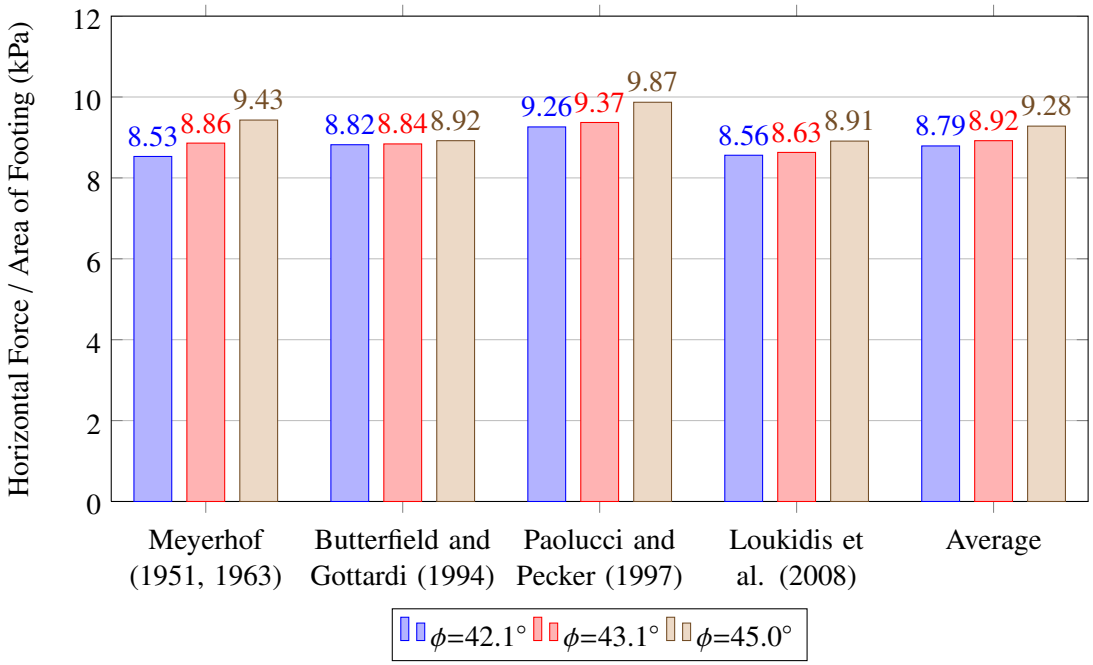

Figure 5.11: Results of selected solutions in literature for sensitivity study on internal friction angle of Case 6

Table 5.12: Results of selected solutions in literature for sensitivity study on internal friction angle of Case 6

Solution from Literature	**ϕ=42.1° (kPa)**	**ϕ=43.1° (kPa)**	**ϕ=45.0° (kPa)**	**ϕ=43.1°/ ϕ=42.1° (kPa)**	**ϕ=45.0°/ ϕ=42.1° (kPa)**
Meyerhof (1951, 1963)	8.53	8.86	9.43	1.04	1.11
Butterfield and Gottardi (1994)	8.82	8.84	8.92	1.00	1.01
Paolucci and Pecker (1997)	9.26	9.37	9.87	1.01	1.07
Loukidis et al. (2008)	8.56	8.63	8.91	1.01	1.04
Average	8.79	8.92	9.28	1.02	1.06
Standard Deviation	0.34	0.31	0.46	0.02	0.04

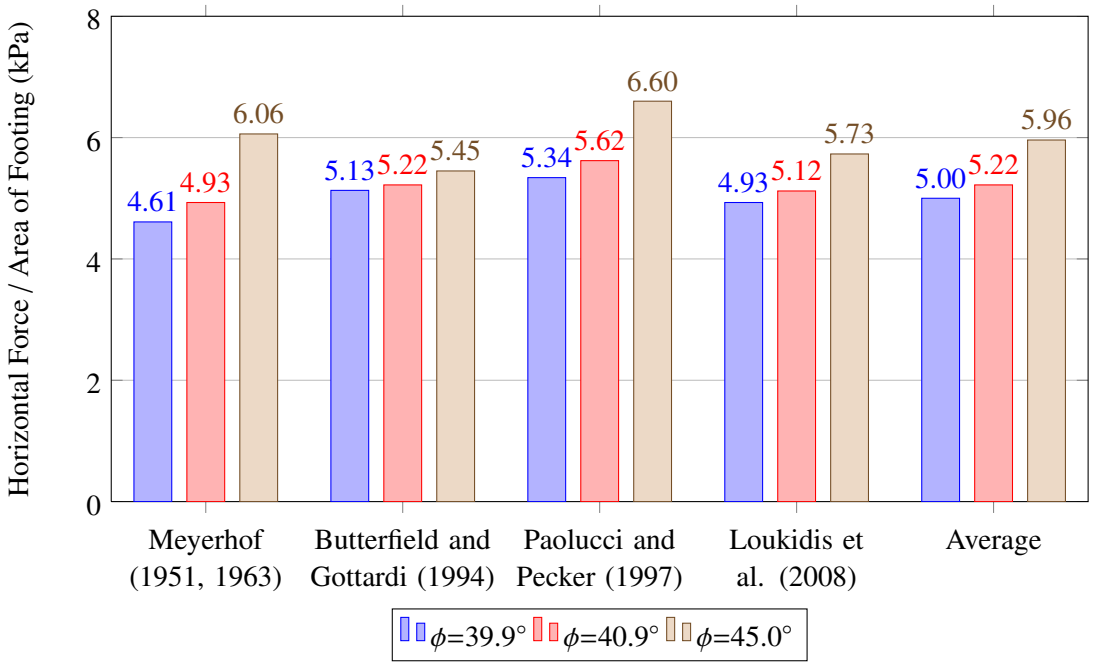

Figure 5.12: Results of selected solutions in literature for sensitivity study on internal friction angle of Case 9

Table 5.13: Results of selected solutions in literature for sensitivity study on internal friction angle of Case 9

Solution from Literature	**ϕ=39.9° (kPa)**	**ϕ=40.9° (kPa)**	**ϕ=45.0° (kPa)**	**ϕ=40.9°/ ϕ=39.9° (kPa)**	**ϕ=45.0°/ ϕ=39.9° (kPa)**
Meyerhof (1951, 1963)	4.61	4.93	6.06	1.07	1.31
Butterfield and Gottardi (1994)	5.13	5.22	5.45	1.02	1.06
Paolucci and Pecker (1997)	5.34	5.62	6.60	1.05	1.24
Loukidis et al. (2008)	4.93	5.12	5.73	1.04	1.16
Average	5.00	5.22	5.96	1.04	1.19
Standard Deviation	0.31	0.29	0.50	0.02	0.11

5.4.2 Analyses Results, Comparisons and Discussions

In order to observe the sensitivity of analyses results and solutions in literature to variation of internal friction angle, for monotonic horizontal loading cases, a sensitivity study is conducted for internal angle of friction. Sensitivity analyses are identical to the analyses, the results of which were presented in Section 5.3.5, except the employed internal angle of friction (ϕ), dilation angle (ψ) and friction coefficient of the interface between foundation and soil (μ). Employed values of these parameters in sensitivity analyses are presented in Table 5.14. Figure 5.13 presents the results of sensitivity analyses, in comparative manner with the experiment results and selected solutions in literature.

Table 5.15 and Table 5.16 presents the comparison of ratio of horizontal load carrying capacity obtained from sensitivity studies to results presented in Section 5.3.5 for the internal angle of friction values presented in experiment manual (Fukui et al., 2005). Analyses and mean of solutions in literature, are in good agreement with each other. It is seen that increasing the internal friction angle results in closing the gap between experiment and analyses results. However, experiment results for Case 6 are still higher than analyses results even when 45° is employed as internal friction angle.

Table 5.14: Parameters employed in analyses

Experiment Case	ϕ (°)	ψ (°)	μ
Case 6	43.1	40.0	0.93578
Case 6	45.0	42.0	1.00000
Case 9	40.9	38.0	0.86623
Case 9	45.0	42.0	1.00000

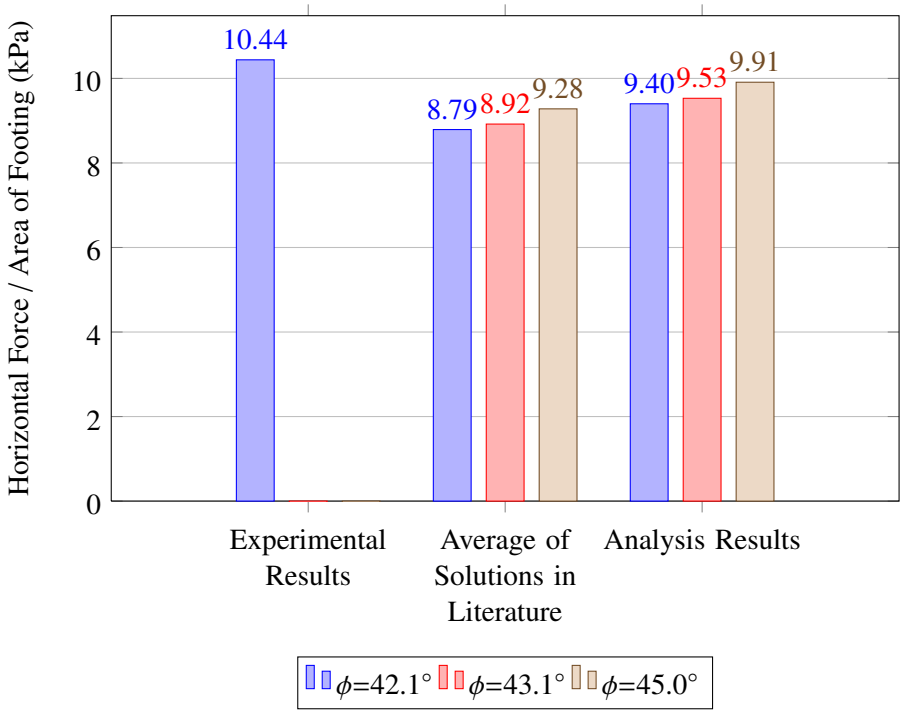

(a) Case 6

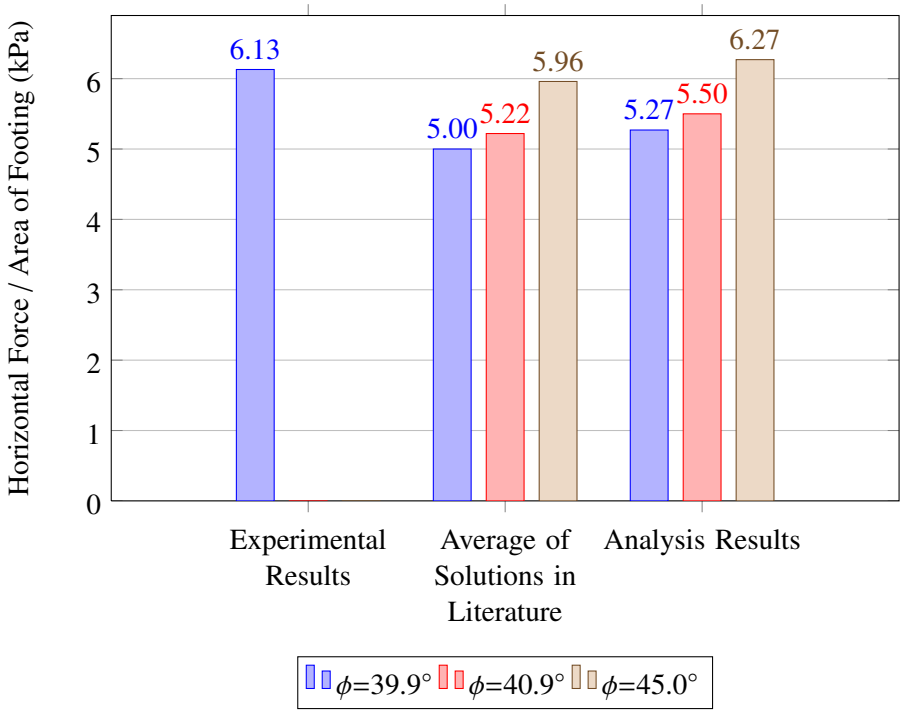

(b) Case 9

Figure 5.13: Comparison of analyses results with experimental results and solutions in literature

Table 5.15: Results of selected solutions in literature for sensitivity study on internal friction angle of Case 6

Solution from Literature	**ϕ=42.1° (kPa)**	**ϕ=43.1° (kPa)**	**ϕ=45.0° (kPa)**	**ϕ=43.1°/ ϕ=42.1° (kPa)**	**ϕ=45.0°/ ϕ=42.1° (kPa)**
Experimental Results	10.44	-	-	-	-
Literature Results	8.79	8.92	9.28	1.02	1.06
Analysis Results	9.40	9.53	9.91	1.01	1.05

Table 5.16: Results of selected solutions in literature for sensitivity study on internal friction angle of Case 9

Solution from Literature	**ϕ=39.9° (kPa)**	**ϕ=40.9° (kPa)**	**ϕ=45.0° (kPa)**	**ϕ=40.9°/ ϕ=39.9° (kPa)**	**ϕ=45.0°/ ϕ=39.9° (kPa)**
Experimental Results	6.13	-	-	-	-
Literature Results	5.00	5.22	5.96	1.04	1.19
Analysis Results	5.27	5.50	6.27	1.04	1.19

CHAPTER 6

OTHER CONDITIONS

6.1 Introduction

In this chapter, based on the conducted finite element method analyses, influence of dilation angle, plane strain assumption and second order moments on analyses results are investigated.

6.2 Influence of Dilation Angle on Results

6.2.1 Influence of Dilation Angle on Monotonic Vertical Loading Analyses

6.2.1.1 Introduction

Influence of dilation angle on monotonic vertical loading analyses conducted in this study is investigated by running the 3D Case 2 experiment with different dilation angles. Four additional finite element analyses, with dilation angles presented in Table 6.1 are conducted for this purpose.

Analyses with dilation angles up to and including 30° are conducted with the fine mesh shown in Figure 3.13(a) with elasticity modulus of 31.6MPa, whereas other analyses are conducted with the coarse mesh shown in Figure 3.13(b) and with elasticity modulus of 41.6MPa. Difference in elasticity modulus does not have significance for ultimate bearing capacity obtained from analysis, whereas employment of different meshes were required due to convergence difficulties as explained in Section 3.4.1.1.

6.2.1.2 Results of Analyses

Table 6.1 and Figure 6.1 presents the ultimate bearing capacities obtained from analyses employing varying angle of dilation magnitudes. Figure 6.2 presents the pressure - settlement variation of theses analyses.

Table 6.1: Influence of dilation angle on monotonic centered vertical bearing capacity according to 3D analysis results for experiment Case 2

$\psi(^\circ)$	q_{ult}(kPa)	$q_{ult}/(q_{ult})_{\psi=37^\circ}$
37	473.9	1.00
35	482.6	1.02
30	478.4	1.01
20	450.0	0.95
10	355.0	0.75

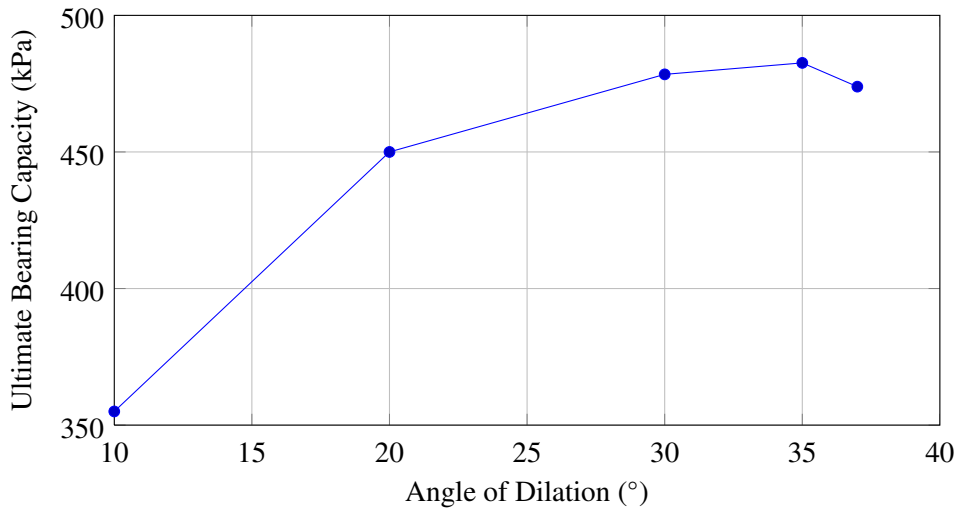

Figure 6.1: Influence of dilation angle on monotonic centered vertical bearing capacity according to 3D analysis results for experiment Case 2

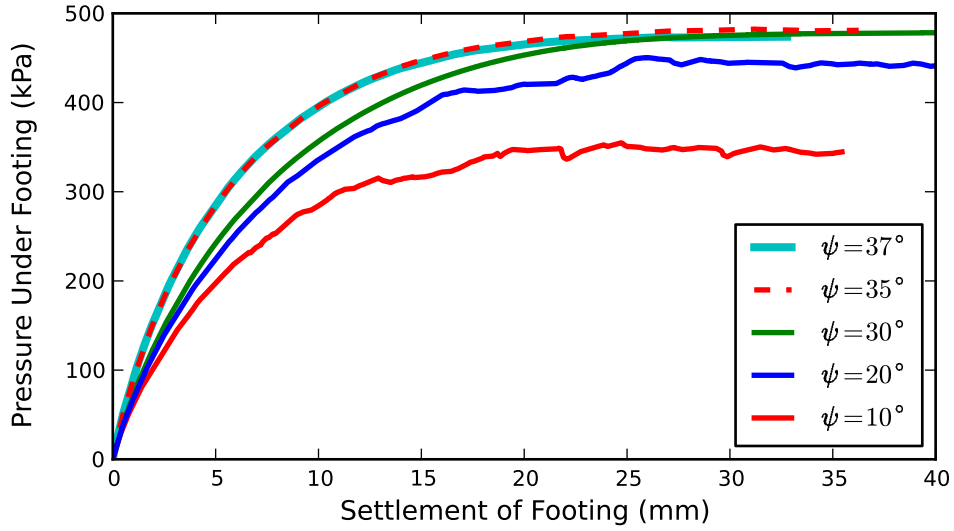

Figure 6.2: Influence of dilation angle on pressure - settlement curve of monotonic centered vertical loading cases according to 3D analysis results for experiment Case 2

6.2.1.3 Results of Study from Literature

In order to assess the quality of analysis results presented in Section 6.2.1.2, in this section Equation 1.3 and Equation 1.4 provided by Loukidis and Salgado (2009) are employed. Equation 1.3 accounts for the influence of dilation angle on bearing capacity factor N_γ and Equation 1.4 presents the shape factor for circular foundations for associated flow rule s_γ^{circ} according to finite element method analysis results. Bearing capacity q_{ult} presented in Table 6.2 and Figure 6.3 by this means is for circular foundation by neglecting the influence of dilation angle on shape factor. Note that the results presented in Section 6.2.1.2 are for square foundation. Considering the comment by Lyamin et al. (2007) that shape factor s_γ for circular foundation is only slightly higher than that of square foundation, comparison is expected to be meaningful. Additionally, if shape factor is independent of angle of dilation, comparison of $q_{ult}/(q_{ult})_{\psi=37^\circ}$ terms would be adequate.

Table 6.2: Results obtained from Loukidis and Salgado (2009) for Case 2, considering influence of dilation angle

$\psi(^\circ)$	N_γ	s_γ^{circ}	q_{ult}(kPa)	$q_{ult}/(q_{ult})_{\psi=37^\circ}$
37	84.04	1.46	472.2	1.00
35	83.87	1.46	471.2	1.00
30	82.76	1.46	465.0	0.98
20	76.32	1.46	428.8	0.91
10	62.73	1.46	352.5	0.75

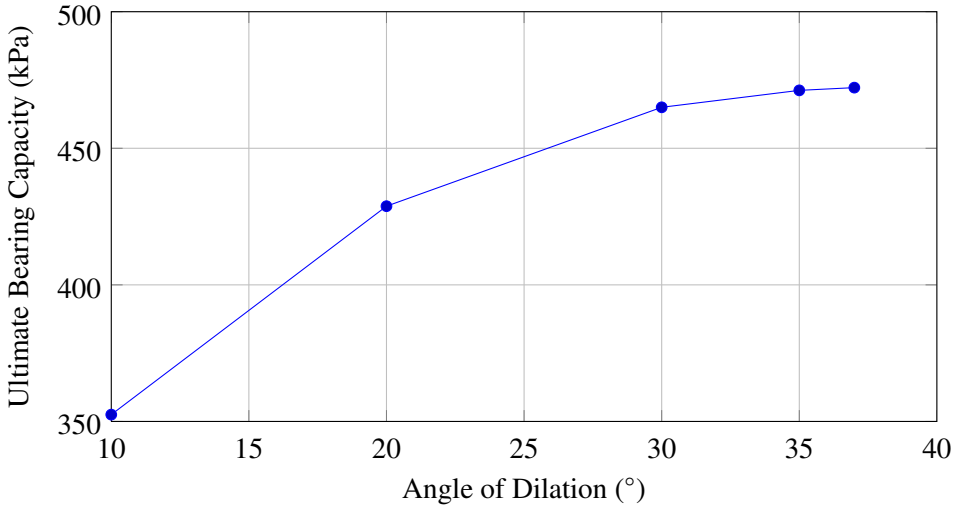

Figure 6.3: Results obtained from Loukidis and Salgado (2009) for Case 2, considering influence of dilation angle

6.2.1.4 Comparisons

Table 6.3 and Figure 6.4 present the comparison of results of analyses of this study presented in Section 6.2.1.2 with the result obtained from proposals of Loukidis and Salgado (2009)) presented in Section 6.2.1.3.

Table 6.3: Analysis results for monotonic centered vertical loading Case 2, considering influence of dilation angle

$\psi(°)$	This Study		Loukidis and Salgado (2009)		T.S. / Lit.	
	q_{ult}(kPa)	$q_{ult}/(q_{ult})_{\psi=37°}$	q_{ult}(kPa)	$q_{ult}/(q_{ult})_{\psi=37°}$	q_{ult}	$q_{ult}/(q_{ult})_{\psi=37°}$
37	473.9	1.00	472.2	1.00	1.00	1.00
35	482.6	1.02	471.2	1.00	1.02	1.02
30	478.4	1.01	465.0	0.98	1.03	1.03
20	450.0	0.95	428.8	0.91	1.05	1.04
10	355.0	0.75	352.5	0.75	1.01	1.00

T.S.: Results of this study presented in Section 6.2.1.2
Lit.: Results of Loukidis and Salgado (2009) calculated in Section 6.2.1.3

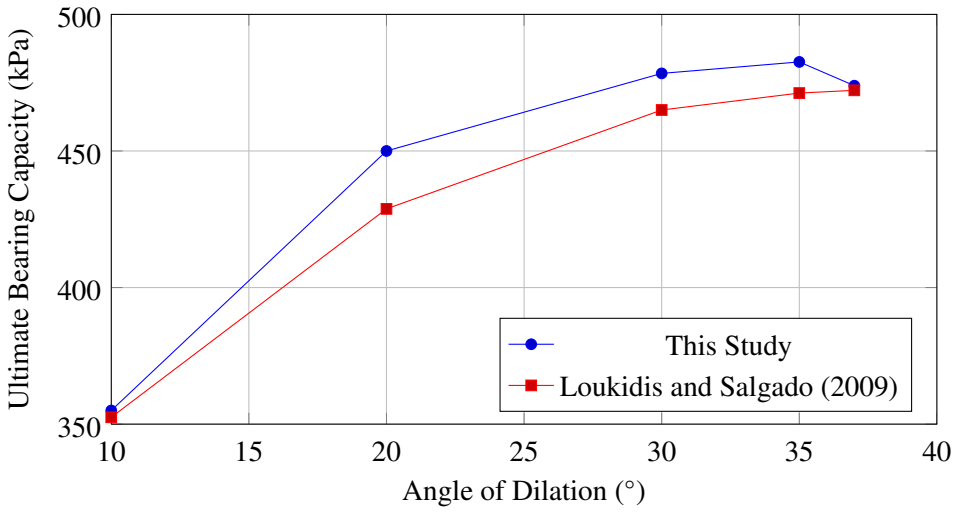

Figure 6.4: Influence of dilation angle on bearing capacity

6.2.1.5 Discussions

According to Figure 6.1 bearing capacity increases, at a decreasing rate, as dilation angle increases. Data point for $\psi = 37^{\circ}$ does not conform to this trend. This may be an error originating from the influence of automatic stabilization on analysis results as investigated in Section 3.6.1. Since influence of automatic stabilization on analysis is expected to increase with decrease in dilation angle. Moreover, order of difference between these results are 2% as shown in Table 6.1, which is could be considered as within the error limits of analyses.

In Figure 6.2 pressure settlement curves of the analyses are presented. It is seen that there are undulations on these curves for low dilation angles. Similar oscillations have been reported by Loukidis and Salgado (2009), they studied bearing capacity of shallow foundations with finite element method considering the influence of unassociated flow rule. They explain that oscillations in pressure settlement curves for small angle of dilation values are observed in studies in literature involving Mohr Coulomb constitutive model. These oscillations are due to the apparent softening exhibited in shear bands and is related to the rotation of the principal stress axes as strains are intensely localized inside the shear bands. Loukidis and Salgado (2009) continues that these oscillations do not undermine the validity of the simulations and that these oscillations are also recorded in footing load tests in the laboratory or at the field; although neither intensity nor pattern of these oscillations match the simulation results, since simulations do not constitute the exact representation of the actual physical process.

Due to employment of automatic stabilization mechanism, explained in Section 3.3.5, magnitude of the oscillations in Figure 6.2 may be less than the study by Loukidis and Salgado (2009).

Comparison of analysis results of this study with Loukidis and Salgado (2009) indicates good agreement between results with at most 5% difference. Difference is at most 1% for dilation angles of 37° and 10°. Little difference between the error levels of quantities q_{ult} and $qult/(q_{ult})_{\psi} = 37^{\circ}$ might suggest that shape factors presented in Table 6.2 are representative for the analyses of this study.

Based on good agreement of results with Loukidis and Salgado (2009), it could be concluded that the employment of automatic stabilization mechanism explained in Section 3.3.5 in finite element method is an adequate approach for mitigating the instabilities originating from

utilization of unassociative flow rule with Mohr-Coulomb yield criterion.

6.2.2 Influence of Dilation Angle on Monotonic Horizontal Loading Analyses

In Figure 6.5, 2D analysis results presented for Case 6 in Section 6.3 are compared with another analysis the only difference of which is magnitude of dilation angle selected for the soil medium. In analysis referred as "ψ = 20°" in the figure, dilation angle of the foundation is selected as 20°. Results of these analyses are compared in order to see the effect of dilation angle on analysis results.

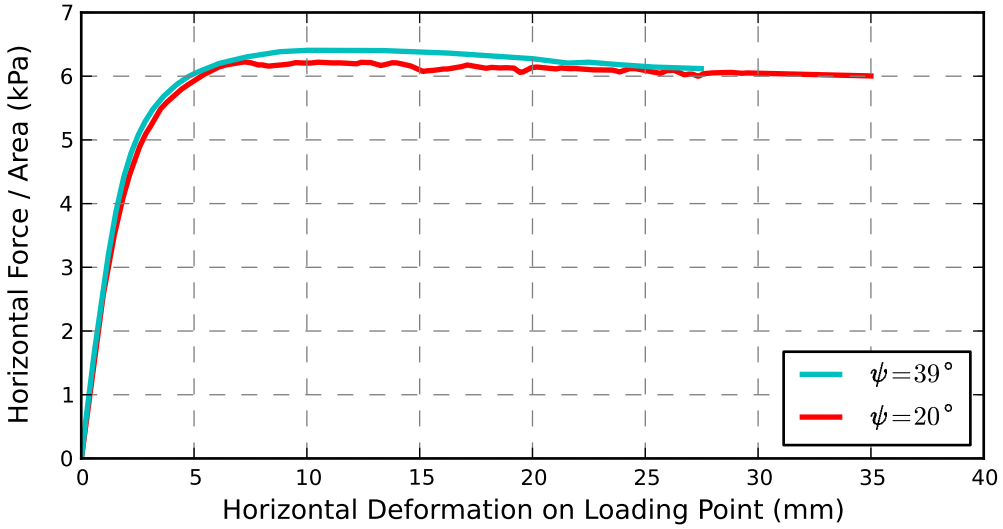

Figure 6.5: Influence of Dilation Angle on Analysis Results

As seen in Figure 6.5, influence of decrease in dilation angle results in decreasing of the load carrying capacity of the foundation, as presented by Loukidis et al. (2008).

6.3 Comparison of 2D and 3D FEM Analysis Results

For each monotonic vertical and monotonic horizontal loading case, one 3D and one 2D analysis was performed with identical material properties. Results of the 3D analyses were presented in Section 4.5 previously. 2D analyses were performed with plane strain assumption, which implies the modeling of a strip foundation instead of the actual square shaped foundation. In this section results of these 2D and 3D analyses are compared with each other

in terms of ultimate plastic loads and shape of force displacement curves.

6.3.1 Results of Analyses

6.3.1.1 Plastic Limit Loads

Table 6.4 and Figure 6.6(a) presents comparison results of 3D and 2D monotonic vertical loading analyses, whereas Table 6.5 and Figure 6.6(b) presents the same comparison for monotonic horizontal loading analyses.

Table 6.4: Ultimate bearing capacities provided by 3D and 2D FEM analyses

Experiment Case	**3D Analysis (kPa)**	**2D Analysis (kPa)**	**3D/2D**
Case 1	801.1	568.2	1.41
Case 2	473.9	358.4	1.32

Table 6.5: Ultimate horizontal loads provided by 3D and 2D FEM monotonic horizontal loading analyses divided by foundation area

Experiment Case	**3D Analysis (kPa)**	**2D Analysis (kPa)**	**3D/2D**
Case 3	4.88	4.61	1.06
Case 6	6.85	6.41	1.07
Case 9	6.27	5.78	1.08

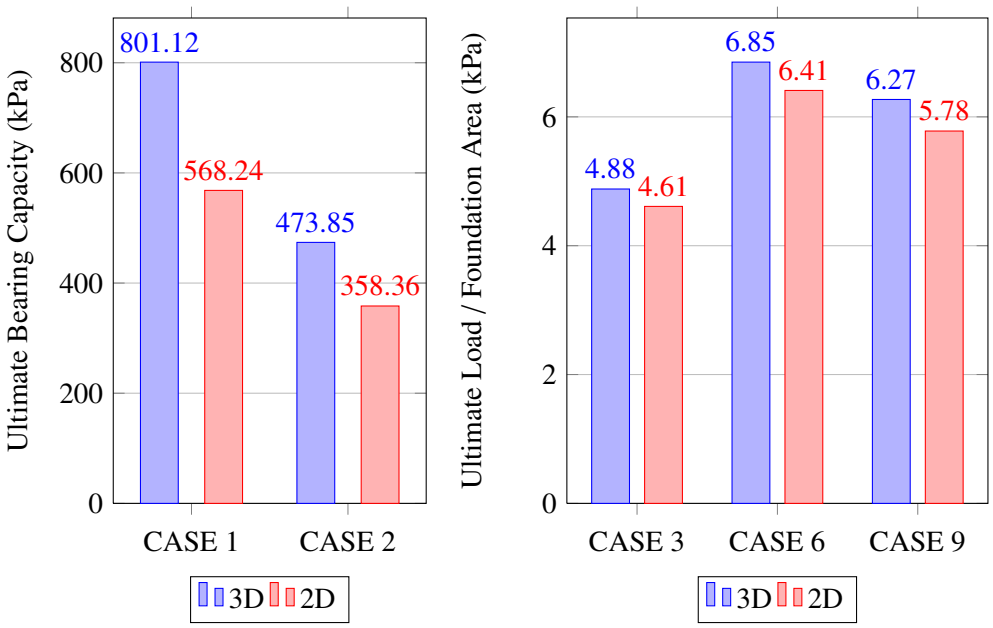

(a) Monotonic Vertical Loading Analyses

(b) Monotonic Horizontal Loading Analyses

Figure 6.6: Comparison of 2D and 3D FEM Analysis Results

6.3.1.2 Load versus Displacement Curves

Figure 6.3.1.2 presents variation of foundation settlement with foundation pressure for monotonic centered vertical loading analyses. Figure 6.8 presents variation of horizontal displacement of load application point with applied experiment loading for monotonic horizontal loading analyses.

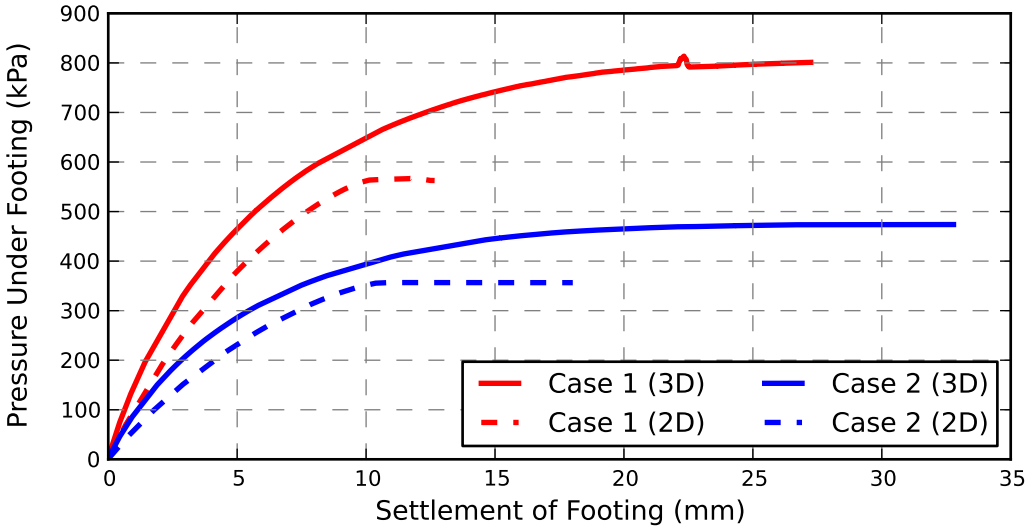

Figure 6.7: Load versus displacement curves of 2D and 3D monotonic vertical loading analyses

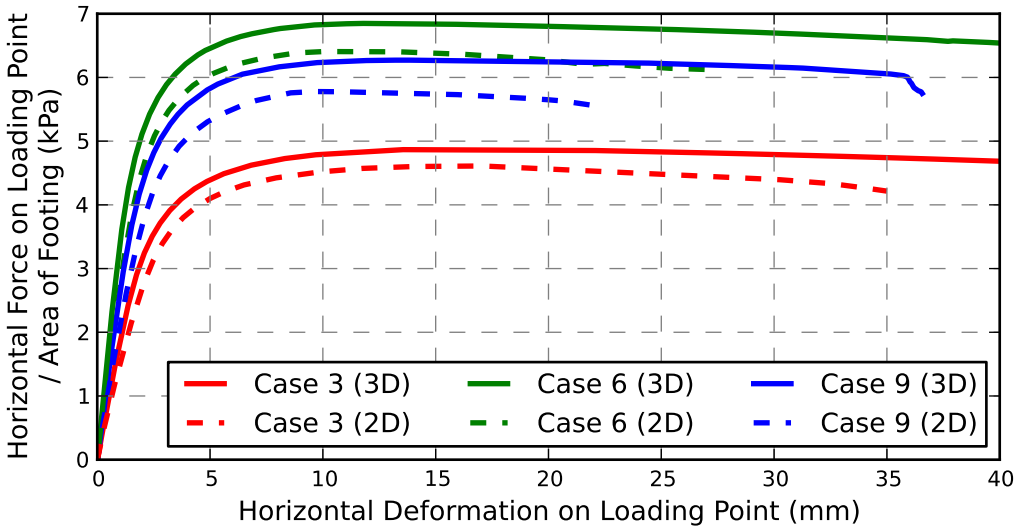

Figure 6.8: Load versus displacement curves of 2D and 3D monotonic horizontal loading analyses

6.3.2 Discussions

Table 6.4 presents ultimate plastic loads provided by 2D and 3D analyses of monotonic centered vertical loading cases. Comparison of the ratio of 3D analysis results to 2D analysis results with shape factors obtained from solutions in literature presented in Table 4.8 reveals

that results of this study are in close agreement with shape factors of Lyamin et al. (2007).

In Figure 6.8 limit loads provided by 2D monotonic horizontal loading analyses are compared with their corresponding 3D analyses. It is seen that strip foundations yield lower ultimate horizontal load capacity compared to square foundations. This observation is similar to the monotonic vertical loading analyses. However, magnitude of the influence of plane strain assumption on ultimate load is not as high as observed for monotonic vertical loading cases. Equations that define interaction envelopes in vertical, horizontal and moment space in literature, such as Paolucci and Pecker (1997), and Loukidis et al. (2008) generally present a linear relationship between vertical load carrying capacity under eccentric and inclined loading with centered vertical load bearing capacity. Therefore accuracy of these equations when employed for square shaped foundations might be of question since centered vertical load bearing capacity increases with a higher rate than the vertical load bearing capacity under inclined and eccentric loading. Hence extension of these equations to take into account the shape factors could be more appropriate.

Figure 6.3.1.2 shows pressure - settlement curves of 3D and 2D analyses of monotonic vertical loading analyses. From this figure it is seen that limit loads are approached with separate paths having different inclinations for 2D and 3D analyses, where 3D analyses shows stiffer response than 2D analyses. Figure 6.8 shows force - displacement curves of 2D and 3D monotonic horizontal loading analyses. It is seen from this figure that square foundations shows stiffer load displacement response than strip foundations. This behavior is in accord with the behavior observed for monotonic vertical loading analyses. However this behavior is more prominent for monotonic vertical loading analyses.

6.4 Influence of Second Order Moments on Results

Considering the experiments modeled in this study were conducted on bridge pier foundation models, which have center of gravity considerably above the foundation base, second order moments due to tilt of the foundation is considered in this study.

In Figure 6.9, 3D analysis results presented for Case 3 in Section 4.5.2.1 are compared with another analysis the only difference of which is the application point of the model weight. In analysis referred as ”Center of Gravity at Pier Base” in the figure, weight of foundation is

applied at bottom of the pier at the middle of the footing. Therefore second order moments are ignored in this analysis. Results of these analyses are compared in order to see the influence of second order moments due to rotation of the foundation model on analysis results.

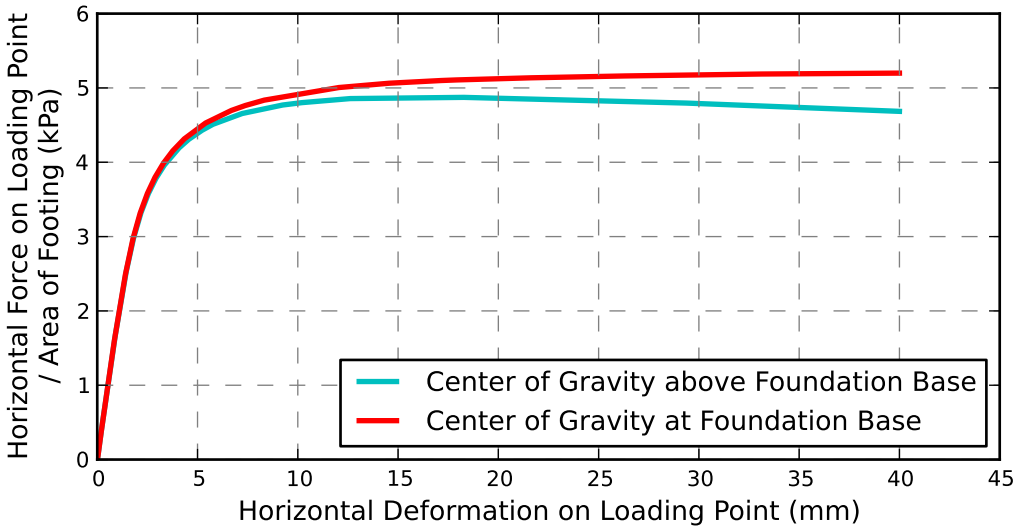

Figure 6.9: Effect of Second order Moments on Analysis Results

As seen in Figure 6.9, both analyses follow the same force - displacement relationship initially. Once the deformations and consequent rotations increase, curves start to deviate from each other as a result of second order moments. Moreover it is also seen that the second order moments are responsible for the decrease in load carrying capacity in analysis results observed after reaching the ultimate load capacity. Ultimate load carrying capacity of analysis ignoring the second order moments is higher. This is in conformance with the analytical solutions, implying that the increase in moment has unfavorable effect on horizontal load carrying capacity.

CHAPTER 7

CONCLUSIONS AND RECOMMENDATIONS

7.1 Summary

Simulation of a set of laboratory model experiments were conducted with finite element method employing linear elastic perfectly plastic material model with Mohr - Coulomb yield criterion. Results of the simulations and experiments were compared with each other and with selected studies from literature.

Simulated experiment cases include monotonic centered vertical loading and monotonic combined loading cases conducted on square shaped shallow foundation models, positioned on surface of air-dried Toyoura standard sand. Relative density of the sand and the employed foundation model, defining the magnitude of moment to base-shear ratio, were the variable conditions among experiment cases.

Main objective of this study was the assesment of capability of finite element method employing Mohr-Coulomb yield criterion and linear elastic perfectly plastic constitutive law for providing plastic limit loads for shallow foundation problems on granular soils. Additionally, influence of plane strain assumption and angle of dilation on limit loads of square shaped foundation models were investigated.

7.2 Conclusions

- Plastic limit loads provided by the analyses are in good agreement with the selected solutions from literature. Therefore, finite element method analyses for bearing capacity of shallow foundations could provide ultimate limit loads of comparable quality with

analytical solutions. This finding is in agreement with Loukidis and Salgado (2009).

- Difference between plastic limit loads provided by the analyses conducted in this study and experiments by Fukui et al. (2005) are relatively large for monotonic horizontal loading cases and error levels are inconsistent among experiment cases. It is concluded that major reason of this situation is the eccentric application of model weight on soil surface before the application of horizontal test load in these cases. Eccentric application of foundation model weight in monotonic horizontal loading analyses is probably due to unbalanced placement of weights on the foundation models. When this condition is taken into account in analyses, and solutions from literature, it is seen that the ultimate horizontal load carrying capacities of experiment cases increased for Case 3 and Case 6, and decreased for Case 9. Hence, resulting in similar differences between analyses of this study and experimental findings by Fukui et al. (2005) for similar experiment cases. According to this condition, it is seen that the results of the modeled experiments are consistent, while providing somewhat higher load carrying capacities than the analyses of this study and selected solutions in literature.

- Bearing capacity factors depend on magnitude of cohesion. Introduction of a small magnitude of cohesion to vertical bearing capacity analyses of purely frictional soil increases the computational efficiency. If the effect of cohesion on bearing capacity is considered as large enough to be deducted from analysis result, deduction of $cN_c s_c$ term may not be sufficient. Instead, effect of cohesion on N_γ and N_c should be considered, possibly by means discussed in Section 3.6.2, as well.

- Dilation angle has significant influence on limit plastic loads. Lower dilation angle results in lower ultimate load capacities for both monotonic horizontal and vertical loading analyses. Influence of dilation angle on limit plastic loads of monotonic vertical loading analyses decreases as the dilation angle increases. Such that, for a granular soil with internal friction angle of 39.9°, change of dilation angle in the range of 30° to 37° does not have significant effect on bearing capacity, whereas 25% reduction in bearing capacity is observed for dilation angle of 10°. These results are in good agreement with Loukidis et al. (2008). Employment of automatic stabilization mechanism in finite element method is an adequate approach to mitigate the instabilities originating from utilization of unassocaited flow rule with Mohr - Coulomb yield criterion.

- Lower limit loads are obtained from finite element analyses both for monotonic vertical and monotonic horizontal loading analyses compared to 3D analyses when plane strain assumption is employed. Shape factors calculated according to analysis results of centered vertical loading cases are in close agreement with the equation proposed by Lyamin et al. (2007). Effect of plane strain assumption on plastic limit loads for monotonic horizontal loading analyses are considerably lower than its influence on vertical loading analysis results. Since equations such as Paolucci and Pecker (1997) and Loukidis et al. (2008) present a linear relationship between vertical load carrying capacity under eccentric and inclined loading with centered vertical load bearing capacity accuracy of these equations when employed for square shaped foundations might be of question considering centered vertical load bearing capacity increases with a higher rate than the vertical load bearing capacity under inclined and eccentric loading. Hence extension of these equations to take into account the shape factors could be more appropriate.

- For monotonic horizontal loading experiments, second order moments have unfavorable influence on horizontal load carrying capacity. Additionally, increase in second order moments after attainment of ultimate horizontal load results in a linear decrease in horizontal load carrying capacity observed in horizontal force versus horizontal displacement curves.

7.3 Recommendations

- Dynamic analyses of cyclic horizontal loading experiments of Fukui et al. (2005) could be conducted.

- More advanced material model could be employed in analyses considering phenomena such as strain dependence of yield surface or dependence of internal friction angle on confining pressure.

- Effect of dilation angle on monotonic horizontal loading analyses could further be investigated by conducting analyses employing lower dilation angles.

- Influence of dilation angle on shape factors for foundations under centered vertical loading could be investigated.

- Influence of foundation shape on bearing capacities of foundations under inclined and eccentric loading could be investigated.

REFERENCES

[1] Abaqus 6.10 Online Documentation, Dassault Systèmes, 2010

[2] Bathe Klaus-JÜrgen (1996), Finite Element Procedures, Prentice Hall Inc., New Jersey

[3] Butterfield R., and Gottardi G. (1994). "A complete three-dimensional failure envelope for shallow footings on sand, Geotechnique, Vol. 44, No.1, pp.181-184.

[4] Cox, A. D. (1962), Axially-symmetric plastic deformations - Indentation of ponderable soils. Int. Journal Mech. Science, Vol. 4, 341-380

[5] Chandrupatla T. R., Belegundu A. D. (1997), Introduction to Finite Elements in Engineering Second Edition, Prentice Hall, New Jersey

[6] Das, B. M. (1997) Advanced soil mechanics, Taylor & Francis, Washington, D.C.

[7] Fukui Jiro, Shirato Masahiro, Nonomura Yoshinori, Asai Ryuichi (2005) Experimental study on the residual displacement of shallow foundations subjected to cyclic loads, Technical Memorandum of PWRI No., 2005.3

[8] Georgiadis, M. & Butterfield, R. (1988). Displacements of footings on sand under eccentric and inclined loads. Can. Geotech. J. 25, 199-212.

[9] Guo PJ (2010) Effect of density and compressibility on K0 of cohesionless soils. Acta Geotech 5:225238

[10] Ishihara, K. (1996). Soil Behaviour in Earthquake Geotechnics., Oxford Science Publications, Oxford, UK, pp. 350.

[11] Jaky J. (1948) Pressure in soils, 2nd ICSMFE, London, Vol. 1, pp 103-107.

[12] Kokusho, T. (1980) Cyclic triaxial test of dynamic soil properties for wide strain range. Soils and Foundations, 20, 45-60

[13] Krizek, R. J., and R. B. Corotis (1975) Synthesis of Soil Moduli Determined from Different Types of Laboratory and Field Tests, in Proc. In Situ Conf. Measurement Soil Procedures, vol. 1, Am. Soc. of Civ. Eng., pp. 225-240

[14] Loukidis, D., Chakraborty, T., Salgado, R. (2008) "Bearing capacity of srip footings on purely frictional soil under eccentric and inclined loads" Can. Geotech. J. 45:768-787

[15] Loukidis, D., Salgado, R. (2009). Bearing capacity of strip and circular footings in sand using finite elements. Computers and Geotechnics, Vol. 36, No. 5, pp. 871-879.

[16] Lyamin, A. V., Salgado, R., Sloan, S. W., Prezzi, M. (2007) Two- and three-dimensional bearing capacity of footings in sand, Geotechnique, Vol.57, No.8, pp.647-662.

[17] Martin C. M. (2005) Exact bearing capacity calculations using the method of characteristics. In: Barla, G., Barla, M., editors. Proceedings of the 11th IACMAG, vol. 4, Turin; 2005. p. 441-50

[18] Martin C. M. User guide for ABC - Analysis of Bearing Capacity Version 1.0 (2004), OUEL Report No. 2261/03 Department of Engineering Science, University of Oxford

[19] Meyerhof, G. G. (1963) Some recent research on the bearing capacity of foundation, Canadian Geotechnical Journal, 1, No. 1, 16-26

[20] Meyerhof, G. G. (1951) The ultimate bearing capacity of foundations, Geotechnique, vol. 2, no. 4, pp. 301-331

[21] Michalowski, R. L. (1997). An estimate of the influence of soil weight on bearing capacity using limit analysis. Soils Found., 37(4), 5764.

[22] Michalowski RL (2005) Coefficient of earth pressure at rest. J Geotech Geoenviron Eng 131(11):14291433

[23] Paolucci R., and Pecker A. (1997). Seismic bearing capacity of shallow strip foundations on dry soils, Soils and Foundations, J.G.S., Vol.37, No.3, pp.95-105.

[24] Plaxis 2D. Reference Manual, version 8.0; 2002.

[25] Potts D. M., Zdravkovic L. (1999) Finite Element Analysis In Geotechnical Engineering : Theory, Thomas Telford Limited, London

[26] Potts D. M., Zdravkovic L. (2001) Finite Element Analysis In Geotechnical Engineering : Application, Thomas Telford Limited, London

[27] Prandtl, L. (1920). Über die Härte plastischer Körper. Nachr. Ges. Wiss. Goettingen, Math.-Phys. Kl., 7485.

[28] Randolph, M.F., Jamiolkowski, M.B., and Zdravkovic, L. 2004. Load carrying capacity of foundations. In Advances in Geotechnical Engineering: The Skempton Conference. Edited by R.J. Jardine, D.M. Potts and K.G. Higgins. Thomas Telford, London. Vol. I. pp. 207-240

[29] Reddy, J. N. (2004). Introduction to Nonlinear Finite Element Analysis, Oxford University Press, New York

[30] Sarma S.K. and Iossofelis (1990). "Seismic bearing capacity factors of shallow strip footings, Geotechnique, Vol.40, No.2, pp.265-273.

[31] Siddiquee M.S., Tanaka T., Tatsuoka F., Tani K., and Morimoto T. (1999). "Numerical simulation of bearing capacity characteristics of strip footing on sand" Soils and Foundations, J.G.S., Vol.39, No.4, pp.93-109.

[32] Siddiquee M.S., Tatsuoka F., Tanaka T., Tani K., Yoshida K., and Morimoto T. (2001). "Model tests and FEM simulation of some factors affecting the bearing capacity of a footing on sand, Soils and Foundations, J.G.S., Vol.41, No.2, pp.53-76.

[33] Siefffert J.G., and Bay-Gress Ch. (2000). "Comparison of European bearing capacity calculaton methods for shallow foundations, Proc. Instn. Civ. Engrs. Geotech. Engrg., No.143, pp.65-74.

[34] Sun D. A., Huang W. X., Yao Y. P. (2008) An experimental study of failure and softening in sand under three-dimensional stress condition, Granular Matter, No.10,pp.187-195

[35] Terzaghi K. (1943). Theoretical Soil Mechanics, Wiley, New York.

[36] Trautmann, C. H., and F. H. Kulhawy (1987) CUFAD-A Computer Program for Compression and Uplift Foundation Analysis and Design, Report EL-4540-CCM, vol. 16, Electrical Power and Research Instititute

[37] Vesic, A. S. (1973) Analysis of ultimate loads of shallow foundations, J. Soil Mech. Found. Div. 99(1), 45-76

[38] Yılmaz M. T. (2004) Seismically Induced Tilting Potential of Shallow Mats on Fine Soils Phd.Thesis, M.E.T.U., 259 p.

[39] Wicaksono, R. I., De Silva, L. I. N., Mulmi, S., Enomoto, T., Kiyota, T., Tsutsumi, Y., Kuwano, R., Koseki, J. (2008) Small Train Stiffness of Toyoura Sand Obtained from Various Techniques in IIS, Seisan Kenkyu, Vol. 60, No. 6, pp.561-564

[40] Zhu, M. and Michalowski, R.L., Shape factors for limit loads on square and rectangular footings. J. Geotech. Geoenviron. Eng., 2005, 131(2), 223–231.

Appendix A

LOAD VERSUS DEFORMATION VARIATIONS

In this appendix variations of applied test load with the horizontal displacement of load application point, sliding of foundation and tilt angle of foundation are provided for monotonic horizontal loading analyses, the results of which were presented in Section 4.5.2.1. Figure A.1 presents the variation of horizontal displacement of load application point with applied horizontal test loading, normalized by the foundation area, for monotonic horizontal loading experimental findings and analyses. Figure A.2 presents variation of tilt and sliding of foundation with applied horizontal test loading normalized, by the foundation area, for monotonic horizontal loading experimental findings and analyses.

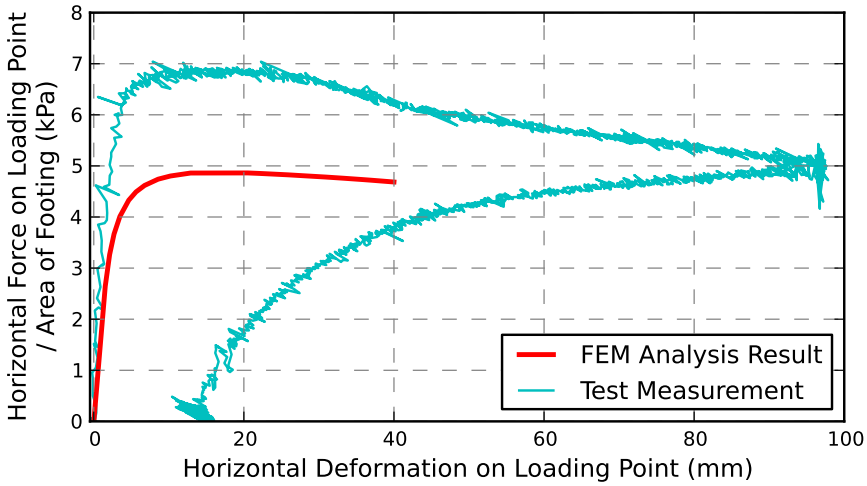

(a) Case 3

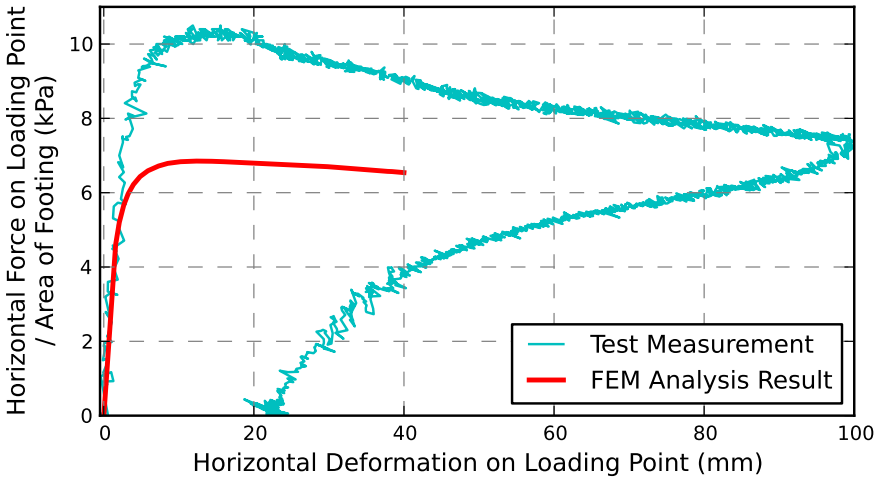

(b) Case 6

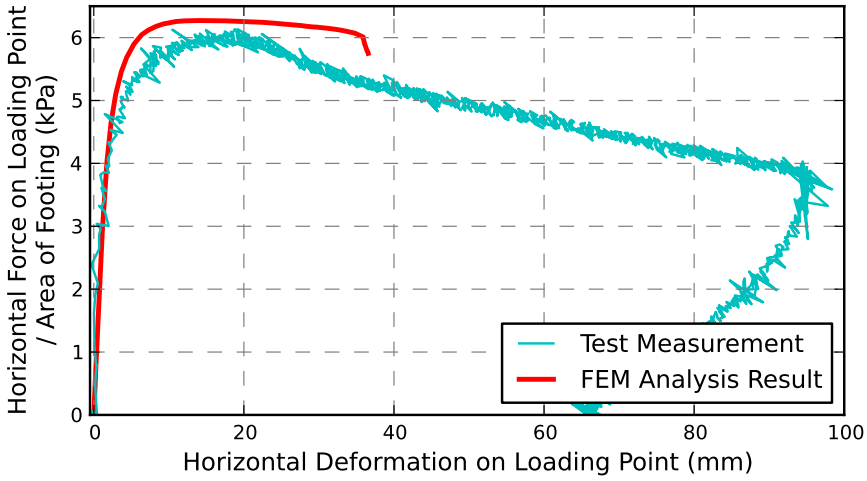

(c) Case 9

Figure A.1: Force displacement curves provided 3D analysis results and experiment measurements

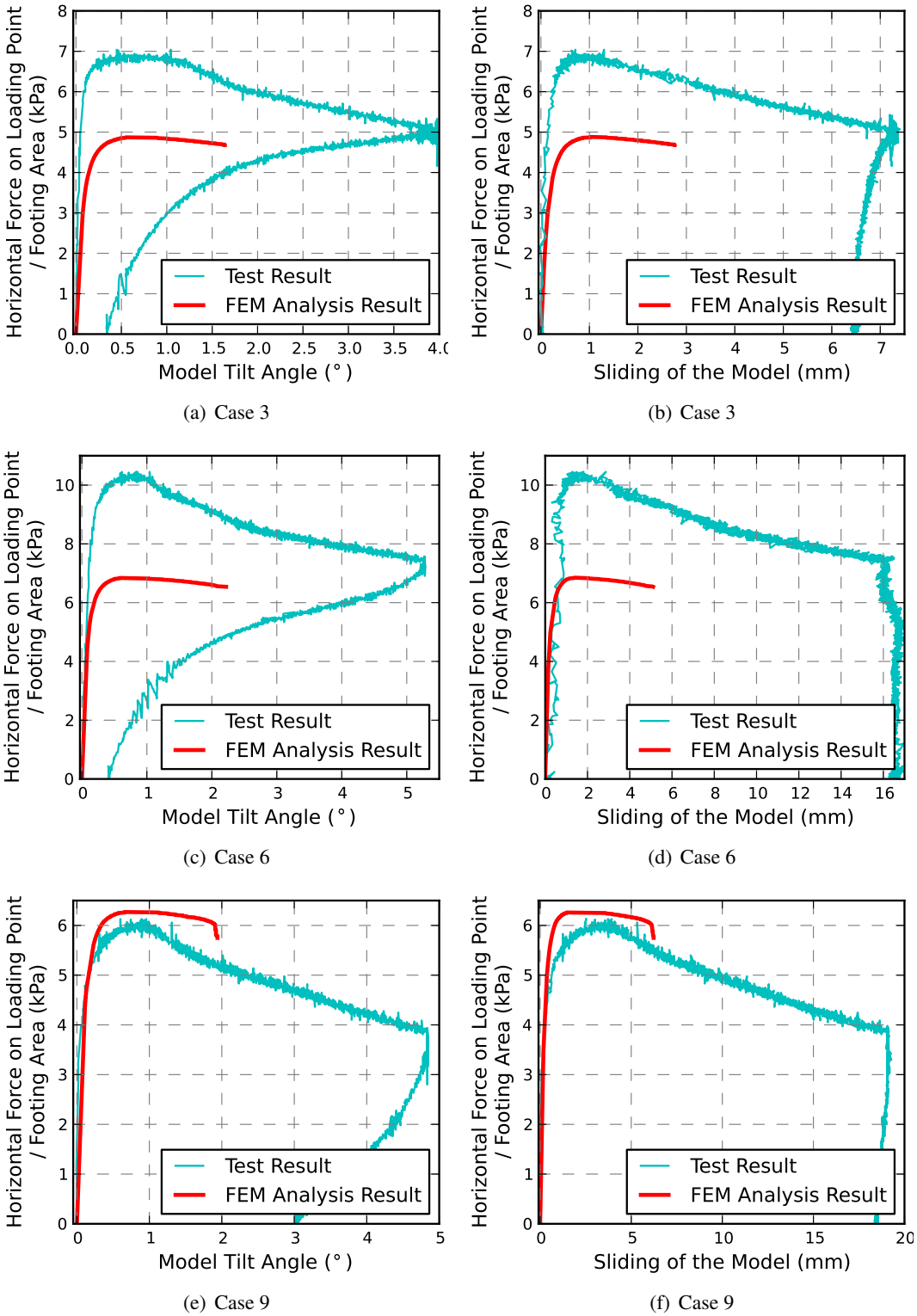

(a) Case 3

(b) Case 3

(c) Case 6

(d) Case 6

(e) Case 9

(f) Case 9

Figure A.2: Sliding and tilt of foundation models provided by 3D analysis results and experiment measurements

Appendix B

VARIATION OF STRESSES AND DEFORMATIONS

In this appendix, variation of stresses and deformations for the three dimensional analyses of monotonic centered vertical and horizontal loading cases, the force versus deformation variations of which were given in Section 6.3, are presented.

B.1 Deformed Meshes

Figure B.1 presents the deformed meshes of the monotonic centered vertical loading analyses plotted on undeformed meshes with deformations scaled by a scale factor of 0.1. Figure B.2, Figure B.3 and Figure B.4 presents the deformed meshes of monotonic horizontal loading analyses, with deformation scale factors of 2.0, for the instant corresponding to 3 cm horizontal displacement of the horizontal load application point (i.e., pier top).

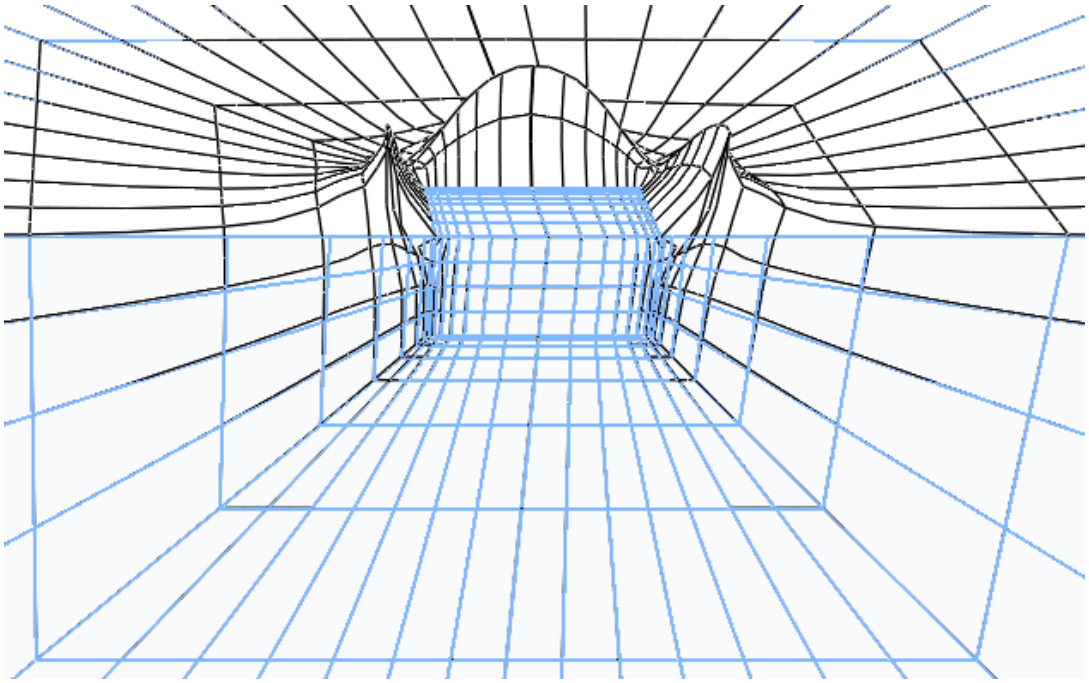

(a) Case 1, at the end of analysis (deformation scale factor: 0.1)

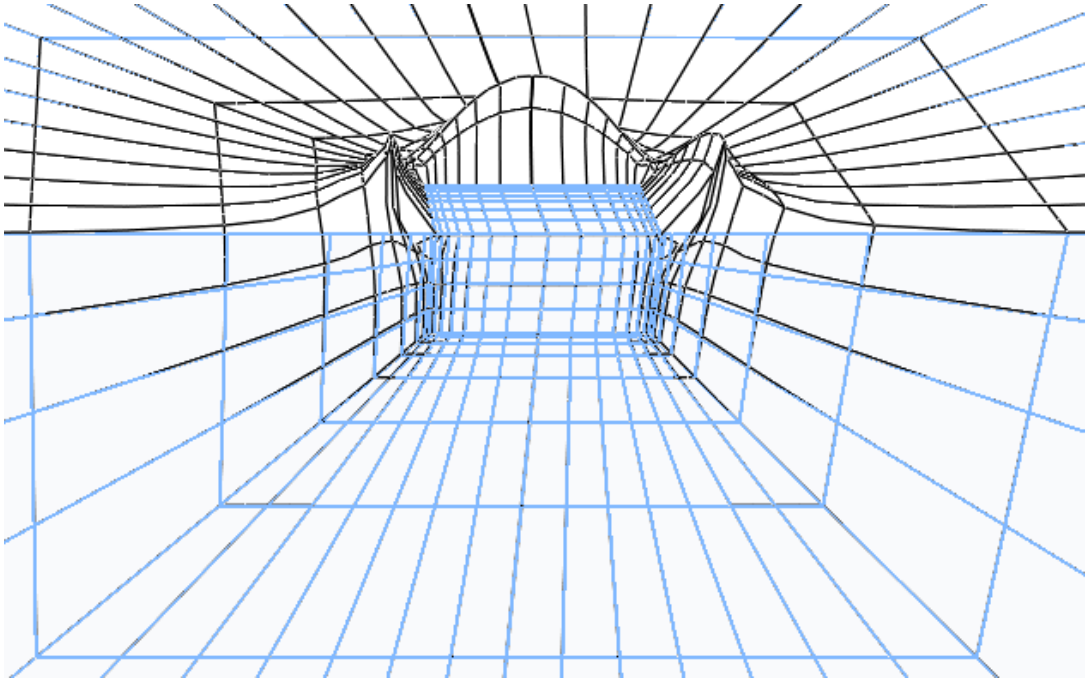

(b) Case 2, for 3 cm settlement (deformation scale factor: 0.1)

Figure B.1: Deformed meshes of 3D centered vertical loading analyses cases

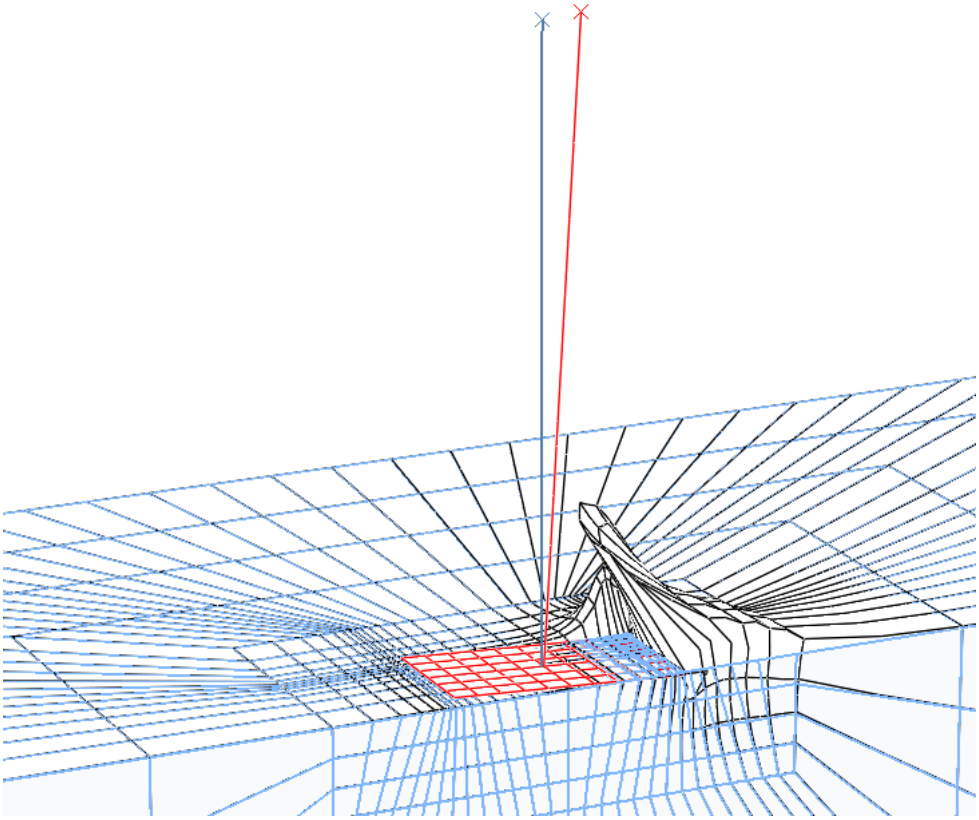

Figure B.2: Deformed mesh of 3D Case 3 FEM analysis - for 3 cm horizontal displacement of load application point (deformation scale factor: 2.0)

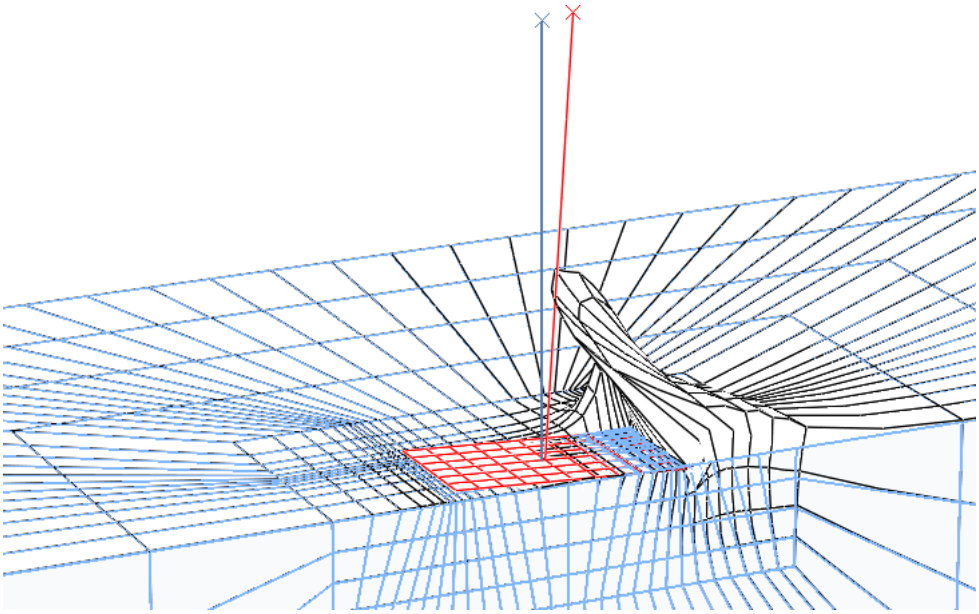

Figure B.3: Deformed mesh of 3D Case 6 FEM analysis - for 3 cm horizontal displacement of load application point (deformation scale factor: 2.0)

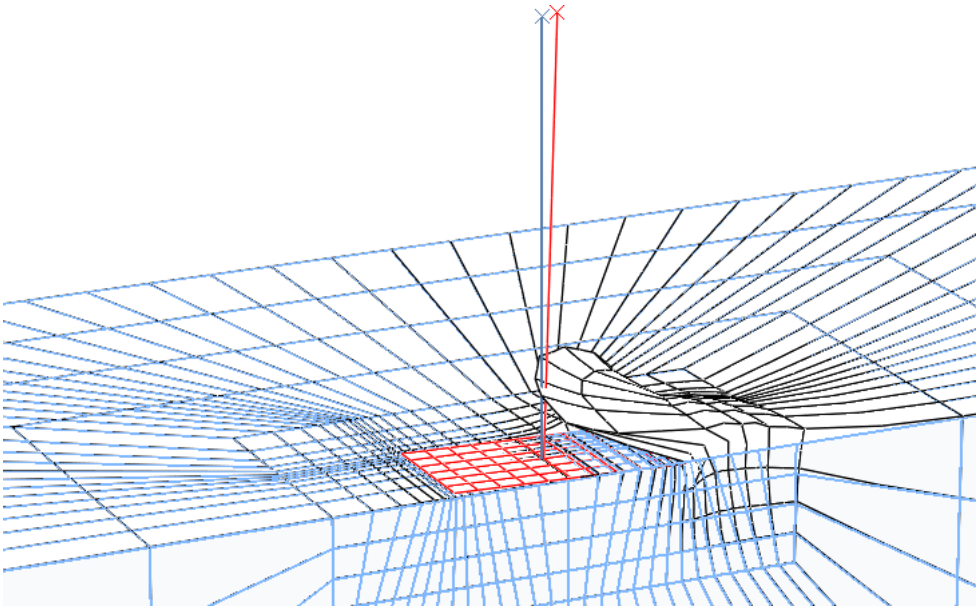

Figure B.4: Deformed mesh of 3D Case 9 FEM analysis - for 3 cm horizontal displacement of load application point (deformation scale factor: 2.0)

B.2 Variation of Vertical Components of Deformations and Stresses

Figure B.5 and Figure B.6 presents the variation of vertical deformations on finite element meshes of monotonic centered vertical, and monotonic horizontal loading analyses, respectively. Figure B.7 and Figure B.8 presents the variation of vertical components of stresses on finite element meshes of monotonic centered vertical, and monotonic horizontal loading analyses, respectively. Figure B.5 and Figure B.7 are obtained for the instant corresponding to 2.5 cm settlement of the foundation in monotonic centered vertical loading cases, and with the deformation scale factor of 0.1. Figure B.6 and Figure B.8 are obtained for the instant corresponding to 2 cm displacement of the horizontal load application point of the horizontal loading analyses with the deformed mesh presented in true scale by employment of a deformation scale factor of 1.0.

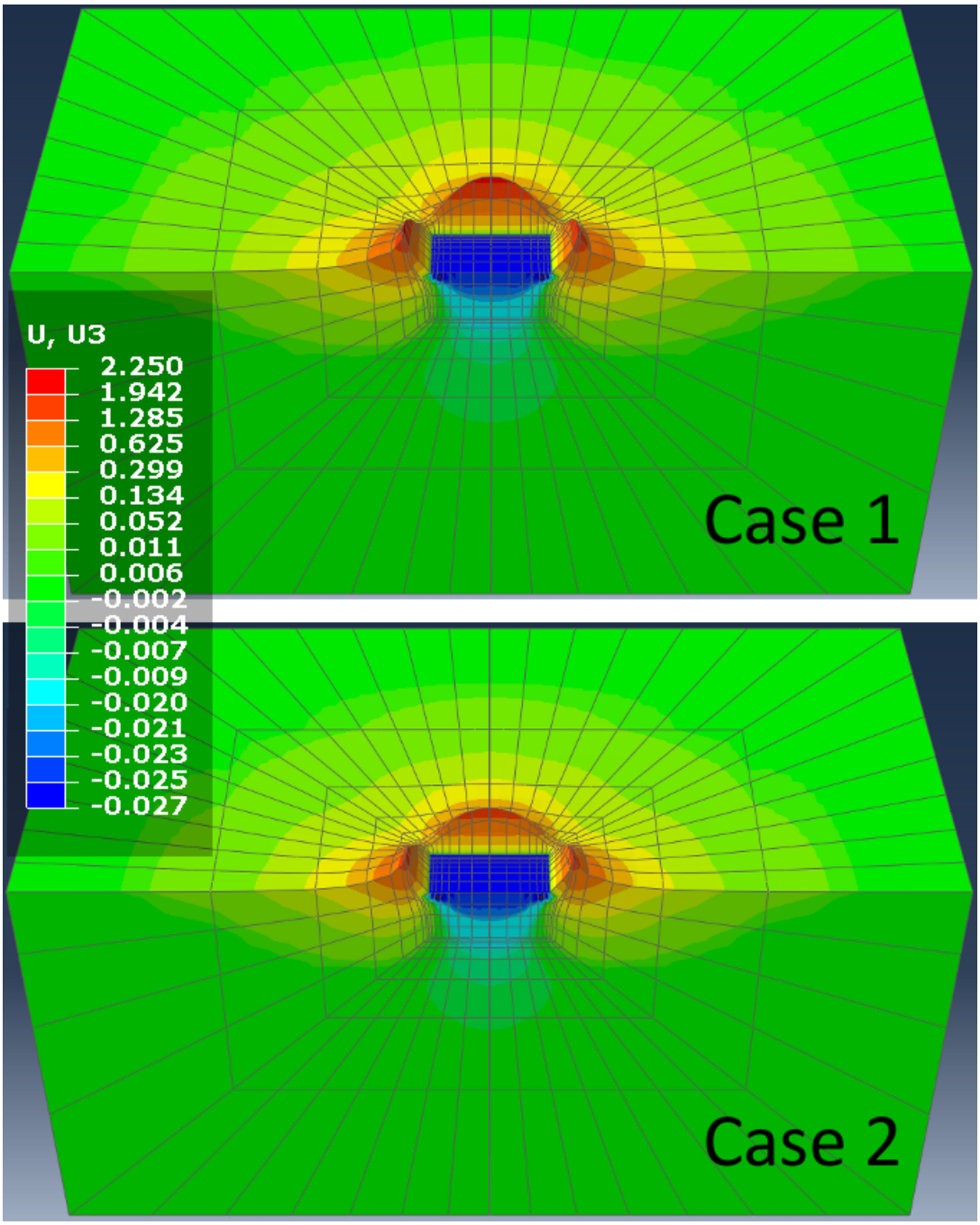

Figure B.5: Vertical component of deformations plotted on deformed meshes of monotonic vertical loading analyses for 2.5 cm settlement of foundation (deformation scale factor: 0.1, units are in meters)

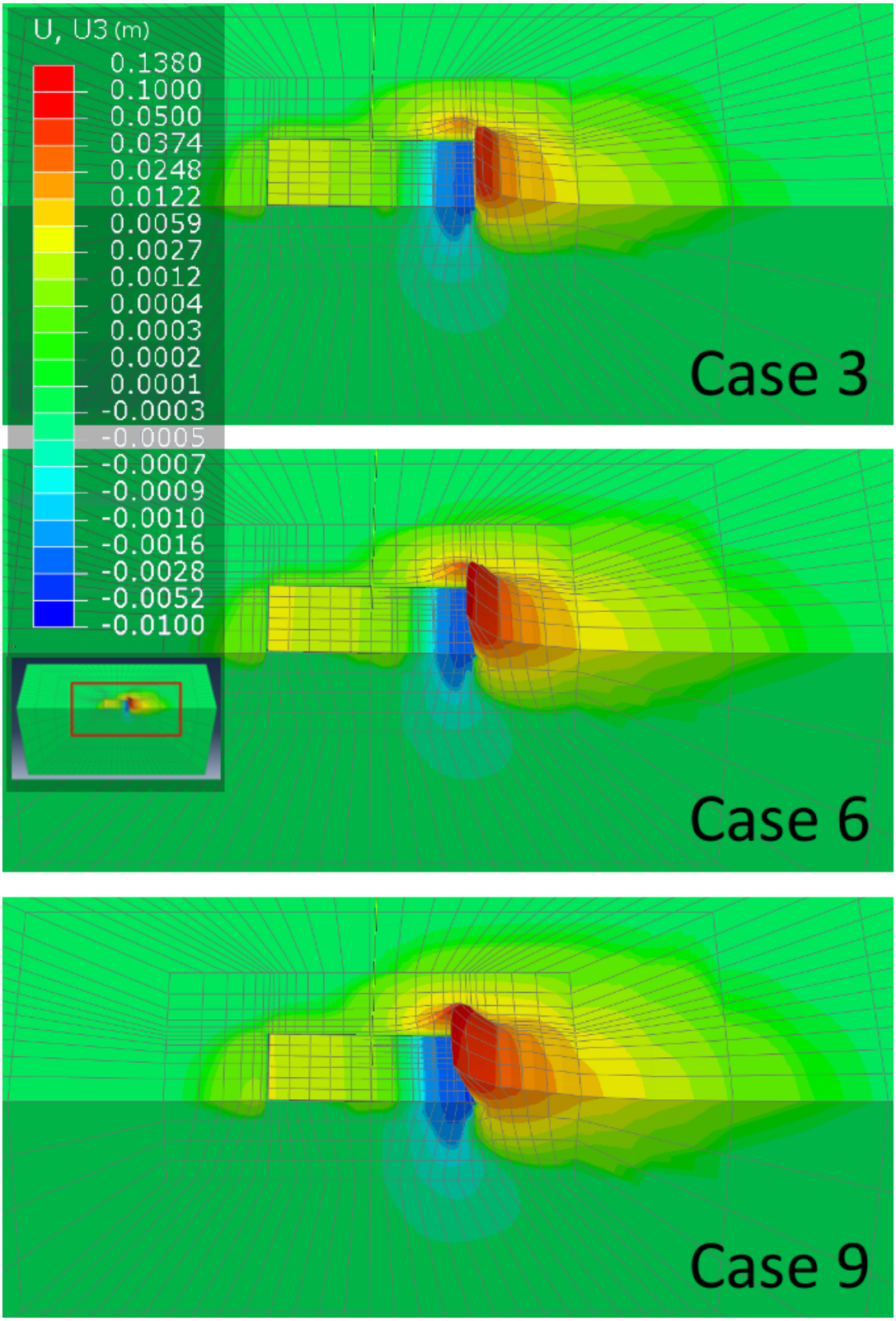

Figure B.6: Variation of vertical component of deformations in FEM mesh for monotonic horizontal loading cases

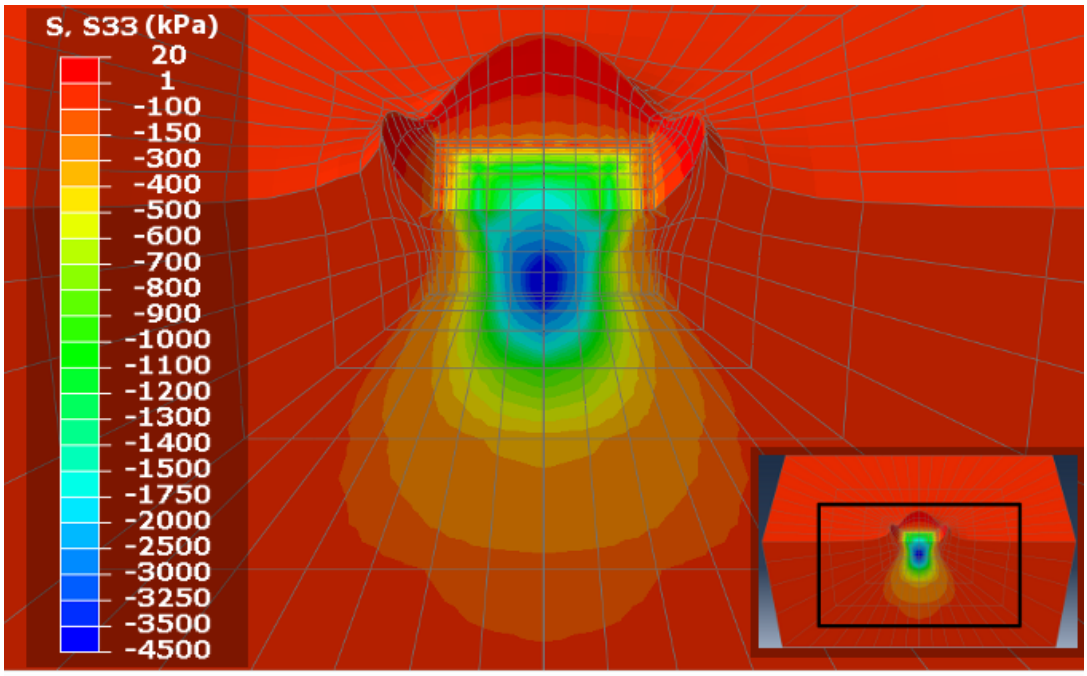

(a) Case 1

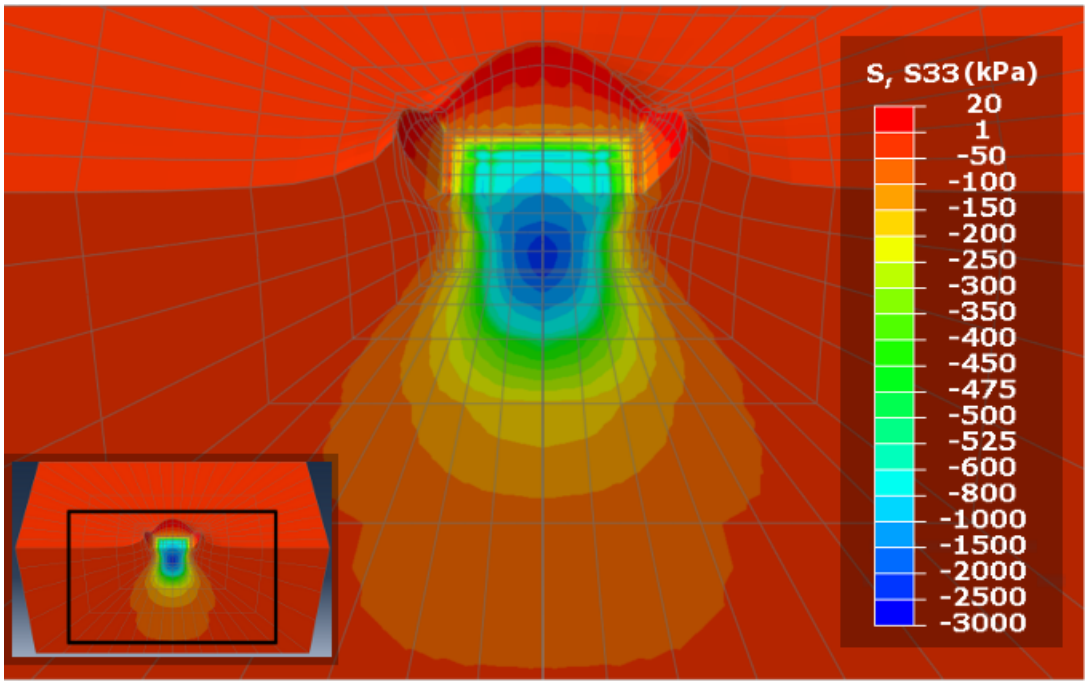

(b) Case 2

Figure B.7: Variation of vertical component of stresses in FEM mesh for monotonic centered vertical loading cases

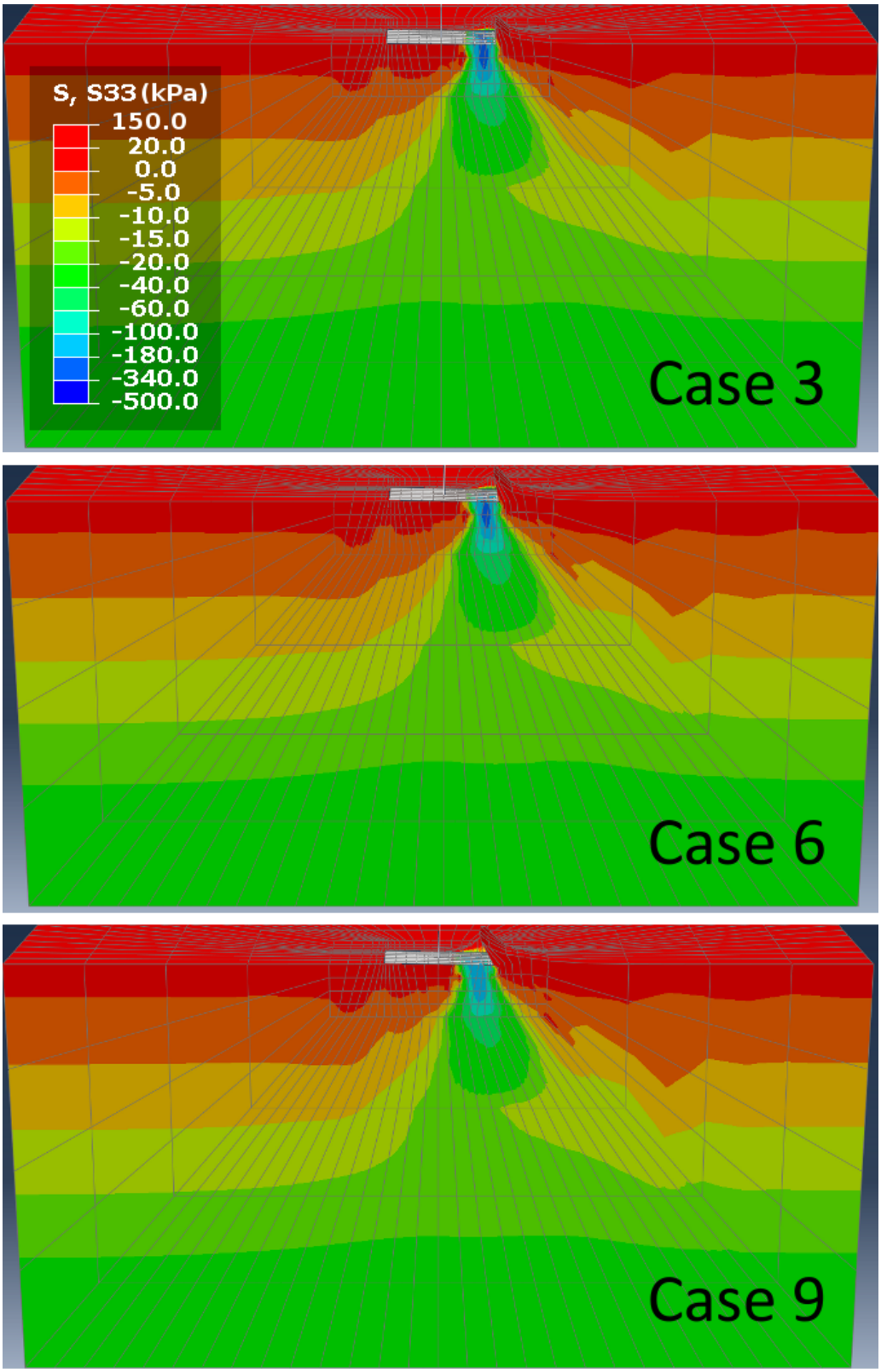

Figure B.8: Variation of vertical component of stresses in FEM mesh for monotonic horizontal loading cases

Appendix C

COMPUTATIONAL COSTS OF ANALYSES

In this appendix, computational costs of a number of analyses, the results of which were presented in this study are presented in terms of analyses run times. Analyses run times (TIME) are presented in Table C.1 and Table C.2 for centered vertical and horizontal loading analyses, respectively. "Section" column in these tables presents the number of the section in this study,where the results of these analyses were presented. It is observed that, for a given analysis, and number of central processing units (CPUS), number of iterations completed per minute is approximately constant. Therefore, analyses run times are obtained by division of total number of iterations (ITERATIONS) completed in the analyses to the number of iterations completed per minute (ITER/MIN).

Table C.1: Computational costs of monotonic centered vertical loading analyses

CASE	SECTION	CPUS	ITER/MIN	ITERATIONS	TIME
Case 1	Section 4.5.1	14	76	301625	66 hours
Case 2	Section 4.5.1	8	59	241654	68 hours
Case 2 ($\psi = 35°$)	Section 6.2.1.2	4	31	135387	73 hours
Case 2 ($\psi = 30°$)	Section 6.2.1.2	44	7	19231	46 hours
Case 2 ($\psi = 20°$)	Section 6.2.1.2	12	3	18524	103 hours
Case 2 ($\psi = 10°$)	Section 6.2.1.2	48	7	14173	34 hours

Table C.2: Computational costs of monotonic horizontal loading analyses

CASE	SECTION	CPUS	ITER/MIN	ITERATIONS	TIME
Case 3	Section 4.5.2.1	4	6	10754	30 hours
Case 6	Section 4.5.2.1	4	6	14885	41 hours
Case 9	Section 4.5.2.1	4	6	24107	67 hours